POLITECNICO DI MILANO

School of Industrial Engineering and Information
Department of Aerospace Science and Technology
Master of Science in Aeronautical Engineering

THUMS NECK INJURY CRITERIA STUDY BASED ON LITERATURE AND COMPARISON WITH HYBRID III DUMMY FINITE ELEMENT MODEL

Advisor: Prof. Marco Anghileri
Coadvisors: Ing. Paolo Panichelli
Ing. Davide Benetton

M.Sc. Thesis by:
Arlotti Ernesto - ID:905221

Academic Year 2020/2021

Alla noia, madre della fantasia

It matters not how strait the gate,
How charged with punishments the scroll,
I am the master of my fate,
I am the captain of my soul.

William Ernest Henley

ABSTRACT

The aim of this study is that of finding injury criteria suitable for neck injury assessment performed on a Human Body Model simulation. In particular, THUMSv4.02 has been used in this work. The purpose has been pursued by considering three possible injury criteria and approaches. The first injury criterion was developed in this work, it is derived from Nij criterion for Hybrid III dummy and it is based on force and moment calculation on THUMS' vertebral sections. The second criterion is based on anatomy studies and in particular on RoM of cervical spine segments. The third criterion is based on osteology and in particular on the plastic strain that causes bone fractures.
The Hybrid III Finite Element model has been validated by the comparison with data from an oblique impact crash test. The peak acceleration magnitude of the test was around $70g$. The first injury criterion development and all the injury assessment were performed using a frontal impact crash simulation. The peak acceleration magnitude of the test was around $62g$.
In addition to the main objective, this study analyse the THUMS and in particular its neck behaviour. A comparison with Hybrid III is proposed in order to understand if the usage of models with high biofedelity has to be increased in injury assessment.
KEYWORD: THUMS, Hybrid III, neck injury, Nij, frontal impact, crash test, Finite Element simulations, LS-DYNA.

ACKNOWLEDGMENT

I surely couldn't have done this thesis work without the help of all the people that supported and guided me in the last year. Therefore, I would like to express my gratitude through these behooved thanks.
First of all, I would like to thank my advisor, Prof. Marco Anghileri, for giving me the possibility to work on a so interesting field of study that is passive safety and Human Body Model in particular. Thanks to FIA for giving me the chance to work with Ing. Paolo Panichelli on this project that was stimulating and educational. Thanks to Paolo himself, for the patience, for guiding me during this amazing journey, for not making me feel deserted and for always being present when I needed an advice, even not related to the work itself. A huge thank to Ing. David Benetton that gave me great support when I needed a technical advice or I couldn't solve a problem. Thanks to LaST personnel, especially Ing. Sergio Bassi and Ing. Mauro Zanella that helped me with the "smart working" issues. I am very sorry that I couldn't work and meet all of you in person due to the pandemic and I wish I could have known you better.
I have written a pseudo-poetic inscription on this thesis because I wanted to somehow give a soul to this work, that I am very proud of. Nevertheless, I have to truly dedicate this thesis to my parents. Mom, thank you for your contagious glee and for always pushing me to experiment, even "blackmailing" me during my childhood; thank you for teaching me what affection is. Dad, thank you for all the stories and anecdote you told me, thank you for teaching me the importance of spiritual self-improvement through art, music and literature. Thank you both for all the support and love you give me every day and for being role models. Thank you for teaching me that whatever happens to me is either my credit or my fault. Thank you for showing me the importance of appreciating and looking for beauty in the life. I love you.
Last but not least, a huge shout-out to all my friend of Ferrara and Milan. Thanks to my roommate Angelo, Giovanni, Italo, Matteo and Michele for all the laugh and the incredible company of these years. Thank you for growing up with me and for sharing with me adventures and everyday life joys but also all the anxiety and problems of university. When I left my hometown, I was eighteen and I felt so lonely and lost. Luckily, I found brothers and for this I will never be thankful enough. You truly are family to me. Thanks to my other brothers Gianmarco, Pasquale and all the guys of Fantasperduti for the affection and for being so present in my life even when we are apart, with you I had the best laugh of my life. Thanks to Filippo and Birra that were my inseparable colleagues in this last years of university. I treasure so much our relationship, how we are so supportive to each other, the jokes and the affectionate insults. Thanks to Andrea, Alessandro and Federica, my Italian buddies in China. Thanks because I had the best time of

my life with you and I will never forget the incredible adventures we had in a so distant country. Thank to Marco, Jacopo, Giacomo, Stefano, Riccardo and all the "regaz" of TTL for tolerating me and treating me as I never left FE whenever I come home, thanks for not making me feel the only old person in the group when I don't want to return home late, for every biretta and ciacara at Reihn, for the daytrips at Lidi and for the summer vacations that were exceptional. Also, many thank for having games with me when I should have studied, I had so much fun. Thank all of you for being part of my most beautiful memories of these years.

Contents

List of Tables

List of Figures

Chapter 1

Introduction

This chapter contains a brief introduction on the main topics analysed in this paper and it explains the main objectives of the work. This thesis was made in collaboration with *FIA*[1].

1.1 Work Objectives

Every year, millions of people are involved in car accident: approximately 1.35 million people die in road crashes each year and 20-50 million suffer non-fatal injuries[28]. Injury may also occur in motor sports, where the pilots drives at higher speed, even following strict safety rules. Neck injuries are one of the most common and dangerous injuries caused by car crashes. In frontal impact, the vehicle is subjected to a forced backward acceleration, but the head lags behind and so the neck is forced into a motion called *whiplash motion*[20]. Depending on the severity of the damage, injuries can compromise the motor skills of the occupants, or even cause death.
In order to prevent this dire consequences, neck injury criteria have been studied and applied in certification tests for cars, motorbikes and safety devices. These tests make use of the so called *Anthropomorphic Test Devices* (ATD) as they guarantee several benefits that will be discussed later in Chapter 2. It is also true that it is not possible to repeatedly perform ATD tests because of their cost in terms of both money and time. Nowadays, *Finite Element Methods* (FEM) are popular and diffused tools for the crash investigation. FEMs offer the possibility to run several numerical simulation saving time and money while maintaining test repeatability. In order to perform *Finite Element Analysis* (FEA), *Finite Element* (FE) models of ATD and *Human Body Models* (HBM) have been implemented. The former has a lower biofidelity than the latter, as it has to match a real dummy. Mannequin are developed to be enough durable to perform repeatable tests. Hence, HBMs provide a better prevision of the human kinematic during crashes. On the

[1] Fédération Internationale de l'Automobile

other hand, injury criteria refer almost exclusively to ATD because they were formulated on dummies as the numerical simulation on complex FE models has been allowed only recently by computer technology development. *THUMS*[2] is one of the most popular HBM in crashworthiness, but there are no official neck injury criteria that are used for assessing neck injury in numerical simulations.

The aim of this thesis is to study THUMS' neck behaviour in order to find possible criteria to apply to injury investigation in frontal impact crashes. The first approach that has been used consisted in using *Nij* criterion[3] as a reference for limit load calculation. Nij is usually applied to a Hybrid III FE model. This approach showed not to take full advantage of the pros of FEA, hence other possible criteria involving cervical spine *RoM*[4] and plastic strain have been assessed. All the numerical simulation has been done using the LS-DYNA® solver software. The LS-DYNA keyword input files were created by using the PRIMER® software environment.

1.2 Problem definition

The first part of the work consisted in the validation of the Hybrid III FE model. The validation of the finite element dummy model was carried out by comparing the results of a crash test conducted on a real dummy with the results of the numerical simulation. FIA provided results of a sled test performed on 06/04/2017 together with pictures and videos of the sled setup and of the test itself. The finite element Hybrid III model and the sled models was provided by FIA, too. Both the Hybrid III and the sled have been positioned in order to match the geometry of the real ones.

Once the Hybrid III had been validated, the second phase consisted in positioning the THUMS into the same setup and then running simulations with the same acceleration pulse. Obviously, the two models are different, so, some modification have been done for fitting the THUMS into the seat.

Finally, the results of Nij criterion performed on the Hybrid III FE model have been compared with the resultant forces and moments on THUMS' vertebral sections and load limits have been found.

As previously said, this approach was still relying on criteria devised for a real ATD and so for punctual measurement. The strengths of THUMS are the biofidelity and the possibility to take measurement everywhere in the model without the need of instrumentation. Therefore, in the last part of the work, the assessment of injury was performed by referring to scientific studies on osteology.

[2]Total HUman Model for Safety
[3]Normalized Neck Injury Criterion
[4]Range of Motion

1.3 Injury Criteria

In this section, the injury criteria used in the thesis are described. The first criterion is commonly used in sled test performed on ATD and was formulated by Mertz et al.[11] also making use of *PMHS*[5]. The other criteria are given by osteology scientific literature.

1.3.1 Nij Criterion

The *Nij* criterion was developed by the *US National Highway Traffic Safety Administration* for the prevention of spinal injuries caused by frontal impacts[18]. It states that the linear combination of normalized neck axial load and normalized moment about the occipital condyle must not be higher than 1.0 at any point in time. The normalization is done using force and moment limits defined for traction, compression (forces), extension and bending (moments). Indeed, the i and j of *Nij* indicates the aforementioned loads: for instance, N_{te} indicated traction-extension injury mechanism. The criterion is expressed as:

$$N_{ij} = \frac{F_z}{F_{1im}} + \frac{M_y}{M_{\text{lim}}} \tag{1.1}$$

F_z is the axial load, M_y is the moment about the occipital condyle and F_{lim} and M_{lim} are the critical values of force and moment. The load limits depend on the dummy involved in the test and are listed in the table below[7][18]:

Dummy	M_y (flexion/extension) (Nm)	F_z (compression/tension) (N)
HIII 50%	310/135	6160/6806
HIII 5%	155/67	3880/4287
HIII 6-year-old	93/37	2800/2800
HIII 3-year-old	68/27	2120/2120

Table 1.1: Critical value of force and moment for different dummies

Abbreviated Injury Scale for Nij criterion

The *Abbreviated Injury Scale* also known as *AIS* is an injury scale that defines the severity of injuries. Table1.2 shows the description of the six levels of AIS[19]. AIS can be applied to different injury criterion for creating the so called risk curves. In Figure 1.1 are reported the risk curves for Nij criterion[24].

[5]Post Mortem Human Subjects

AIS	Level	Description
1	minor	Light lesion to the brain, headache, vertigo but no loss of consciousness; light cervical lesion, whiplash and contusions.
2	moderate	Contusions with or without cranium fractures, less than 15 minutes of loss of consciousness, little corneal crack, retina separation, nose fracture and face damages.
3	serious	Contusions with or without cranium fractures, more than 15 minutes of loss of consciousness without severe neurological damage, clean break of the cranium or compound break but no loss of consciousness; other damages as vision loss, fracture of face bones, cervical fracture with no marrow damage.
4	severe	Cranium fracture with severe neurological damages.
5	critical	Concussion with or without cranial fracture, more than 12 hours of unconsciousness, hemorrhage in the vicinity of the cranium and/or critical neurological damages.
6	fatal	Death, partial or total damages to the brainstem or to the upper part of the cervical zone, fracture and torsion of the cervical spine with marrow damages.

Table 1.2: AIS - Abbreviated Injury Scale

$$\text{Prob AIS2 } N_{ij} = 100 \cdot \left(1 + e^{2.0536 - 1.1955 \cdot N_{ij}}\right)^{-1}$$

$$\text{Prob AIS3 } N_{ij} = 100 \cdot \left(1 + e^{3.227 - 1.969 \cdot N_{ij}}\right)^{-1}$$

$$\text{Prob AIS4 } N_{ij} = 100 \cdot \left(1 + e^{2.693 - 1.196 \cdot N_{ij}}\right)^{-1}$$

$$\text{Prob AIS5 } N_{ij} = 100 \cdot \left(1 + e^{3.817 - 1.196 \cdot N_{ij}}\right)^{-1}$$

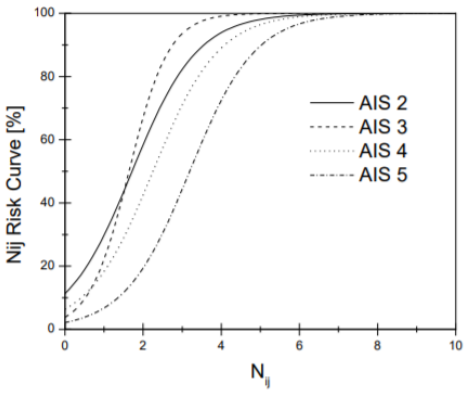

Figure 1.1: Neck injury risk curves corresponding to Nij criterion

1.3.2 Head-neck mobility

The neck contains seven cervical vertebrae that are linked with the occipital bone through the *atlanto-occipital joint*. The cervical segment itself is made of several joint. This structure allows the head to perform complex movements in the space. These movements are basically a combination of four main rotation: flexion and extension in the sagittal plane, lateral flexion in frontal plane and axial rotation in transverse plane (shown in Figure 1.2).

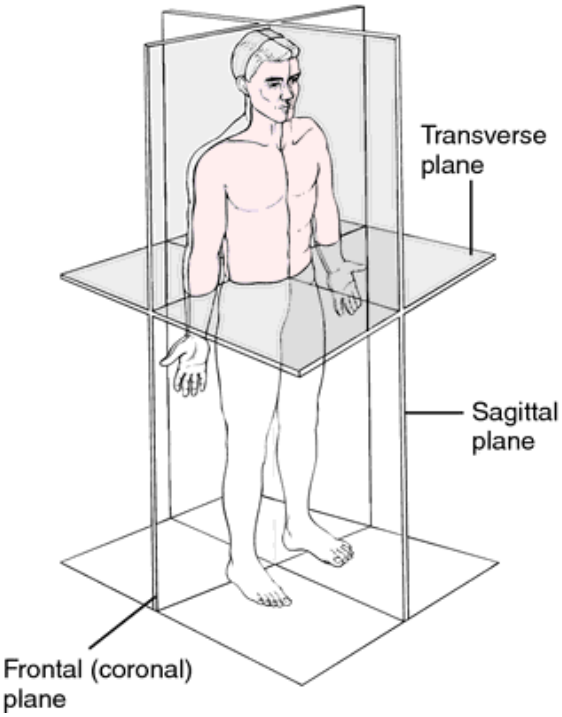

Figure 1.2: Body planes

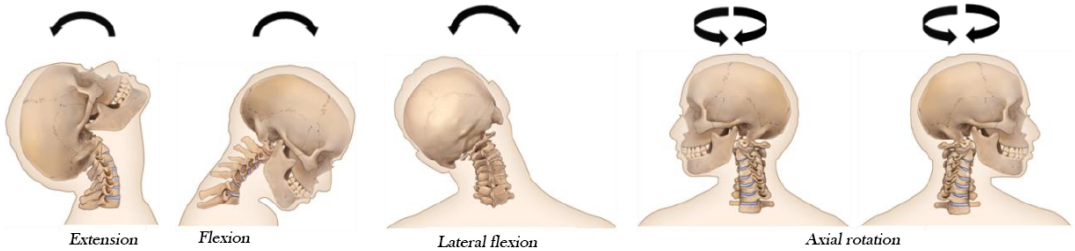

Figure 1.3: Head-neck kinematic movements

The mobility of the cervical spine has been widely studied in the recent years by using different methods; in vivo, by imaging or in vitro with cadaveric specimens.

The kinematic of the cervical spine is studied by defining a *Funcional Spinal Unit* (FSU) that is composed of two vertebrae and a connecting elements that usually is an intervertebral disc (*IVD*). For better understanding of the vertebrae anatomy, the reading of Chapter 2.4 is recommended. The range of motion of different FSUs and of the segments of the cervical spine has been studied through cadavers' tests. In Table 1.3 are listed some RoM[3] for cervical FSU together with RoM for the upper cervical segment (C0[6]-C2) and for the lower segment (C2-C7).

Average Values (degrees)	C0-C1	C1-C2	C2-C3	C3-C4	C4-C5	C5-C6	C6-C7	C0-C7 (total)	C0-C2 (total)	C2-C7 (total)
Flexion/ Extension	26.9 ± 11.8	18.4 ± 8.8	11.2 ± 4.8	16.4 ± 6.1	17.1 ± 5.3	18.7 ± 6.7	15.9 ± 4.9	116.9± 20.2	45.2 ± 14.8	85.1 ± 18.9
Lateral flexion	9.8 ± 2.3	12.2 ± 8.5	11.7 ± 7.0	11.9 ± 6.0	10.9 ± 4.8	10.1 ± 5.2	9.3 ± 4.7	79.5 ± 20.8	20.2 ± 7.6	60.1 ± 24.9
Axial rotation	6.7 ± 6.4	73.4 ± 16.3	11.6 ± 8.6	11.6 ± 6.6	10.0 ± 5.9	10.3 ± 4.3	7.5 ± 4.3	128.5± 19.4	80.4 ± 16.8	59.5 ± 26.9

Table 1.3: Range of motion for cervical FSU, upper, lower and whole segments during the main movements

The cervical spine mobility can also be analysed macroscopically, thus focusing on the movement of the whole spine through a global evaluation, but in this work the mobility was analysed microscopically. It has to be noted that the mobility of cervical spine articulations has been shown not to differ significantly between men and women. It is also true, that can be consistently compromised by aging and by several pathologies[23].

1.3.3 Bone failure due to plastic strain

Another way for evaluating bone fracture consist in evaluating plastic strain. The plastic strain failure of bones has been studied by Burstein et al.(1976) and McCalden et al.(1993). These studies defined a fracture criterion of 3% strain[31], valid for cortical bone material. Later studies on vertebrae attested the limit at 1-2%[8]. In this work we used a plastic strain limit equal to 2% because it was previously used by FIA in other projects as it was a reasonable average value.

[6] Occipital condyle

1.4 Thesis structure

This thesis is organized in the following chapters:

- Introduction
- State of the Art
- Hybrid III model validation
- THUMS' numerical simulation
- Injury criteria development and assessment
- Conclusions and future development

Chapter 2

State of the Art

This chapter gives the reader an overview on the development and history of passive safety and describes the anatomy of the neck and of the cervical spine in particular. Regarding passive safety, the main focus will be the development of numerical models and the reasons behind their implementation. The FE models used in the work are described, too, as they are indispensable to understand the work done.

2.1 Anthropomorphic Test Devices' history

From the beginning of automotive industry to the 1950s, little attention was given to safety measure for vehicle accidents. Only after the end of Word War II, aviation service personal began to understand the importance of comprehending the effects of deceleration on human body. Colonel John Paul Stapp[1] can be considered a pioneer in this field of study. Starting from 1947, Stapp run several rocket sled tests, sometimes even offering himself as volunteer, for studying the effect of high deceleration on human body[22].
Initially, the purpose of these studies was to increase the safety for aeronautic pilots during deceleration situation e.g. during ejection from the aircraft, but soon were applied to the automotive safety. Even if Stapp program was fundamental to set the starting point for passive safety development, it soon became clear that his methods were not feasible, so human volunteers were replaced with inanimate object, animals or PMHS.
The first test mannequin, *Sierra Sam*, was created in 1949 by Samuel W. Alderson, at Alderson Research Labs, together with Sierra Engineering Co., the project supported by the *United States Air Force* (USAF). The dummy was involved in ejection seats, aviation helmets and pilot restraint harnesses tests. As it has to

[1] Colonel John Paul Stapp (July 11, 1910 – November 13, 1999), M.D., Ph.D., was an American career U.S. Air Force officer, flight surgeon, physician, biophysicist, and pioneer in studying the effects of acceleration and deceleration forces on humans. He became known as "the fastest man on earth" after he reached a speed of 632 mph (1,017 km/h) as a volunteer for a deceleration test and survived.

Figure 2.1: Colonel Stapp during rocket sled test

represent a member of aviation the mannequin was a 95^{th} percentile male dummy (heavier and taller than 95% of human males)[6]. Regarding biofidelity, Sierra Sam had humanlike exterior shape, good weight and height reproduction and average accuracy of the ranges of motion for its articulated limb joints. The instrumentation installed was not particularly comprehensive: it was possible to measure only orthogonal linear head acceleration components. These defects encouraged the creation of other dummies.

So, firstly in 1971 and secondly in 1972, General Motors released Hybrid I and Hybrid II mannequins[12]. The former combined the best features of two improvement of Sierra Sam: the VIP series (made by Alderson) and Sierra Stan (made by Sierra Engineering). It was a 50^{th} percentile male dummy, hence, it reproduced an average male in height, mass, and proportion. The latter had improved shoulder, spine, and knee responses, and more rigorous documentation. Hybrid II became the first dummy to comply with the *American Federal Motor Vehicle Safety Standard* (FMVSS) for testing of automotive lap and shoulder belts. Despite being used for tests and development of seat belts, Hybrid II was still unrefined.

All these models set an important milestone in the passive safety development and were fundamental for the creation of the most employed dummy of today: Hybrid

III that is described thoroughly in the following section.

Figure 2.2: Sierra Sam

2.1.1 Hybrid III

"Humanetics harmonized Hybrid III 50^{th} Male ATD is the most widely used crash test dummy in the world for the evaluation of automotive safety restraint systems in frontal crash testing. Originally developed by General Motors, the Hybrid III 50^{th} percentile male design is now maintained and developed by Humanetics in conjunction with the Society of Automotive Engineers' (SAE) Biomechanics Committees and the National Highway Transport and Safety Administration (NHTSA).

Figure 2.3: Hybrid III

The Hybrid III is a regulated test device in the USA Code of Federal Regulations (Part 572, Subpart E) and also in the European ECE Regulations. It is considered to have excellent biofidelity and instrumentation capability. Recent revisions have improved biofidelity in the femur range of motion, and also the ankle and foot. The dummy is also used in many non-automotive applications such as wheelchairs and medical and sports equipment". This is the description that can be found on the website of Humanetics[13] together with a list of key features that makes Hybrid III better than his predecessor Hybrid II:

- Improved biofidelity in the head, neck, thorax, pelvis, and knees
- Anatomically-improved head
- Neck has different flexion and extension response which is tested
- Thorax has improved biofidelic response to impact
- Lower torso uses the driver's slouch position with a curved lumbar spine, with two spine cables for better representation of dummy posture
- Tibia displacement measurement allowed for ACL[2] damage estimation

[2]anterior cruciate ligament

- Ankle bumpers minimize mechanical noise

Furthermore, the Hybrid III has a huge instrumentation capacity providing 44 slots between accelerometers, load cells and displacement transducers.
In order to perform test on subjects with a different physique from the 50^{th} percentile one, Humanetics created other dummies:

- 95^{th} percentile male dummy
- 5^{th} percentile female dummy
- ten, six and three year old dummies

Table 2.1 shows the anthropometric data of the mannequins previously listed.

Hybrid Model	**Anthropometric Data**		
	Mass [Kg]	Stature [m]	Total sitting height [m]
5^{th} percentile	49	1.4896	0.7874
50^{th} percentile	77.70 ± 18[3]	1.7458	0.8839
95^{th} percentile	101.15	1.8502	0.9347
3-year old	16.17	0.94488	0.5461
6-year old	23.4	1.1405	0.635
10-year old	35.2	1.2014	0.7239

Table 2.1: Anthropometric data for different Hybrid III models

2.2 Requirements for dummies

According to J.H.Marcus[15] that studied dummy and injury criteria for crashworthiness, ATDs must meet several requirements in order to be useful and convenient:

- *biofidelity*: ability to reproduce the behavior of the human body given different configurations, to estimate movements and forces involved and to provide compliant values, in terms of injury criteria.
- *repeatability*: ability to provide concordance between a series of measures, when the measurement conditions are left unchanged.
- *reproducibility*: ability to provide concordance between a series of measurements while varying one or more conditions (e.g. measuring instrument).

[3] weight variation related to the presence of the complete instrumentation

- *durability*: ability to survive test conditions without damage, opposite to what happens to human beings.

- *standard calibration*: as all measuring instruments, it is appropriate that the ATDs are subjected to periodic calibrations to ensure results accuracy. For many ATDs, calibration techniques are listed in the Code of Federal Regulations.

2.3 Finite Element Models

In Chapter1 we already disclosed some of the reasons behind the increasing usage of ATDs FE models in crashworhtiness areas. Experimental tests are expensive in term of both time and money because they are difficult to arrange and because they require expensive tools and instrumentation. Meanwhile, numerical simulation are becoming more and more fast and accurate thanks to the continuous improvement of calculators. The FE models themselves are more realistic and reliable than in the past and thus they allow to run less and less experimental tests in favor of the numerical ones. Moreover, they permit to analyze and visualize deformation, loads and energy everywhere in the model model during the entire simulation.
On the other hand, it is necessary to use experimental tests as a reference for the validation of numerical models. In this work in particular, two highly detailed FE models (provided by FIA) have been used: LSTC[4] Hybrid III DETAILED 50^{th} percentile and THUMS AM50v4.02 (50^{th} percentile). The first model is the representation of an ATD, while the second is a HBM, hence there are of course many differences between the two.

2.3.1 Hybrid III: LSTC DETAILED model

In this thesis, the Hybrid III FE model that has been used was developed by LSTC and it represents a male 50^{th} percentile occupant. It was provided by FIA together with a sled model that is described in Section 2.3.3, as both were used in a previous FIA's study. It is $174cm$ tall and weights $79kg$. The type of model is DETAILED, hence the model is very complex and detailed, indeed. It is formed by approximately 466000 elements, the articulation are modeled as joints and several contact card manage the contact between subsystems. The articulation allows limb movements with RoMs similar to the real ones and can be managed by using the pre-processor software (PRIMER has been used for this work). Thus, it is possible to position the dummy without running simulations.
The model has been provided with an helmet because this study has been performed in order to be useful for motor sport passive safety. The helmet weights

[4]Livermore Software Technology Corporation

1.3kg that is a standard weight for an integral helmet. Hybrid III has been positioned to better fit the seat during the work activity, but was already seated as it was used in the previous study cited before.

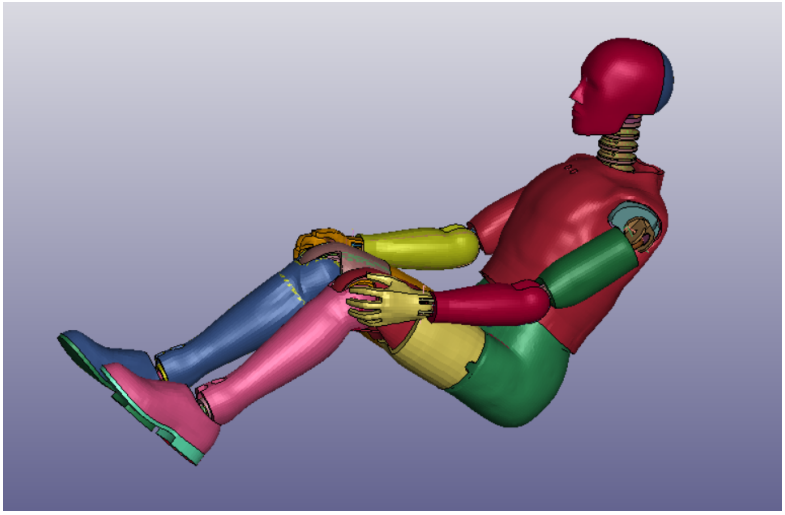

Figure 2.4: Hybrid III finite element model

2.3.2 Total Human Model for Safety

"Total Human Model for Safety (THUMS) is a human body finite element model jointly developed by Toyota Motor Corporation and Toyota Central R&D Labs., Inc. THUMS is capable of simulating human body injuries such as bone fracture, brain and internal organs damage in vehicle collisions. Compared to the physical crash dummies commonly used in vehicle collision tests, THUMS is able to analyze collision-related injuries in more detail because it precisely represents the shapes and durability of human bodies. THUMS has continually evolved to add a range of models with different genders, ages and physiques that include skeletal structures, brains, internal organs and muscles"[5].
For a better understanding of the FE model it is important to examine the history of THUMS. As previously said, in the 1980s automotive company began to explore the potential of numerical simulation. In the 1990s, Toyota Motor Corporation (Toyota) and Toyota Central RD Labs began to collaborate on extending this simulation technology to the human occupants of a vehicle and in 2000 they launched the first virtual human body model (THUMS v1). The model represent not just the structures of the body, including bones, organs, muscles etc. but also their durability in response to force and impact. These features has been based on studies on biomechanics and injuries conduced by the Toyota engineers at Wayne State University in Detroit, Michigan during the 1990s. Toyota engineers manually designed three-dimensional meshes that would reproduce the shapes of the

human body, and implemented the mechanical properties for its component parts, including bones and internal organs[30].

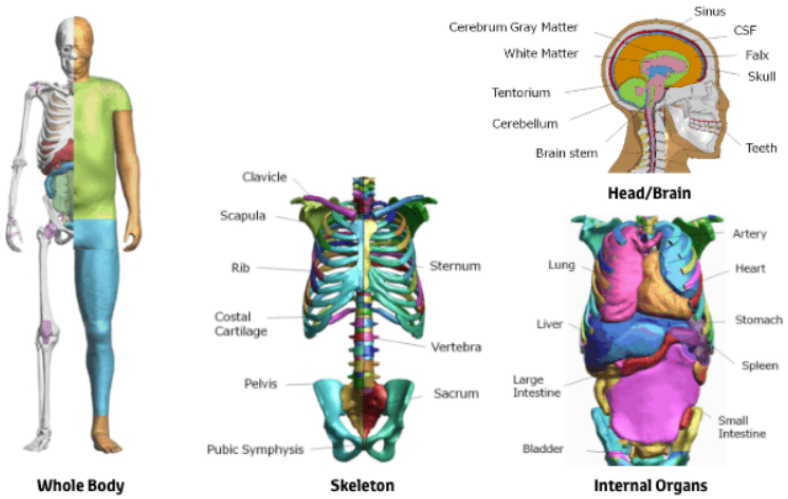

Figure 2.5: THUMS' structure

The aim was to create a tool that could go above and beyond what was possible with vehicle collision tests. Virtual HBM are indeed intrinsically more accurate than ATDs. The latter are limited in how accurately they can represent a human body because they are designed to be durable as seen in Chapter 2.2.

Toyota launched THUMS Version One in the year 2000 and has followed with six more versions that evolve and broaden the model's scope, the differences are shown in Figure 2.6.

Considering different factors, including gender, age, physique, brains, internal organs and muscles, other variation in age and physiques of THUMS v4 were developed. THUMS was validated against loading tests both to body components and whole body. A total of 38 tests with postmortem human subjects (PMHS) were cited from the literature[5].

The THUMS used in this work was provided by FIA and is a version 4.02. It is $177cm$ high and it weighs $74kg$. The model is made of about 1900000 elements and 1322 parts. Hence, it is easy to comprehend that the numerical simulations are very heavy and require good calculators. It is provided with shoes. The model was already in a seated position as the Hybrid III model.

The positioning was performed in order to fit the THUMS into the seat. This process was more complex than Hybrid III positioning because THUMS has no tools for moving in the pre-processor environment. The positioning has been done though numerical analysis and is described later.

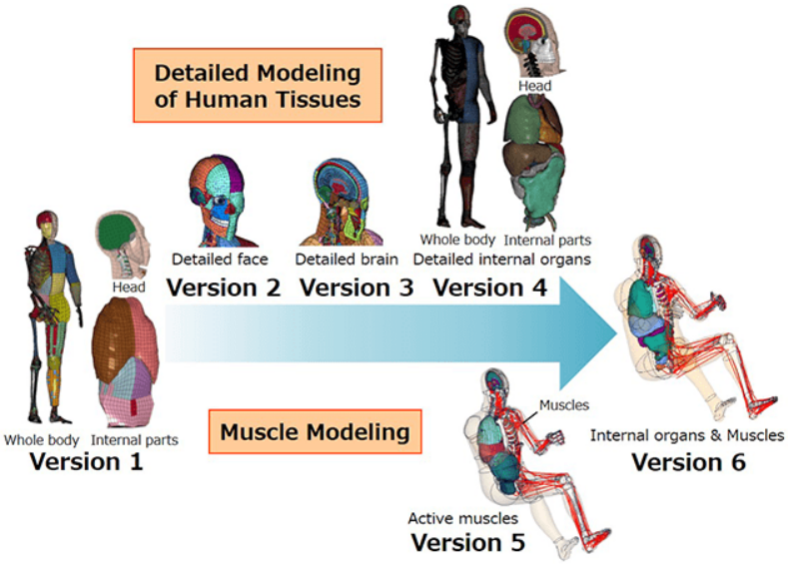

Figure 2.6: THUMS' evolution

Figure 2.7: THUMS in the original seated position

2.3.3 Reclined sled seat model

The sled seat model that has been provided for the work activity is made of seven part:

- Seat back: 500mm high, 400mm large and 20mm thick
- Foot floor: has a L form; the base is a square, side 400mm long; the vertical part is 100mm high; the thickness of the floor is 20mm

- Seat pad: measures=345x390x40mm
- Seat kick: placed under the seat pad; measures=465x390x20mm
- Foot floor: oblique parallelepipedon; measures=400x400x20mm
- Two seat null shell with the same length and width of the seat pad and 1mm of thickness.

Seat back, foot floor and seat kick are made of shell elements and rigid materials. The foot rest is made of solid elements, the material is steel and in particular the card MAT_PLASTIC_KINEMATIC was used. The seat pad is made of solid elements, the material card is MAT_LOW_DENSITY_FOAM[16], thus it guarantees a viscous damping that emulates the texture of a typical seat pad. Two shell parts of null material are placed on and under the seat pad. The seat sled is shown in Figure 2.8. It is possible to notice that the seat pad already shows a deformed form.

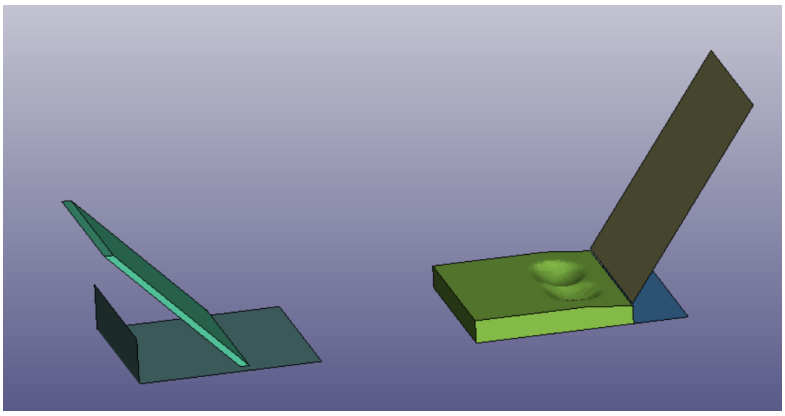

Figure 2.8: Reclined seat sled model

The headrest and the seatbelts were modelled and fitted during the work activity, hence are described in the next chapter.

2.4 Cervical spine anatomy

The vertebral column forms the central pillar of the human body and is divided into 24 mobile vertebrae (cervical, thoracic and lumbar) and a group of nine fused sacro-coccygeal vertebrae (pelvic). Its equilibrium is conditioned by the presence of vertebral curvatures which are similar to an S shape. In the sagittal plane, these curvatures are four in number: cervical curvature in lordosis, thoracic curvature in kyphosis, lumbar curvature in lordosis and sacrococcygeal curvature in kyphosis. According to the previous studies[32], these curves make it possible to absorb the mechanical stresses due to the movements of the body. The spine can support loads

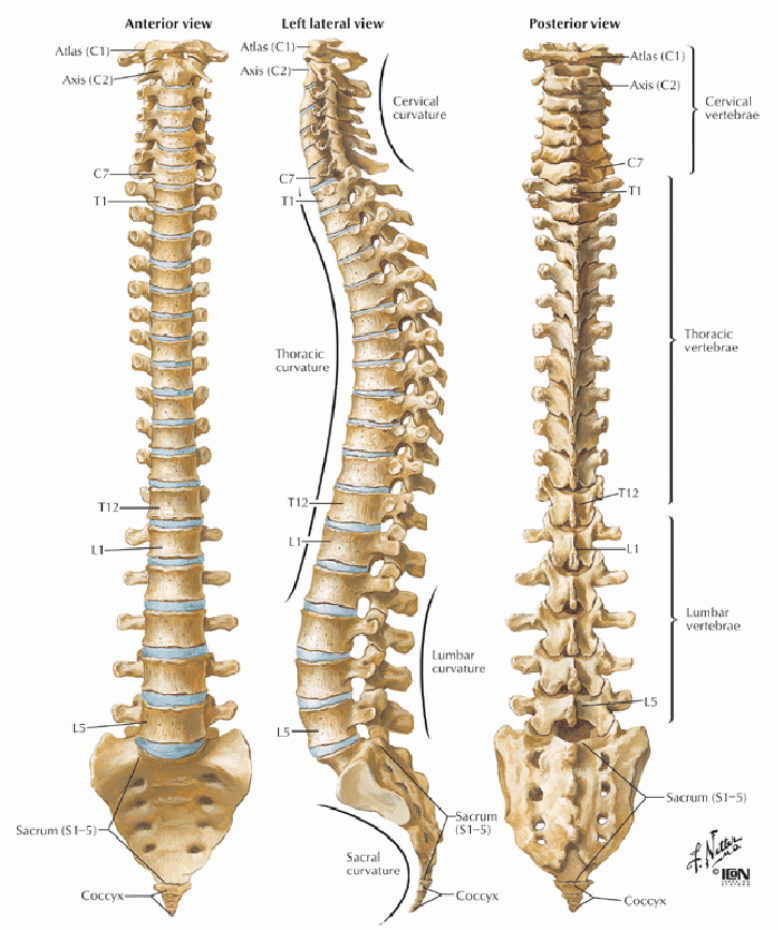

Figure 2.9: Human vertebral column with its curvatures in anterior view, left lateral and posterior view[10]

up to 6000 N. Regarding structure organisation, the spine also has a protective function for the spinal cord and spinal nerves. The connection between the skull and the rest of the spine is made by the cervical spine which supports the head and allows its mobility. In the same way as the rest of the vertebral column, the cervical spine consists of vertebrae, ligaments, intervertebral discs and the nervous system.

2.4.1 Cervical spine bone structures

The cervical spine is the most superior portion of the vertebral column and it lies between the skull and the thoracic spine. It consists of seven distinct vertebrae (C1 to C7[5]).

[5]the name of the cervical vertebrae is given by the letter "C" that stand for "cervical" and by the number of their position starting from the one nearest to the cranium

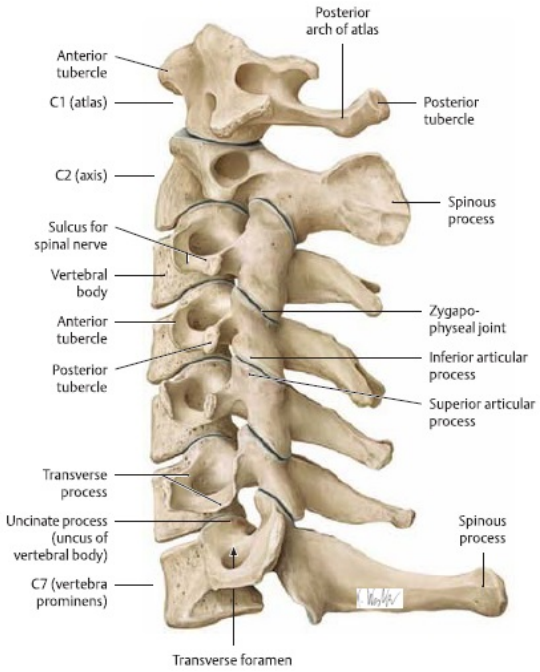

Figure 2.10: Anatomy of the cervical spine

Two of the cervical vertebrae have unique names: C1 is called *atlas* and C2 is called *axis*[29]. The atlas is the first cervical vertebra and articulates with the occiput of the head and the axis. It differs from the other cervical vertebrae in that it has no vertebral body and no spinous process. It's important to highlight the position of the occipital condyle, that is positioned on the occiput because it is essential for the definition of Nij as seen in Chapter 1.3.1. It is shown in Figure 2.11.

The axis (C2) is easily identifiable due to its dens (odontoid process) which extends upwards from the anterior portion of the vertebra. The dens articulates with the anterior arch of the atlas and it creates the medial atlanto-axial joint. This joint allow the rotation of the head independently from the torso.

The vertebrae C3 to C7 have similar geometry and composition. The vertebral body is made of cancellous bone covered with cortical bone. This composition allows to carry compression loads. The spinous process and the transverse processes serve as points of intersection and leverage for muscles and ligaments. The spinal cord is located in the spinal canal. The articular facets guide the movements between two consecutive vertebrae.

Figure 2.11: Occipital condyle highlighted in red

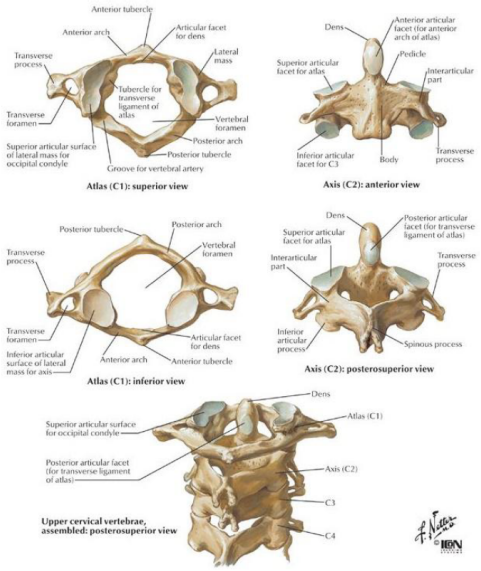

Figure 2.12: Anatomy of cervical vertebra C1 (atlas), C2 (axis) and upper segment C1-C4

2.4.2 Ligaments

The mobility and stability of the spine are provided by the spinal ligaments made of bands of fibrous tissue[29]. The posterior longitudinal ligament (PLL) and the anterior longitudinal ligament (ALL) provide the connection between the vertebral bodies and limit movements in flexion and extension. The yellow ligaments or ligamentum flavum (LF), interspinous (ISL), nuchal (NL), which becomes the

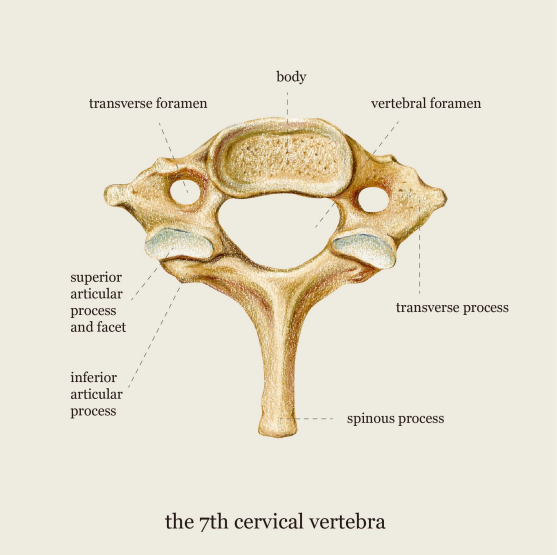

Figure 2.13: Top view of C7

supraspinous ligament below the C7 level, and capsular (CL) protect the spinal cord and limit many movements (flexion, extension, tension, translation rotation). The transverse ligaments are linked to the inner part of the atlas (C1) and around the odontoid process of the axis (C2).

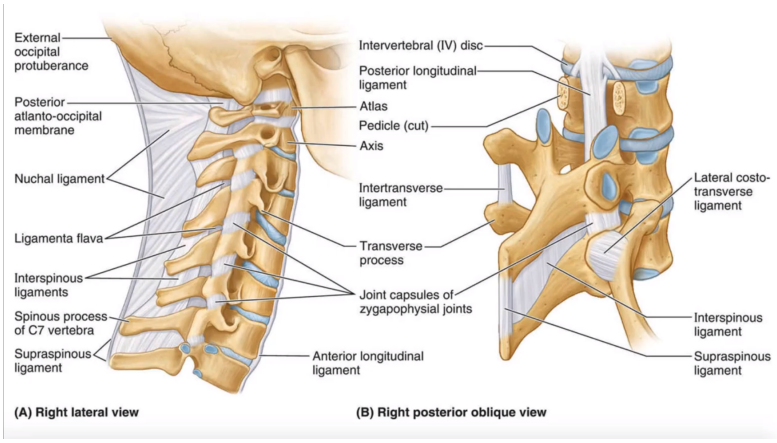

Figure 2.14: Principal ligaments of the cervical spine

2.4.3 Intervertebral discs

The intervertebral discs, located between each of the vertebrae, allow the vertebrae to be held together. These discs also allow movement between each of the vertebrae as well as shock absorption and load transfer between two vertebrae. There are 23

intervertebral discs in total. Each disc consists of a ring of fibrous cartilage with a gelatinous nucleus (80% water) in the center. This core provides the disc with elasticity and compressibility while the ring limits movement and expansion of the core[9].

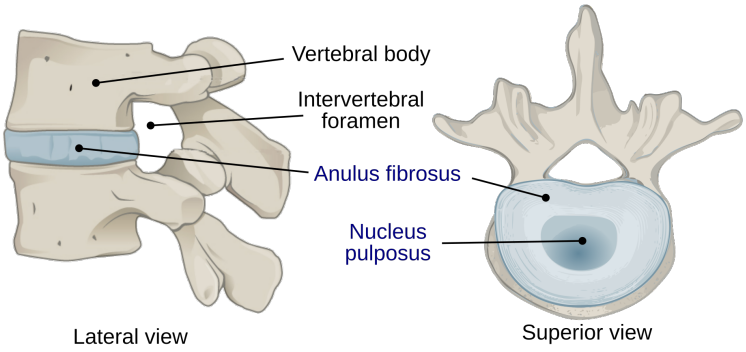

Figure 2.15: Lateral and superior views of IVDs

2.4.4 Spinal cord and nervous system

The spinal cord is an integral part of the central nervous system (CNS). Its shape is similar to a cylinder about $1cm$ in diameter and $45cm$ in length. Its main function is to transmit electrical signals between the central nervous system and the different parts of the body. The spinal cord passes through the spinal canal and is protected by the vertebral column. Its morphology is not constant on the transverse plane and shows the emergence of 31 pairs of spinal nerves which are subdivided into 8 cervical nerves, 12 dorsal nerves, 5 lumbar nerves, 5 sacral nerves and a coccygeal nerve. The vertebral levels are associated with different functions. For example, breathing and the movements of the head and neck are managed at levels C1-C4, the heartbeat and movement of the shoulders are provided by levels C4-C6[9].

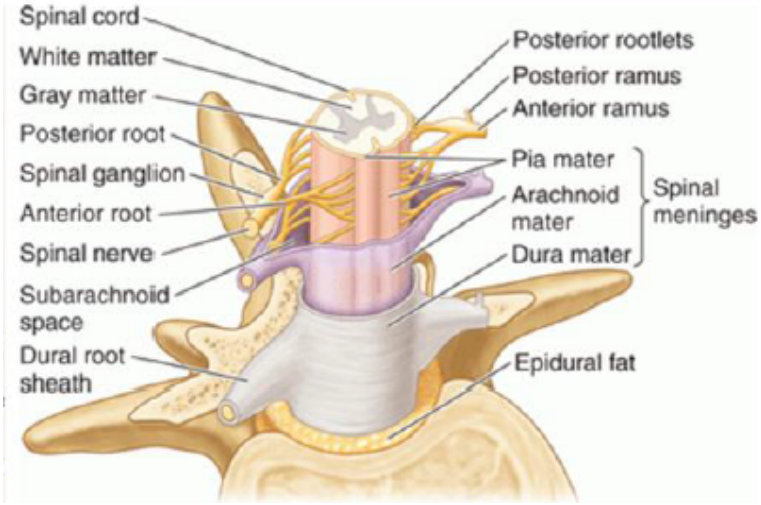

Figure 2.16: Spinal cord and nervous system

Chapter 3

Hybrid III model validation

In this chapter, we discuss the validation of the Hybrid III FE model. This model will be used later on as a reference for studying the behaviour of the THUMS neck and then for formulating a neck injury criterion valid for the latter model. The first step was to reproduce the setup of the sled test conduced by FIA on 06/04/2017. Then some numerical simulations were run and the results were compared with the experimental results. A special attention was given to the seatbelt modelling. The neck model formulation was modified on the basis of the thesis of S.Motta, former Politecnico of Milan student. In the end, the best configuration among those analysed was chosen and then it was used in the Nij calculation and in the subsequent steps of the activity.

3.1 Sled test configuration

FIA provided the data of the aforementioned experimental test, in particular the used instrumentation was:

- Sled accelerometer: measurement of crash pulse
- Upper neck load cells: measurements of forces and moments on the upper neck (i.e. $F_x, F_y, F_z, F_{tot}, M_x, M_y, M_z, M_{tot}$)
- Head and chest accelerometers: measurements of head and chest accelerations (x,y,z components and total)
- Seatbelt tension force sensors: measurement of seatbelts tension forces

For the reproduction of the geometry of the sled we had as a reference some pictures and videos of the sled test, but no numerical data were available. So the sled seat model was modified in order to match the pictures with enough accuracy, but complete congruence cannot be guaranteed. Here a list of the changes:

- The seatback was rotated in a more vertical position (i.e. 55°).

- The footrest was moved so that the knees match the geometry of the ATD (i.e. they form an angle of about 120°).
- The head was rotated in a more vertical position (i.e. 85°).
- A headrest was added for giving support to the head in the first part of the simulation and for being coherent with the experimentation sled seat; the material and section chose for the headrest were the rest ones (dimensions=70x240x50mm).
- The seatbelts were created (their geometry is discussed later).

In Figure 3.1 are shown the numerical test configuration and the experimental one. Hybrid III FE model was equipped with all the database card necessary for

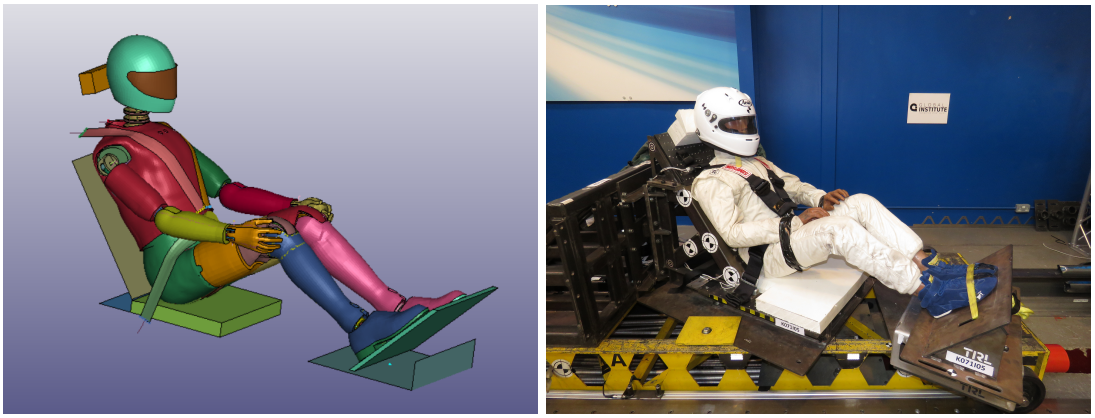

Figure 3.1: Hybrid III numerical and experimental configuration

the calculation of such quantities. In particular, in Figure 3.2 is shown the cross-section on the upper neck that operates as a load cell. In LS-DYNA there are two categories of cross-sections:

- set cross-sections: a set of element and the forces and moments are calculated only for the contribution of the selected set; a reference system is requested for the output.
- plane cross-sections: a plane is defined and a set part is selected, the software automatically generates a set of element through which the loads are evaluated. If no set part is selected LS-DYNA will include all the part of the model; a reference system is requested for the output.

The upper neck cross-section is a set cross-section for the calculation of forces and moments. In Figure 3.3, the accelerometers used for head and chest accelerations are shown . The accelerometers' outputs are affected by high levels of noise, so the solver is requested to do a preliminary filtering by the use of the control card CONTROL_OUTPUT with IACCOP set to 1[16].

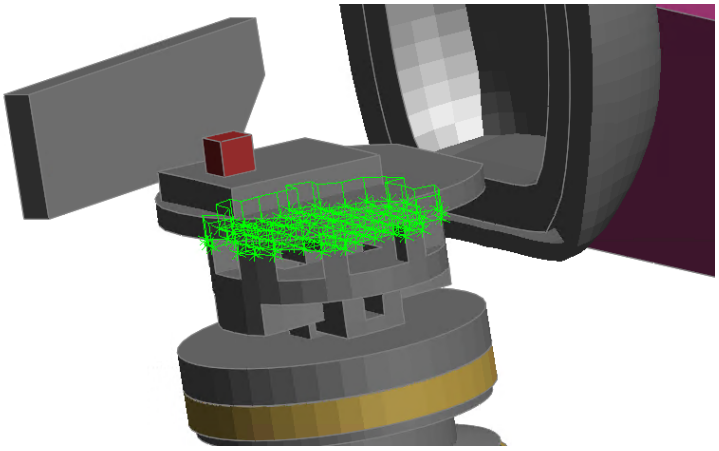

Figure 3.2: Hybrid III UNeck section

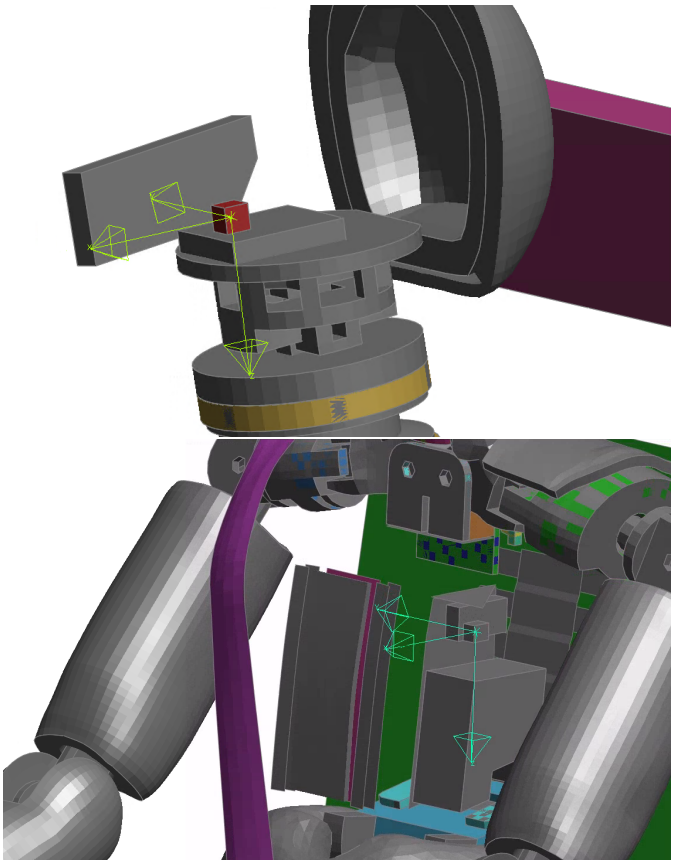

Figure 3.3: Hybrid III head and chest accelerometers

3.1.1 Crash pulse

The experimental sled test was intended to simulate a motor sport crash, i.e. rally race crash, so the crash pulse was set in order to have the deceleration magnitude around $70g$. The acceleration was bi-axial, i.e. in both the x and y direction (Figure 3.4 shows the global reference system). It has to be noted that the experi-

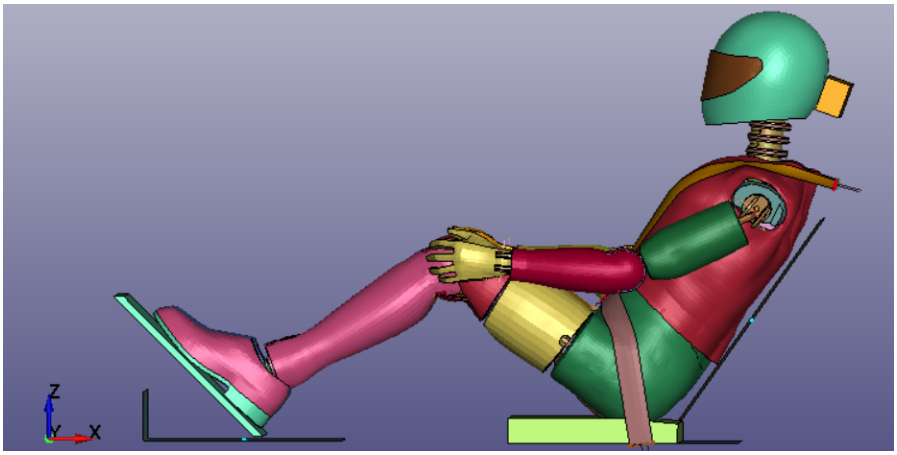

Figure 3.4: Hybrid III global coordinate system

mental and numerical tests use different approach for simulating the crash. In fact, the former simulate the crash deceleration by stopping the sled while it is moving at high speed. Thus the observer is not concurrent with the sled itself. This approach correctly emulate the crash and is commonly used in crashworthiness. On the other hand, the latter tests use the so called lagrangian approach, namely the observer in concurrent with the sled that is perceived as stationary in the initial instant of the simulation. Then a deceleration equal to the experimental one is applied and the sled starts to move. This is done to decrease the heaviness of the calculations that have to be performed by the calculator, hence the time needed to finish the simulation. Obviously, both the approach are physically correct and should provide the same results.

The crash pulse used for the numerical simulation is obviously equal to the one used for the experimental test and it lasts around $45ms$. The crash pulse is provided by prescribing an acceleration on the sled by using the LS-DYNA card PRESCRIBED_MOTION[16]. Prior to the pulse, a period of adjustment was set so that the dummy could correctly lean against the seat (namely $50ms$) because the dummy at the beginning of the simulation is not in contact with the seat to avoid compenetration errors. After the pulse, the simulation continues until the total time left is $150ms$ (hence the CONTROL_TERMINATION[16] card is set to 0.15). The pulse is shown in Figure 3.5. It has to be noted, that the graphs represents the absolute value of the acceleration components and that the x and y

components are directed in the x and y direction of the global reference system.

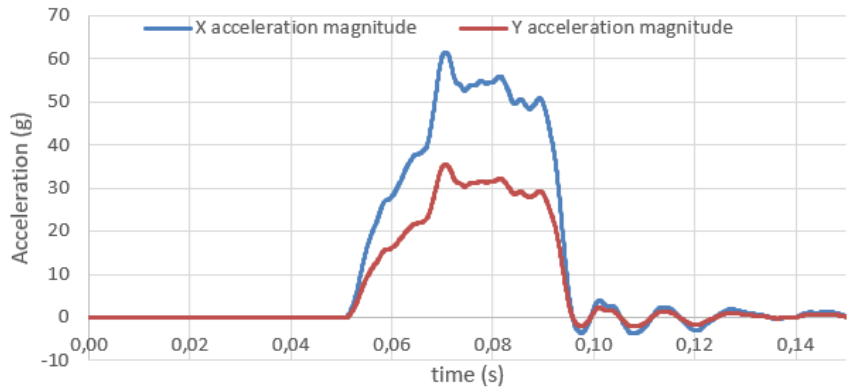

Figure 3.5: Sled acceleration in x and y directions

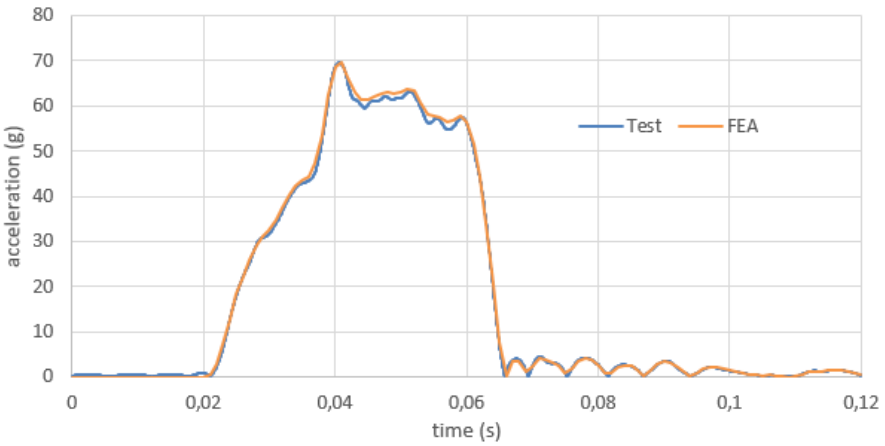

Figure 3.6: Sled total acceleration comparison

By controlling the contact force between the Hybrid III and the seat pad is possible to assess if the dummy is correctly seated on the sled seat at the beginning of the crash pulse. At $50ms$ the reaction force between the dummy and the seat reaches a value of approximately $700N$, that is coherent with the dummy weight.
Figure 3.6 shows the comparison between experimental and numerical total sled acceleration. It has to be noted that the crash pulse starts at $20ms$ in the experimental test, so from now on in this chapter the numerical graphs will be shifted in order to match the experimental data.

3.1.2 Seatbelts

Here follows a brief description of the seatbelts modelling together with some data obtained by running different analysis.

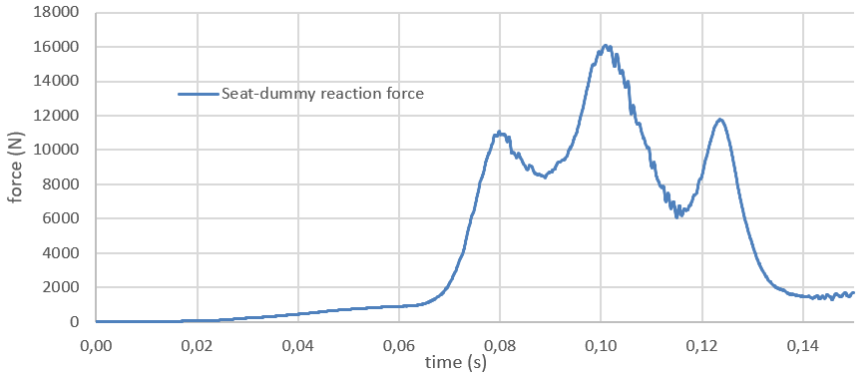

Figure 3.7: Hybrid III-seatpad contact force

The seatbelts were modeled by using the safety seatbelt tool of PRIMER. Because of the fact that the test subject is a motor sport vehicle occupant, the choice was to use a six-point harness in the experimental test, so five seatbelts were modelled and linked to a central buckle in the FE model. The crotch seatbelts were modeled as one seatbelt but the stiffness was two times higher than in the other belts. Each seatbelt is made of three part: the central part is modelled with 2D seatbelt shell elements (four elements in the width direction, elements size equal to 12.5x10.25mm, so a total belt width of 50mm), meanwhile the ends are modelled as 1D seatbelt elements. The shell elements material is defined by the card PIECEWISE_LINEAR_PLASTICITY[17] that represents polyester. The thickness of the seatbelts is 1.35mm for the shoulder belts and 1.21mm for lap and crotch belts. In motor sport there are no type of retractors, so once the seatbelts are tighten they do not loosen up like civilian vehicles seatbelts. In order to reproduce this behaviour, five retractors and five sliprings were implemented. In the analysis, the retractors are left able to tighten the seatbelts during the adjustment phase (until 50ms) then the sliprings block the seatbelt so that the retractor is not able to loosen the seatbelts up.

Because of the retractors, the 1D elements enter in the slipring and "disappear", thus it is important to add enough 1D elements to the ends near the sliprings. Given the dimensions of the elements and 50ms of adjustment, three elements per seatbelt were enough.

The position of retractors and sliprings, hence the geometry and inclination of the seatbelts was chosen referring to the experimental test geometry that is described in Table 3.1 and Figure 3.8. However, this data don't provide enough information (e.g. the length of the belts is unknown). A particular attention was given to the lap belts. In order to obtain numerical results that match the experimental data, several analysis have been done with the following parameters:

Shoulder angle	Lap angle	Crotch angle
$-15°$	$82°$	$-10°$

Table 3.1: Experimental seatbelts angles

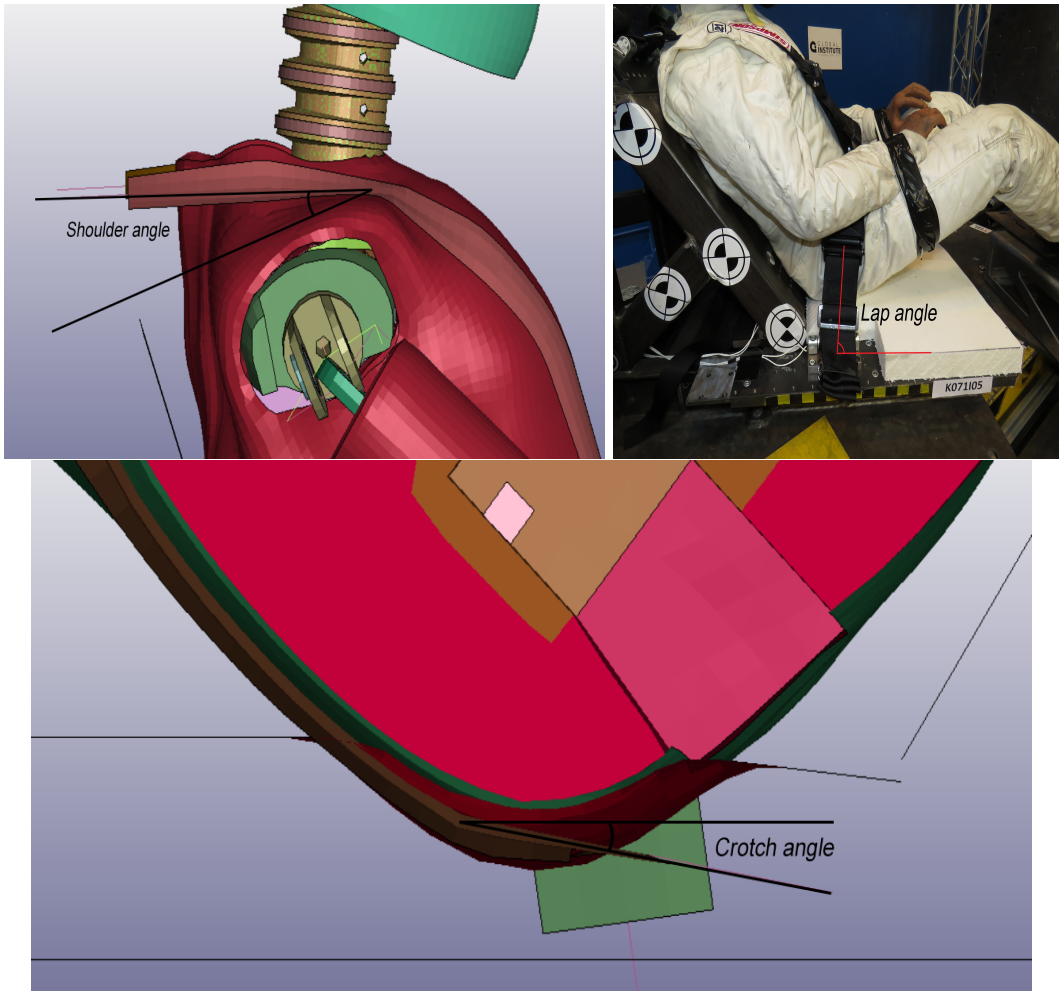

Figure 3.8: Seatbelt angles definition

- Lap belt angle equal to $82°$ as indicated before[1].
- Lap belt angle equal to $50°$[2].
- Lap belt angle equal to $82°$ as in the first configuration, but with belt length increased by $10mm$[3].

[1] this analysis is named FEA2.4 in this work
[2] this analysis is named FEA2.5 in this work
[3] this analysis is named FEA3.3 in this work

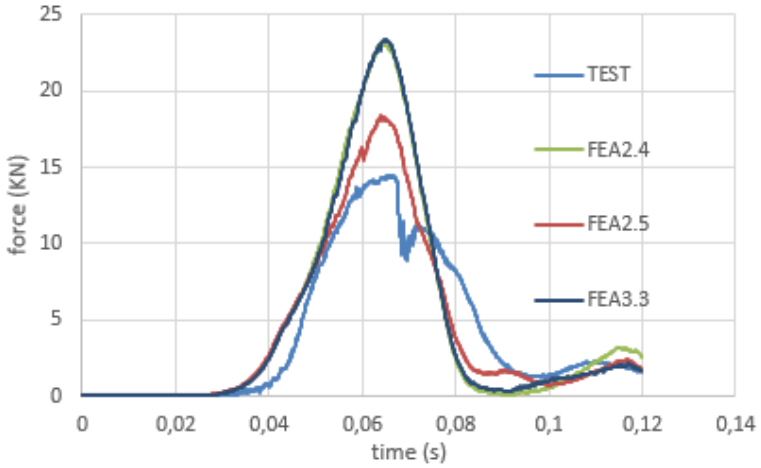

(a) Left shoulder belt force

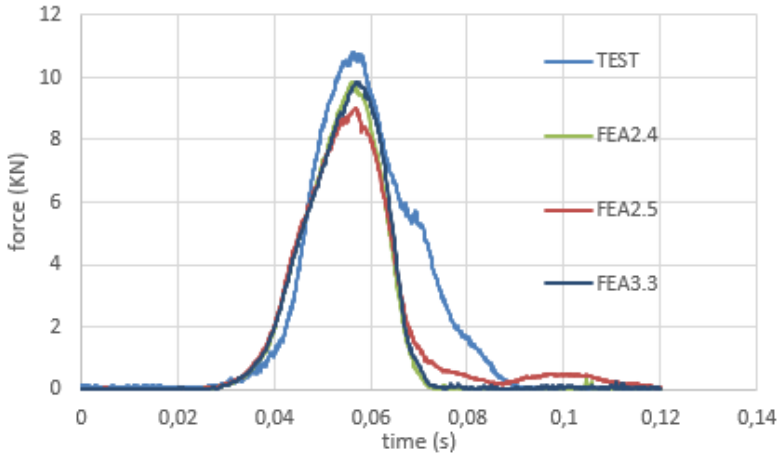

(b) Right shoulder belt force

Figure 3.9: Shoulder force graphs; Hybrid III validation

The second configuration has been considered in order to solve some problems with the data. In particular, the force overestimation in left shoulder and right lap seatbelts. The same goal has been pursued by using the experimental lap angle and increasing the length of the lap belts. Some explanatory results are shown in Figure 3.9 and 3.10, the complete series of graph for FEA2.4, 2.5 and 3.3 can be found in Appendix A.1. The main focus is on the seatbelts forces in this part of model validation due to the fact that variations of head and chest accelerations and upper neck forces and moments are less significant. By looking at the graphs it is possible to notice some important features. The left shoulder belt force is overestimated by all the analysis, with FEA2.5 that gives a better peak value estimation (error of 27.5%). Right shoulder belt force is underestimated by all the analysis but this time the error is lesser and the best peak estimation is given by

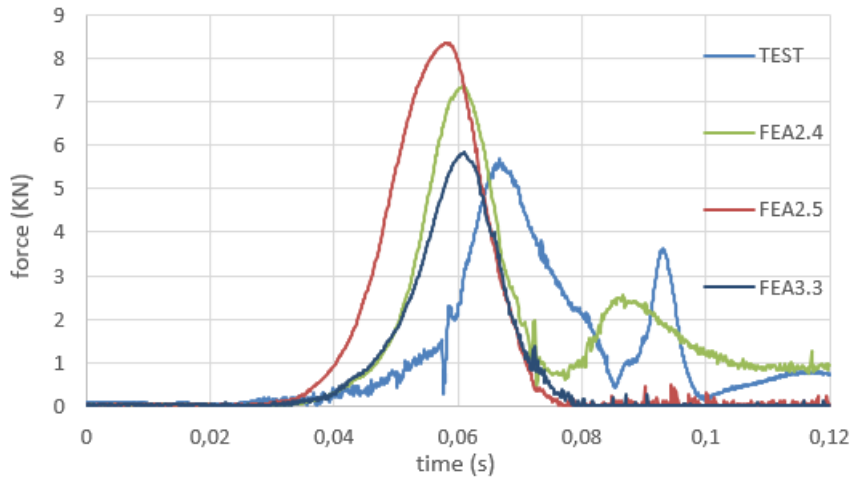

(a) Left lap belt force

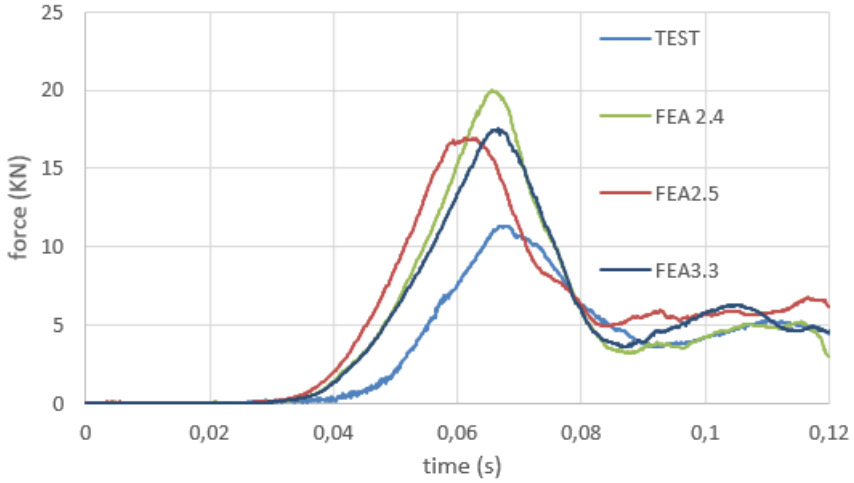

(b) Right lap belt force

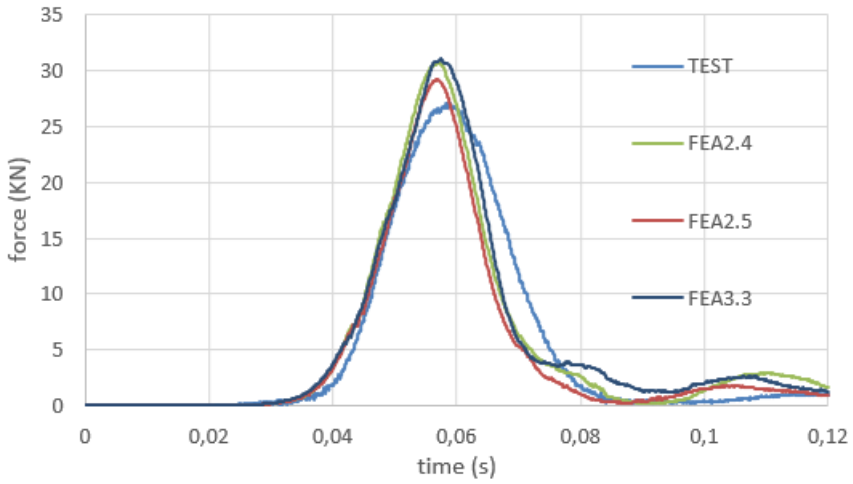

(c) Crotch belt force

Figure 3.10: Lap and crotch seatbelt force graphs; Hybrid III validation

FEA3.3 (error of 9%). As regard left lap belt force it is easily noticeable that the peak time of numerical simulations is $5.5ms$ earlier than the one of experimental test. Nevertheless the peak estimation of analysis 3.3 is very accurate (2.4% error). Right lap force comparison is again critical with FEA2.5 and 3.3 that present the lower errors (49% and 54% respectively), but the latter has a better peak time estimation (less than $0.5ms$ delay). Finally the crotch forces are quite similar with FEA2.5 peak that is the closest to the test one; all the numerical peaks arrive early (around $1ms$).
As already said, the simulations present some criticality, in particular the representation of left shoulder and right lap seatbelts forces. Nevertheless other results were quite accurate. The final choice was to use the FEA3.3 configuration because of two main reasons: firstly the results provided by the simulation were the best overall, even with the exception of the left shoulder forces, and secondly the geometry was compliant with the one indicated by Table 3.1.

3.2 Hybrid III neck modification

The first simulations performed on Hybrid III showed a good reproduction of head and chest accelerations and upper neck forces. Nevertheless the upper neck moments estimation was not accurate enough. Hence, some modification on the neck FE model were performed by using the MSc thesis "*Optimization of head and neck behaviour in Hybrid III FEM models and validation through sperimentation*" by S.Motta, former Politecnico of Milan student, as a reference[26]. The model by Motta was validated by several experimental and related numerical test such as: static tests, dynamic impact with rigid sphere, pendolum tests, impact against guardrail barrier. The change applied to Hybrid III FE model's LS-DYNA cards[16] are here listed:

- Headbase SECTION_SOLID card: ELFORM changed from 2 to 1. This means that the solid formulation is no more fully integrated, namely the elements become constant stress solid elements. Therefore, the response will become less stiff.
- Face PART 50100010 MAT_NULL[17]: the density was changed from $1Kg/m^3$ to $0.1Kg/m^3$.
- Neck assembly PART 50200012 MAT_NULL: the density was changed from $1Kg/m^3$ to $0.1Kg/m^3$.
- Neck assembly PART 50200012 MAT_NULL: the Young's Modulus was changed from $50000MPa$ to $400MPa$, hence decreasing the neck stiffness.

The implemented model has the same setup of FEA3.3 that was previously chosen among the other configurations and the Hybrid III dummy with the parameter

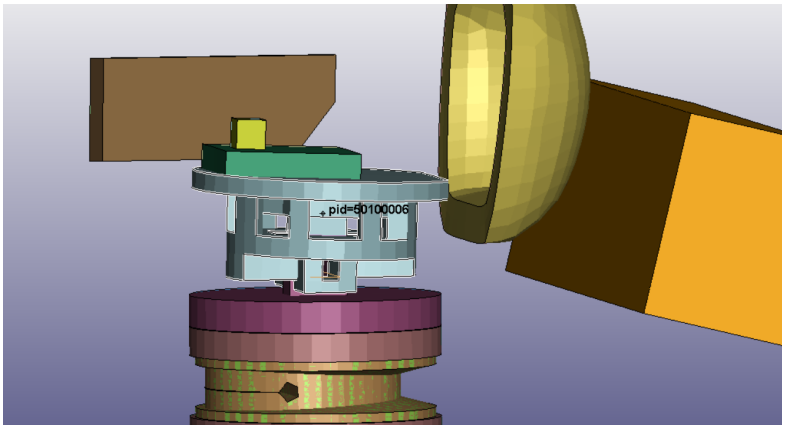

Figure 3.11: Hybrid III "Headbase" PART5010006

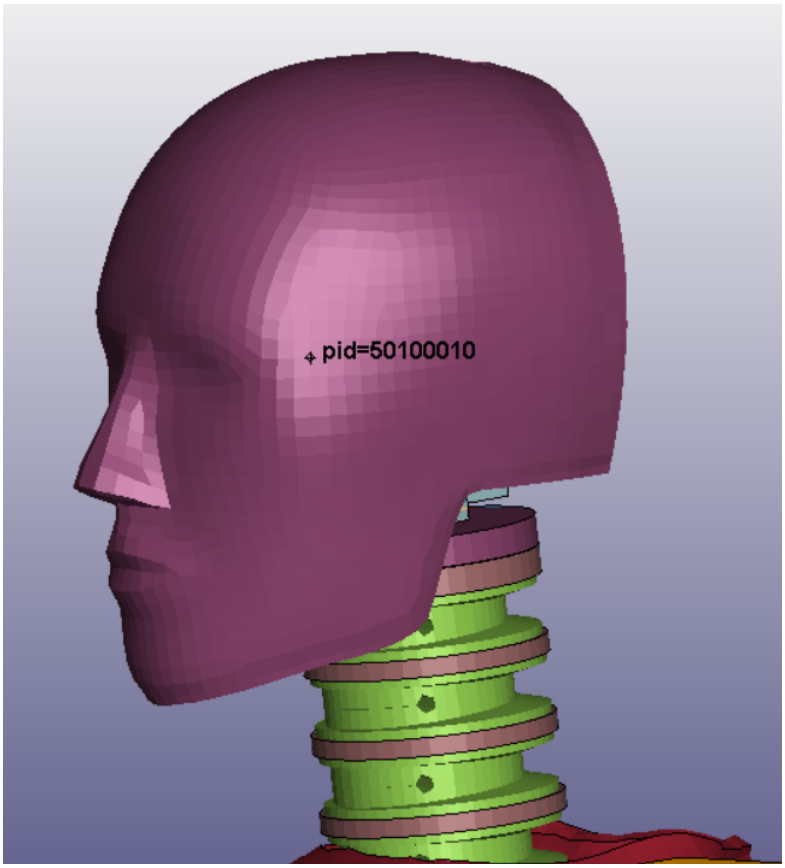

Figure 3.12: Hybrid III face PART5010010

discussed before. The analysis will be present in the graphs under the name of

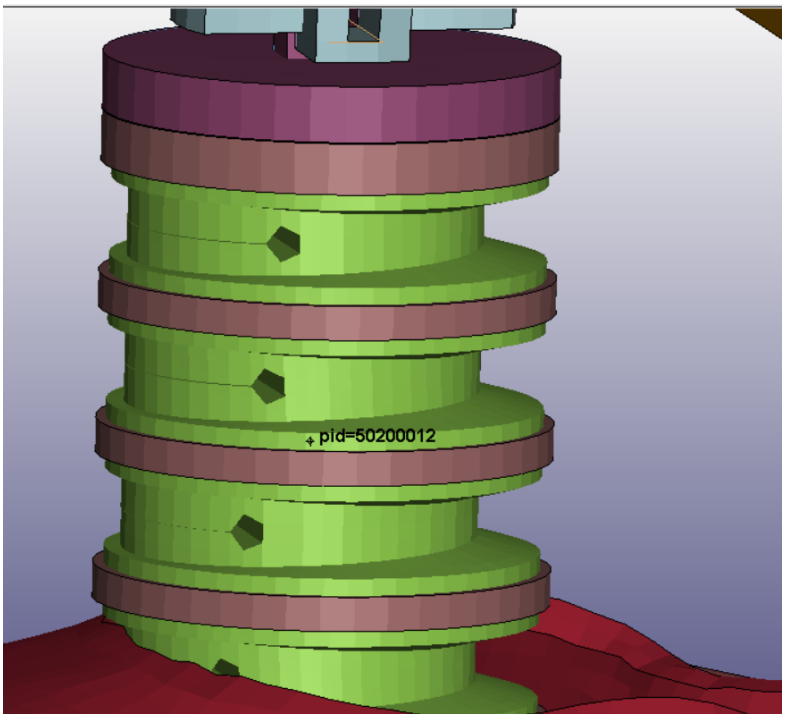

Figure 3.13: Hybrid III neck assembly PART5020012

FEA3.3LaST[4], the complete set of graphs can be found in Appendix A.1.
Firstly, the head acceleration graphs are useful to asses the congruence of head motion between real and numerical dummy. In Figure 3.14 it's shown the compared results of the experimental test and of the numerical tests. The measures are calculated through the use of the head accelerometer (see Figure 3.3 for local reference system) both in the numerical and in the experimental test. Both the numerical tests show a good estimation of the two acceleration peaks (around $140g$ and $120g$ respectively), however the curve trend in between the peaks is not accurate and the second peak is reached with $1ms$ of delay.
Let us consider now the force on the upper neck section of the Hybrid III (see "UNeck" section in Figure 3.2 as a reference). The experimental data in the section is collected by using a load cell. The numerical data is collected by defining a cross-section as described before, the local reference system for the load evaluation is described by the head accelerometer. The upper neck force reproduction is very important because it will be needed later on for the calculation of Nij. In particular the criterion make use of the axial component of the force F_z. The graphs in Figure 3.15 show similar trends, but the second force peak is delayed and underestimated in numerical analyses. The first peak reproduction is quite accurate. In both cases the LaST modified Hybrid III model provides better results for peak estimation

[4]Laboratorio Sicurezza Trasporti: the modification on the Hybrid III model have been studied at LaST

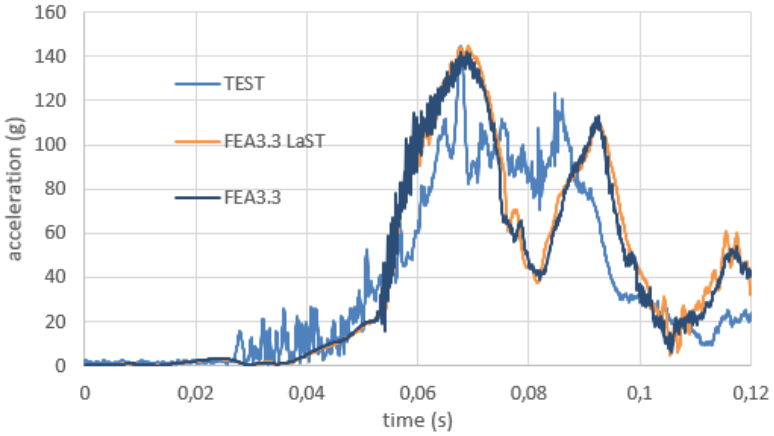

Figure 3.14: Head acceleration graphs; Hybrid III validation

with similar trend, even if the highest value is reached in the first peak and not in the second as it happens in the experimental test.

Finally, the upper neck moment reproduction can be assessed by comparing the data collected by the real dummy load cell and the data provided by the aforementioned cross-section in the FE model. Likewise the upper neck force, the momentum is used in the Nij calculation, in particular the M_y moment (bending in sagittal plane), hence the estimation must be as accurate as possible. This is the reason why, in the first place, it has been decided to modify the Hybrid III model. It should be noted that the considered local reference frame convention produce extension moment when M_y is negative and flexion moment when M_y is positive. It is possible to notice by looking at Figure 3.16a that the moment reproduction was not very accurate in FEA3.3 both in peak time and value, even if the trend was similar to the real one. The LaST modifications guarantee a $20000N$ increase of the total bending moment magnitude and a better estimation of the extension moment, too.

By looking at Figure 3.16b it is possible to notice an interesting behaviour of the neck during frontal impact, the aforementioned whiplash effect that is better shown by the simulation frames in Figure 3.21. The upper neck section is firstly subjected to extension moment because the head tends to remain behind because of inertia. The forces transmitted by the vehicle accelerate the head forward with a delay that causes the typical motion of a whiplash. This motion is the first cause of injury in the frontal impact scenario and so it is important to design safety system able to prevent it. It is interesting to note that the experimental results shown in Figure 3.16b don't show flexion moment until the later instants of the test when the head is almost touching the chest.

The results show that the LaST modifications improve the model, indeed, so the Hybrid III modified model has been used for all the subsequent analysis. For

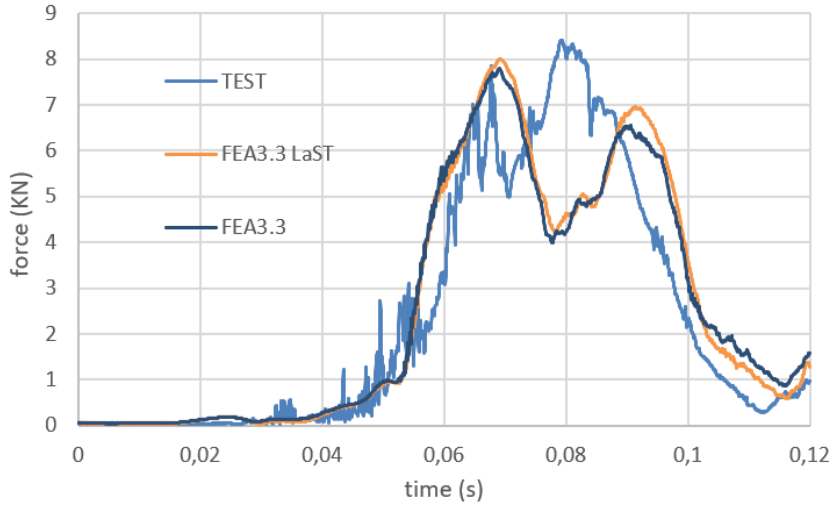

(a) Total force magnitude

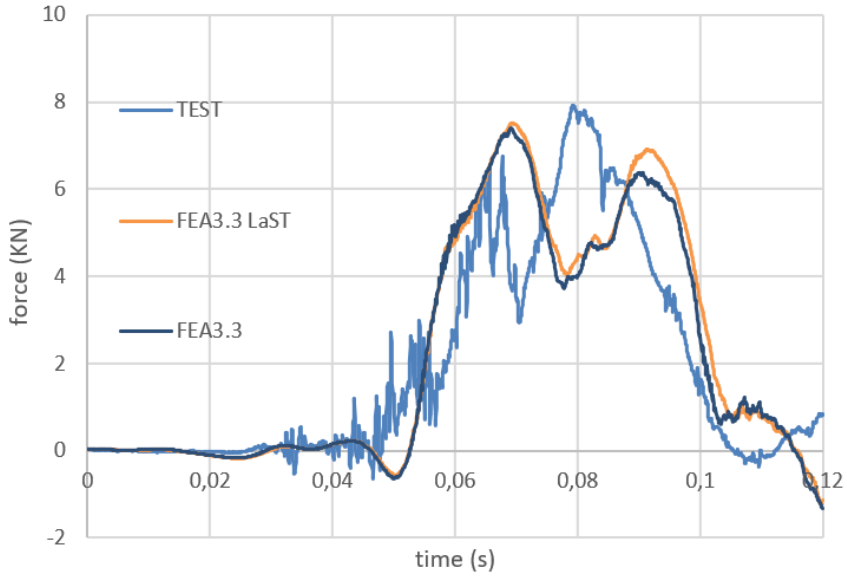

(b) Z force magnitude

Figure 3.15: Upper neck force graphs; Hybrid III validation

completeness, in Table 3.2 are shown in detail the results in term of peak value and peak time of FEA3.3 and FEA3.3LaST, together with their error with respect to the experimental test data. The error for the peak value are calculated in percentage with respect to the experimental peak value, while the peak time error is represented by the time difference.

$$err\% = \frac{||val_{num}| - |val_{\text{exp}}||}{|val_{\text{exp}}|} \tag{3.1}$$

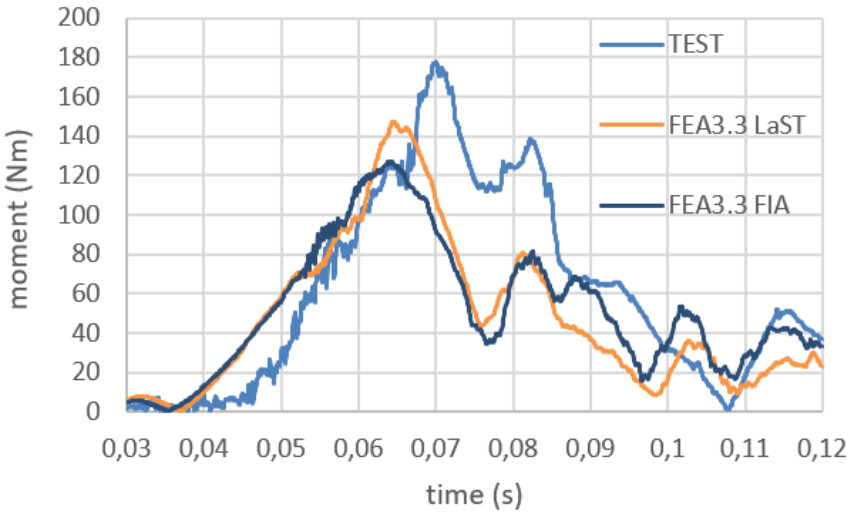

(a) Total bending moment magnitude

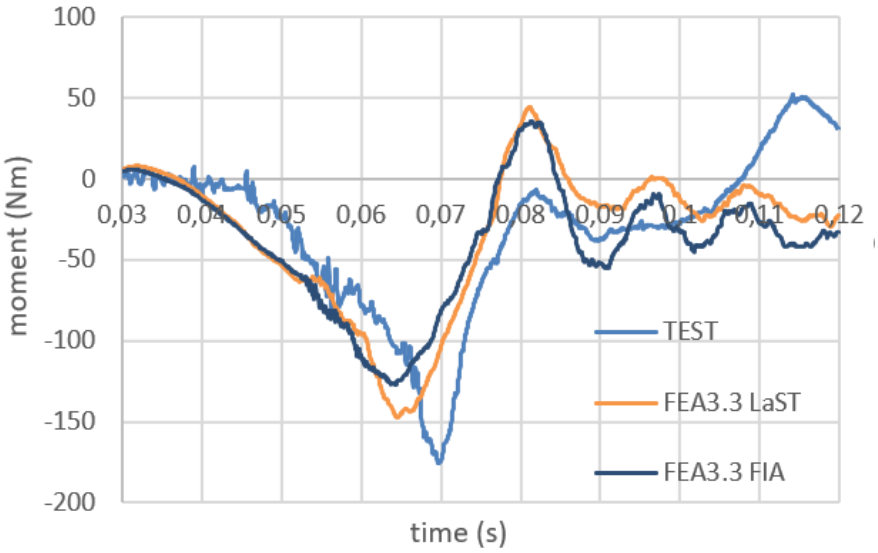

(b) Y bending moment magnitude

Figure 3.16: Upper neck moment graphs (sagittal plane); Hybrid III validation

Where val_{num} is the value given by the numerical simulation data and val_{exp} is the value given by the experimental data.

Graph		Peak value	error%	Peak time(s)	error(s)
Head acceleration (g)	ET[5] Total	138, 95		0.0682	
	NM[6] Total	141.99	2.18%	0.0687	0.0005
	NML[7] Total	144.79	4.20%	0.0692	0.001
	ET x	−87.99		0.0858	
	NM x	−104.81	19.11%	0.092	0.0063
	NML x	−104.23	18.46%	0.0923	0.0066
	ET y	55.86		0.0844	
	NM y	44.27	20.75%	0.0925	0.0082
	NML y	33.61	18.46%	0.0931	0.0088
	ET z	107.90		0.0682	
	NM z	130.93	21.35%	0.0687	0.0005
	NML z	132.61	22.90%	0.0692	0.001
Chest acceleration (g)	ET Total	211.22		0.0836	
	NM Total	111.52	47.20%	0.0621	−0.0214
	NML Total	113.25	46.38%	0.0629	−0.0206
	ET x+	78.69		0.0848	
	NM x+	78.65	0.05%	0.086	0.0012
	NML x+	71.22	9.50%	0.0862	0.0014
	ET x−	−186.99		0.0661	
	NM x−	−88.66	52.59%	0.0621	−0.0040
	NML x−	−92.33	50.62%	0.069	−0.0007
	ET y	198.65		0.0836	
	NM y	78.70	60.38%	0.0668	−0.017
	NML y	76.21	61.64%	0.0684	−0.015
	ET z	−137.68		0.0664	
	NM z	−51.00	34.77%	0.0600	−0.0064
	NML z	−51.21	34.50%	0.0619	−0.0045
	ET Total	8.411		0.0792	
	NM Total	7.803	7.22%	0.0691	−0.01
	NML Total	8.006	4.82%	0.0691	−0.01
	ET x	−4.083		0.0699	

[5]Experimental Test
[6]Numerical Model
[7]Numerical Model with LaST parameters

Graph		Peak value	error%	Peak time(s)	error(s)
UpperNeck force (KN)	NM x	−2.661	34.83%	0.065	−0.0048
	NML x	−2.973	27.18%	0.0667	−0.0031
	ET y	1.604		0.0664	
	NM y	0.984	38.65%	0.1041	0.0378
	NML y	0.797	50.32%	0.1048	0.0385
	ET z	7.929		0.0792	
	NM z	7.408	6.57%	0.0691	−0.01
	NML z	7.512	5.26%	0.0692	−0.0099
UNeck moment (Nm)	ET Total	177.75		0.07	
	NM Total	127.86	28.63%	0.0642	−0.0058
	NML Total	147.22	17.18%	0.0646	−0.054
	ET x+	138.15		0.0822	
	NM x+	73.86	46.54%	0.0825	0.0003
	NML x+	68.78	50.21%	0.0823	0.0001
	ET x−	−73.94		0.0635	
	NM x−	−42.96	−41.90%	0.0553	−0.0081
	NML x−	−37.28	−49.58%	0.0552	−0.0082
	ET y+	51.87		0.1142	
	NM y+	35.47	31.62%	0.1113	−0.0028
	NML y+	44.02	15.13%	0.1112	−0.0029
	ET y−	−175.74		0.0697	
	NM y−	−126.82	27.84%	0.0642	−0.0054
	NML y−	−147.19	16.25%	0.0646	−0.0050
	ET z	36.14		0.0731	
	NM z	6.29	82.60%	0.0558	−0.0172
	NML z	2.68	92.57%	0.0599	−0.0133
	ET LS[8]	14.44		0.0655	
	NM LS	23.38	61.95%	0.0648	−0.0007
	NML LS	23.48	62.62%	0.0649	−0.005
	ET RS[9]	10.81		0.0565	
	NM RS	9.84	8.97%	0.0571	0.0006

[8]Left Shoulder
[9]Right Shoulder

Graph		Peak value	error%	Peak time(s)	error(s)
Seatbelt force (KN)	NML RS	9.67	10.53%	0.0578	0.0013
	ET LL[10]	5.68		0.0667	
	NM LL	5.83	2.63%	0.0609	−0.0058
	NML LL	5.83	2.59%	0.0606	−0.0061
	ET RL[11]	11.34		0.0669	
	NM RL	17.54	54.72%	0.0668	−0.0004
	NML RL	17.10	50.85%	0.0663	−0.0006
	ET C[12]	27.125		0.0584	
	NM C	31.04	14.44%	0.0574	−0.0010
	NML C	31.34	15.53%	0.0572	−0.0012

Table 3.2: Peak values and times for Hybrid III validation analysis

It has to be noted that the chest acceleration graphs of the experimental test are very noisy, as it is possible to see in Appendix A.1. Hence, the errors for peak value and time are very high. It is also true that the overall trend of the data is very close, so the numerical results were considered satisfactory.
The values contained in Table 3.2 shows that the configuration of FEA3.3LaST is the best between the analysed ones; the finite element analysis represents well enough the experimental test. Hence, the model was chosen for the Nij calculation described in the next subchapter and for all the other activities of next chapters.

3.3 Hybrid III numerical model Nij calculation

Once the numerical model has been validated is possible to calculate the Nij that will be needed later on in the study. The Nij criterion is described in Chapter 1.3.1 and its calculation has been done by considering the data of upper neck section (UNeck) that has been described in Chapter 3.1. We already assessed that in the numerical simulation the section force and moment data were close enough to experimental ones (especially F_z andM_y). Nevertheless, the Nij value will be confronted. Remembering that:

$$N_{ij} = \frac{F_z}{F_{1im}} + \frac{M_y}{M_{\text{lim}}} \tag{3.2}$$

the Nij has been calculated in each instant and has been plotted into a graph.

[10]Left Lap
[11]Right Lap
[12]Crotch

During the definition of Nij, we specified that the forces and moments have to be calculated on the occipital condyle section. In the experimental test the load cell was not installed on the section equivalent to the occipital condyle, but was installed above for technical reasons. This positioning of the load cell force us to apply a correction to the aforementioned formula. M_y hence is substituted M_y^{OC}, where OC stands for occipital condyle:

$$M_y^{0C} = M_y + F_x \cdot d \tag{3.3}$$

where F_x is the shear force and d is the distance between the UNeck section and the occipital condyle, namely $18mm$. It is important to remember that in the Nij calculation the moment is positive when the section is subjected to extension and negative when is subjected to tension (which is the contrary of the convention used in the moment graphs shown in the thesis). Hence, the moment contribution given by the shear force has to be considered consequently. Figure 3.17 shows the distance between occipital condyle and Uneck section.
Hybrid III numerical model features a joint on the occipital condyle that permits to calculate the moment directly on the OC, hence avoiding the use of Equation 3.3 (in ASCII jntforc it is possible to select "21-theta-moment-total" relative to JStifR of joint 50100001[16][25]).
Nij criterion was developed for frontal impact, so it should not be applied to oblique impact like the one of experimental test. Nevertheless, the calculation here presented is made with the purpose of confronting numerical and experimental data, namely to further validate the numerical model. The Nij criterion will be used later for the study of THUMS' neck and so it is important that the results given by the Hybrid III FE model are as accurate as possible. In Figure 3.19 is shown a comparison between M_y^{OC} of experimental and numerical data, namely with the shear force correction done already. It is possible to notice that trend peak time and peak value are all quite accurate.
As regard Nij, Figure 3.20 shows the Nij values for each time instant. Again, trend peak time and peak value are quite similar. The peak value, namely the maximum Nij during measurement and simulation is around 1.6 in both the curves. The Neck injury risk curves (Figure 1.1) indicate a probability of moderate, serious and/or severe injury superior to 30% and a critical injury probability of around 10% for this Nij value. Therefore is is quite clear that for crash pulse the analysed one (that is typical of motor sport crash) is necessary to provide the occupant with additional safety device like *HANS*[13] devices[21].

[13]Head and Neck Support device; it is a type of head restraint

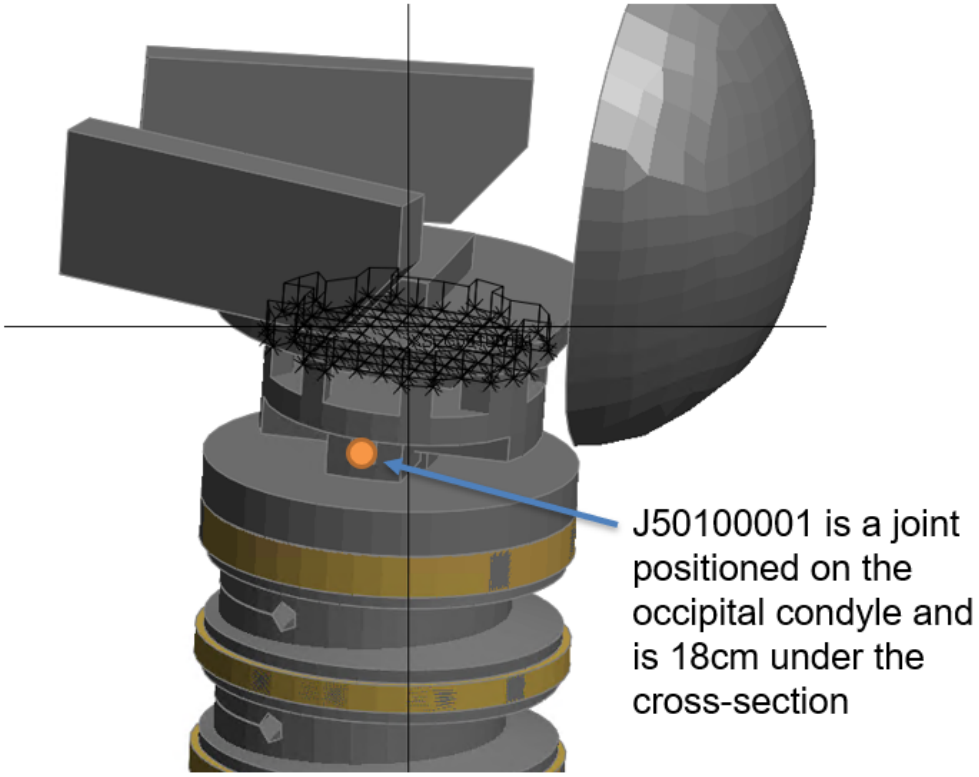

Figure 3.17: Position of the occipital condyle in the Hybrid III FE model

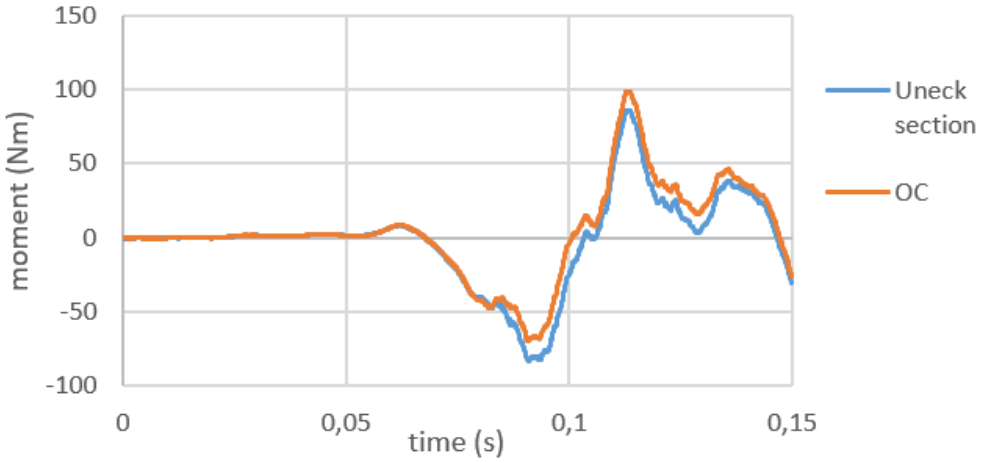

Figure 3.18: M_y moment calculated on the upper neck section and in the occipital condyle joint for a frontal impact

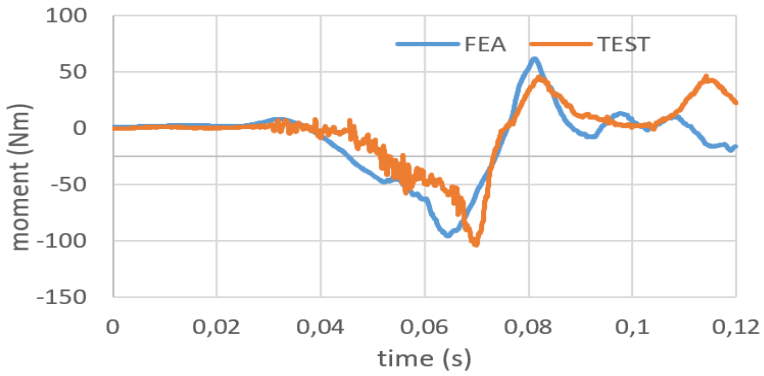

Figure 3.19: M_y around the occipital condyle in FEA and experimental test

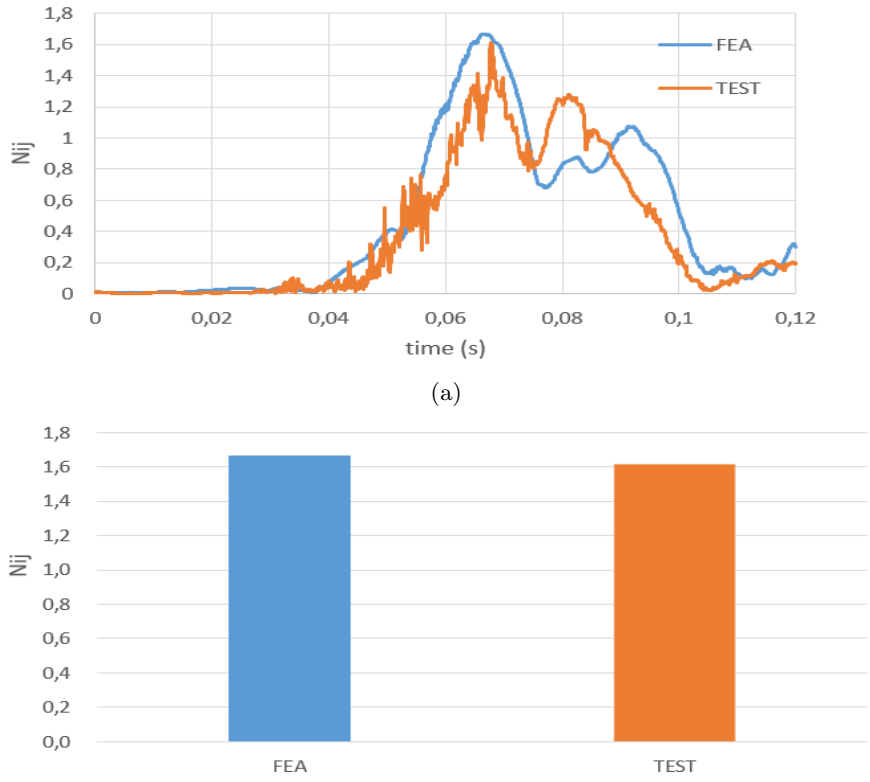

(a)

(b)

Figure 3.20: Nij time-value graph for experimental test and numerical simulation (a) and Nij bar chart (b)

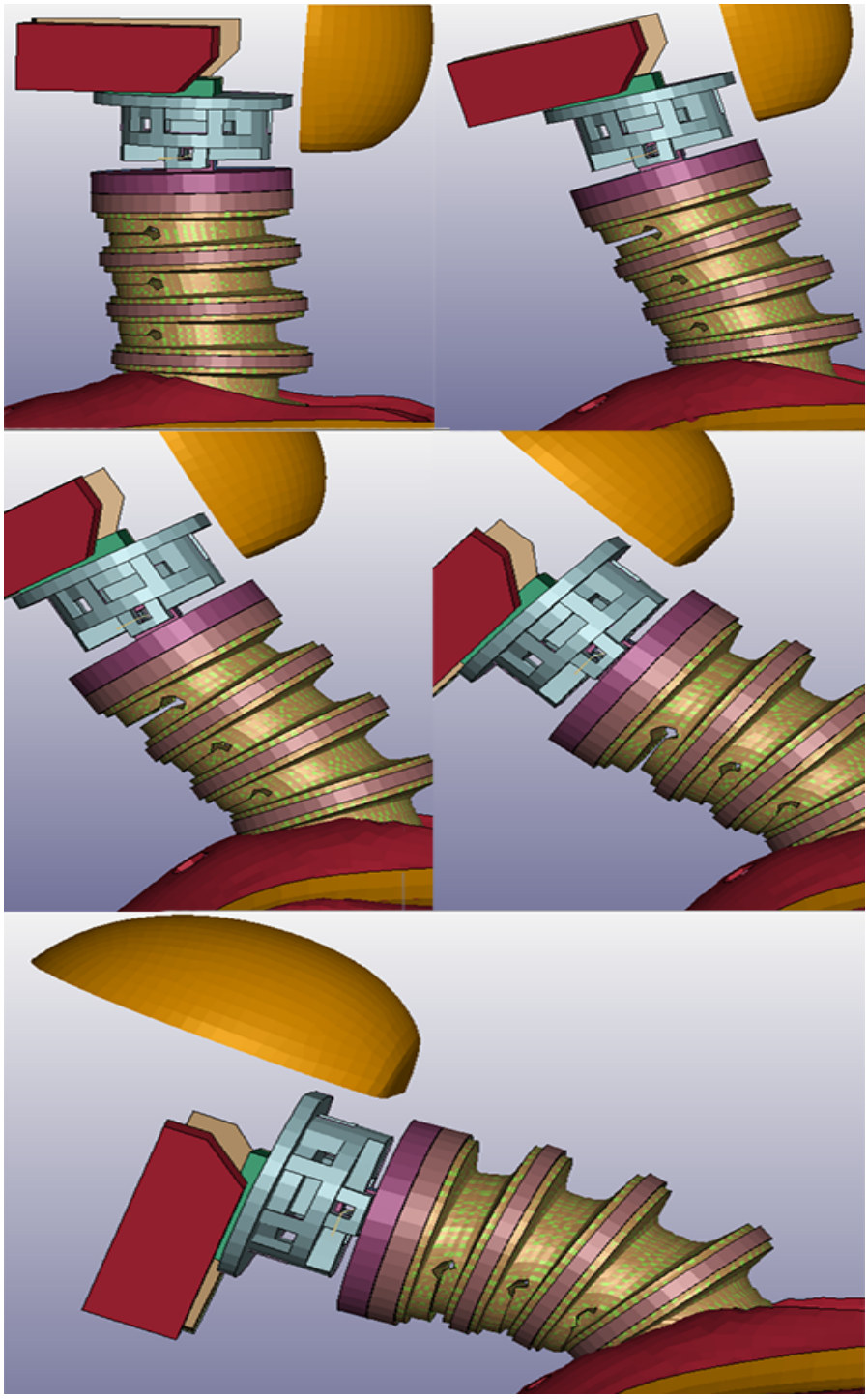

Figure 3.21: Whiplash effect visualization in a frontal impact numerical simulation

Chapter 4

THUMS' numerical simulations

This chapter describes the method used to perform the THUMS' setup and the analysis run to compare THUMS with Hybrid III FE model. In particular, in the first part the process of positioning, the sled seat modification, the instrumentation implementation and the prescribed motions are explained. Then, the obtained data are discussed and the two FE models are compared.

4.1 THUMS' sled test configuration

Now that the Hybrid III model has been validated, it is possible to use the sled seat setup for running FEA on THUMS, and then confront the obtained results. Of course, as described in Chapter 2 the two FE models are very different from one another, so some modification to seatbelts and headrest are necessary to fit the THUMS into the sled seat while maintaining the same geometry (e.g. seatbelts angles, head inclination etc.). These modification will be discussed later on.

4.1.1 THUMS' positioning

The positioning of THUMS is different from the Hybrid III one, because there is no tool in PRIMER or LS-DYNA environments that can perform body part movement. That is why, it is necessary to run simulation and then import the moved nodes into an updated model. We used two analysis precisely. Both the analysis where performed without the helmet, the seatbelts and the headrest (they have been added and fitted once the positioning was completed). The first analysis consisted in letting THUMS to lean on the seat by applying the gravity acceleration and by prescribing a rigid motion on the rigid part 80000000, that is located inside the head. With this method, legs, bottom and back were positioned. The second analysis consisted in a prescribed motion of the same rigid part. The aim was to reach the correct head inclination.

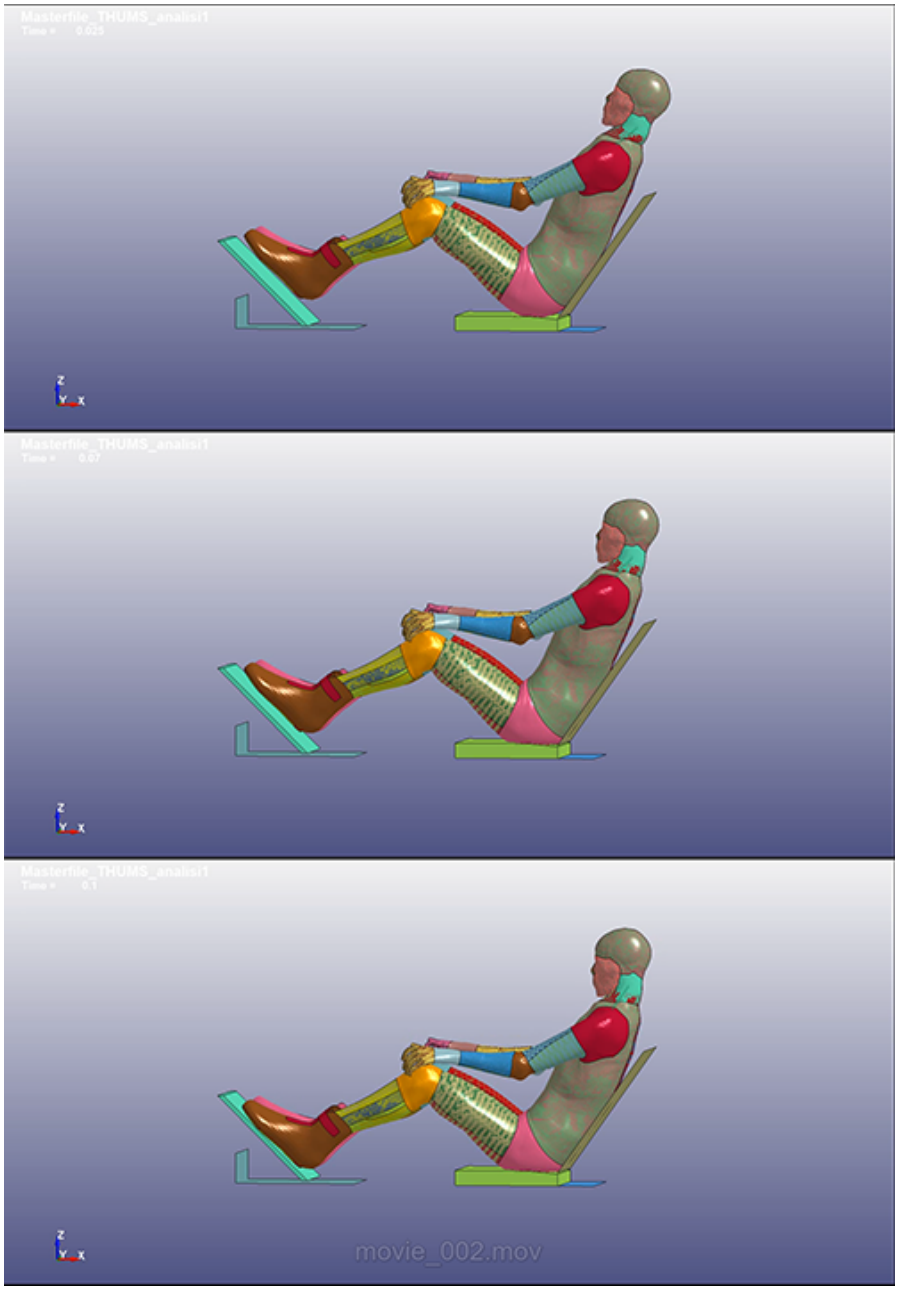

Figure 4.1: THUMS positioning first analysis

Once the THUMS is correctly positioned, the seatbelts, the helmet and the headrest were re-inserted. The seatbelts ends were moved to match the geometry of Table 3.1 so that the two models were consistent. The headrest were moved behind because the THUMS is obviously different from Hybrid III FE model. The neck is shorter and the chest is higher and so, given the same head inclination, the

headrest has to be placed behind his previous position.

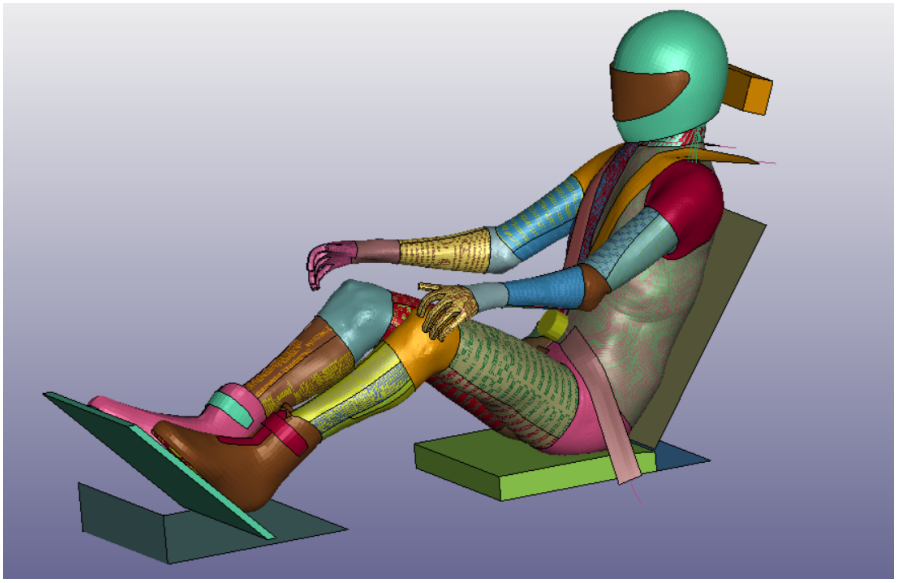

Figure 4.2: THUMS final configuration

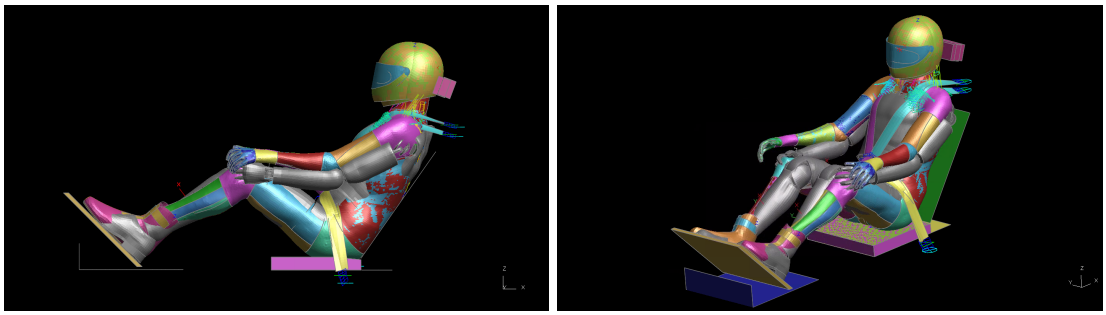

Figure 4.3: Hybrid III and THUMS model comparison

4.1.2 Accelerometer and cross-section definition

Because THUMS is a HBM, it is not provided of any type of instrumentation. So accelerometers and cross-sections have to be implemented. In this work, we implemented a head accelerometer, several plane cross-sections in the neck and in the cervical vertebrae and a chest accelerometer. The accelerometers' outputs are, as in Hybrid III FE model, affected by high levels of noise, so the solver is requested to do a preliminary filtering by the use of the control card CONTROL_OUTPUT with IACCOP set to 1[16].
The head accelerometer was defined by using the nodes of the rigid part 80000000 that is shown is Figure 4.4 and the reference frame was chosen so that the axis

were consistent with the head accelerometer of Hybrid III FE model. Analogously, the chest accelerometer where defined using the rigid part 8000000.
In order to compare the upper neck section loads, two neck plane cross-sections were defined in the THUMS together with other plane cross-sections in each cervical vertebra. The upper neck sections resulted useful for the understanding of

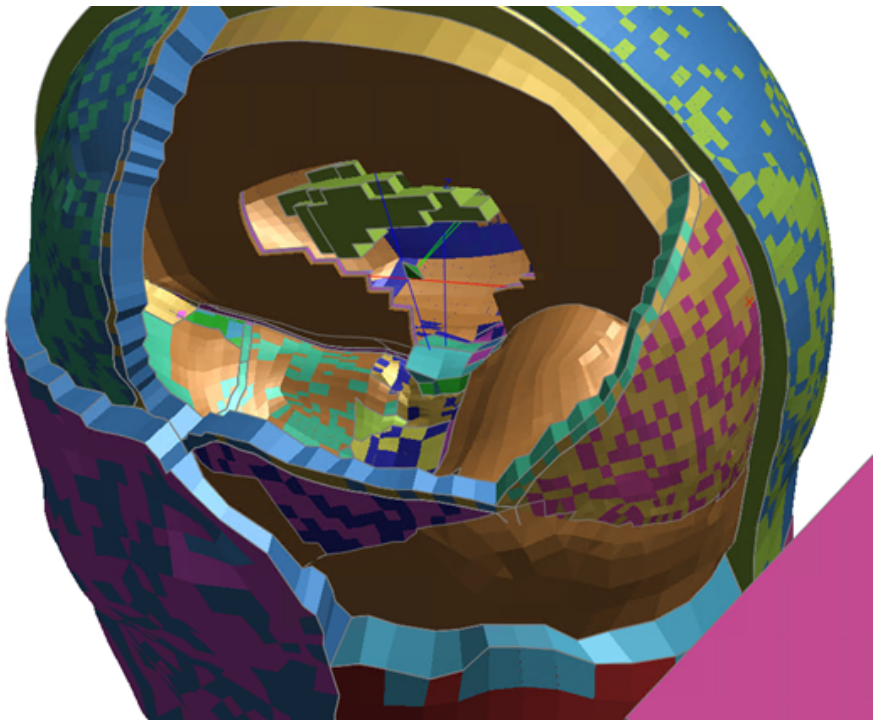

Figure 4.4: THUMS part 80000000 (green tetrahedron), used for head accelerometer definition and positioning

load transfer in THUMS neck. However, the loads on the upper neck cross-sections were not comparable with the Hybrid III upper neck loads due to the differences between the neck models. THUMS' neck section is made of bones, ligaments and other tissue, hence its formulation is way different from the Hybrid III neck that is made of steel and rubber.
On the other hand, the vertebrae cross-sections could be useful for definition of limit loads on the vertebrae themselves. The cross-sections definition has been made in order to be consistent throughout the cervical portion. The cross-sections of each vertebra were defined using a plane that cuts the vertebra in the middle. The geometry of the sections is analysed later and has been chosen following some criteria that should guarantee consistency throughout the cervical spine (an example of cross-section is shown in Figure 4.5).
Originally, the THUMS model provided by FIA featured one triangle shell for each vertebra. The triangles were used for defining the coordinate systems for each ver-

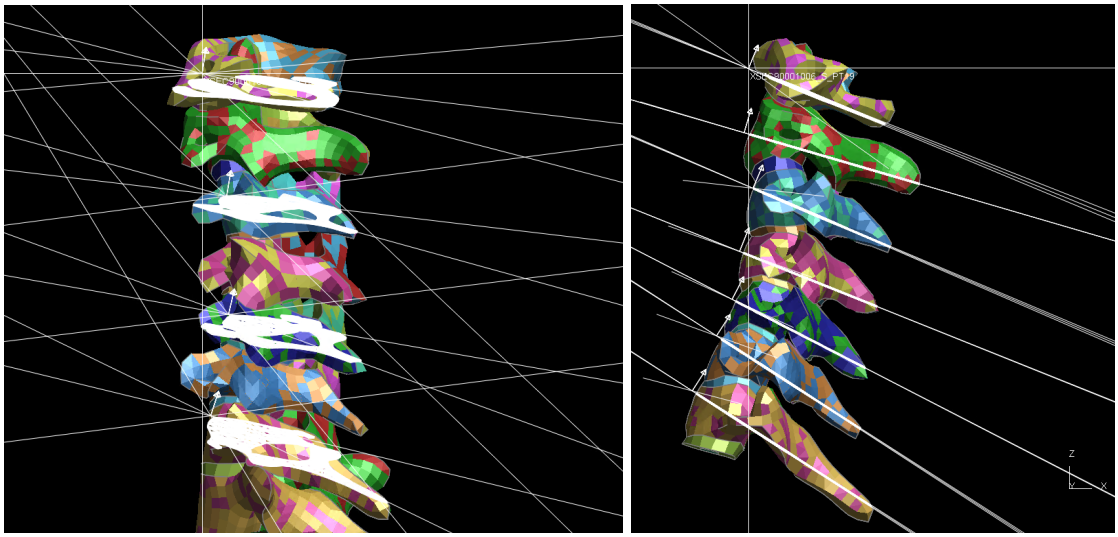

Figure 4.5: Vertebrae cross-sections planes

tebra in order to be used as reference frames in cross-section definitions. These shells were constrained to the bones with a CONSTRAINED_EXTRA_NODES card[16]. In order to avoid an excessive stiffening of the vertebrae due to the constraints, the triangles have been removed and have been substituted by coordinate systems defined directly on the vertebral nodes. The choice has been made so that the reference frames were coherent with the section plane. It is possible to do this operation because the vertebral deformations in the nodes zone are usually very low (less than 2%) and so their effect on the reference frame definition is negligible.

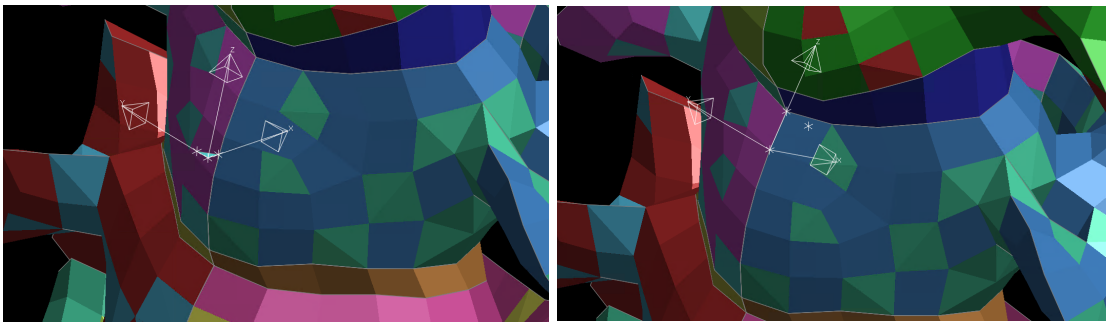

(a) (b)

Figure 4.6: C3 coordinate system defined with a shell triangle (a) and with vertebral nodes (b)

4.1.3 Crash pulse

In the previous chapter we validated the Hybrid III model, so that it could be used for following simulations. Now, it is not the aim of this work to perform THUMS analysis in order to confront the results with the Hybrid III experimental test. The aim of the first part of this work is to confront Hybrid III FE model and THUMS results. So it is acceptable to change the crash pulse for next simulations. The Nij criterion that is subject to study is valid for frontal impact, so a mono-axial acceleration has been considered. Therefore, the chosen crash pulse was the x direction pulse used in the Hybrid III validation (see Figure 3.5). This time, the adjustment period is set to $50ms$ likewise the Hybrid III validation. It has to be noted that THUMS is affected by numerical errors that compromise reliability when the simulation last more that $100ms$ so the analysis could be affected by these errors in the final part of the simulation.

4.2 THUMS and Hybrid III data comparison

Both THUMS and Hybrid III models were used for running FEAs with the aforementioned boundary conditions and prescribed motions. The obtained data are here displayed and analysed.

4.2.1 Head acceleration comparison

The comparison of head acceleration is important to understand if the head of the two models moves in the same way during the simulation. The head motion is, of course, linked to the neck movement (and to the vertebral spine movement in the THUMS case), too. By looking at Figure 4.7 it is possible to observe the total magnitude of head acceleration of the two model. The data of THUMS suffer of noise, so they have been filtered by using a SAE filter with cutoff frequency equal to $180Hz$. The filter is discussed in Appendix **??**. The THUMS' peak value is lower than the Hybrid III's one, it is underestimated of around $25g$ (in the non filtered graph). Meanwhile, the peak times and the trends are close, the THUMS' peak have a $2ms$ delay. Let us consider, now, the three components of head acceleration. Again, the THUMS data are affected by noise. Nevertheless, likewise the case of total acceleration, it is possible to do some observation. Component z of the head acceleration presents a difference of magnitude peak values similar to the total acceleration, the same happens for peak times between the two models. Component y of THUMS is highly affected by the noise, but the filtered signal shows a curve similar to the Hybrid III's, where the y component of acceleration is almost null. THUMS and Hybrid III's x acceleration components are not similar. The peak value in THUMS is around $30g$ lower than in Hybrid III (the exact value depend on if the filtered or not filtered value is considered), with a high percent

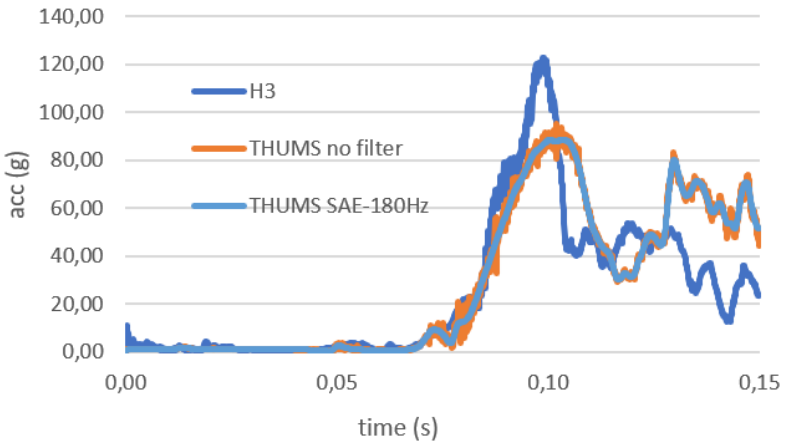

Figure 4.7: Total head acceleration magnitude comparison

error. Trends are also different. Overall, the data shows that the head behaviour is comparable in the two model to some extent.

4.2.2 Seatbelts' forces comparison

The seatbelts forces are useful to understand the behaviour of the models' bodies and are indicators of the forces that are effecting the models. Hybrid III and THUMS are different, indeed, so the belts' forces are not expected to be equal. Figure 4.9 reports seatbelts forces graphs. The shoulder belt has graphs that are similar with a peak difference of around $2500N$. The peak time is delayed in the THUMS of around $5ms$. THUMS lap belts are subjected to a bigger force ($3000N$ of difference), the peak time is delayed again (around $10ms$). On the other hand, crotch belt force are higher in Hybrid III. It is interesting to notice that crotch belt force presents a huge peak difference (almost $17000N$). For both lap and shoulder, left and right belts withstand the same force, as it is expected from a frontal impact simulation. In each seatbelt, the peak value is reached later in THUMS. These considerations highlight the viscous behaviour taht is typical of HBM.

4.2.3 Chest acceleration comparison

The chest acceleration data of THUMS were very affected by noise, so they have been filtered using two different cutoff frequency. Otherwise, a comparison between models would have been almost impossible to perform. It is expected to obtain data that tend to zero in the y direction because the models are seated and constrained by the seatbelt. Nevertheless, the backlash of the seatbelts should

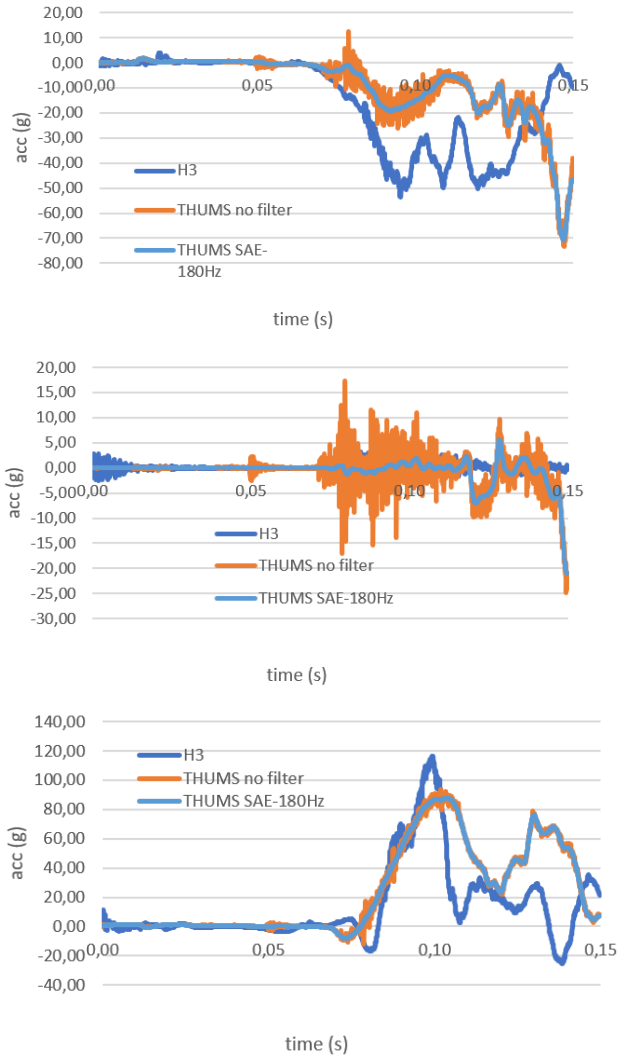

Figure 4.8: Comparison between magnitudes of head acceleration in x, y and z directions

allow accelerations in x and z direction. Figure 4.10 and 4.11 shows the graph of the acceleration components' magnitudes.

By looking at the filtered data it is possible to observe that the results are in agreement with what have been discussed before. The x component's graphs in particular have similar trends, peak values and peak times. THUMS y component data show a tendency to the expected trend only when filtered with a low cutoff frequency, in Figure 4.11b it is $20Hz$

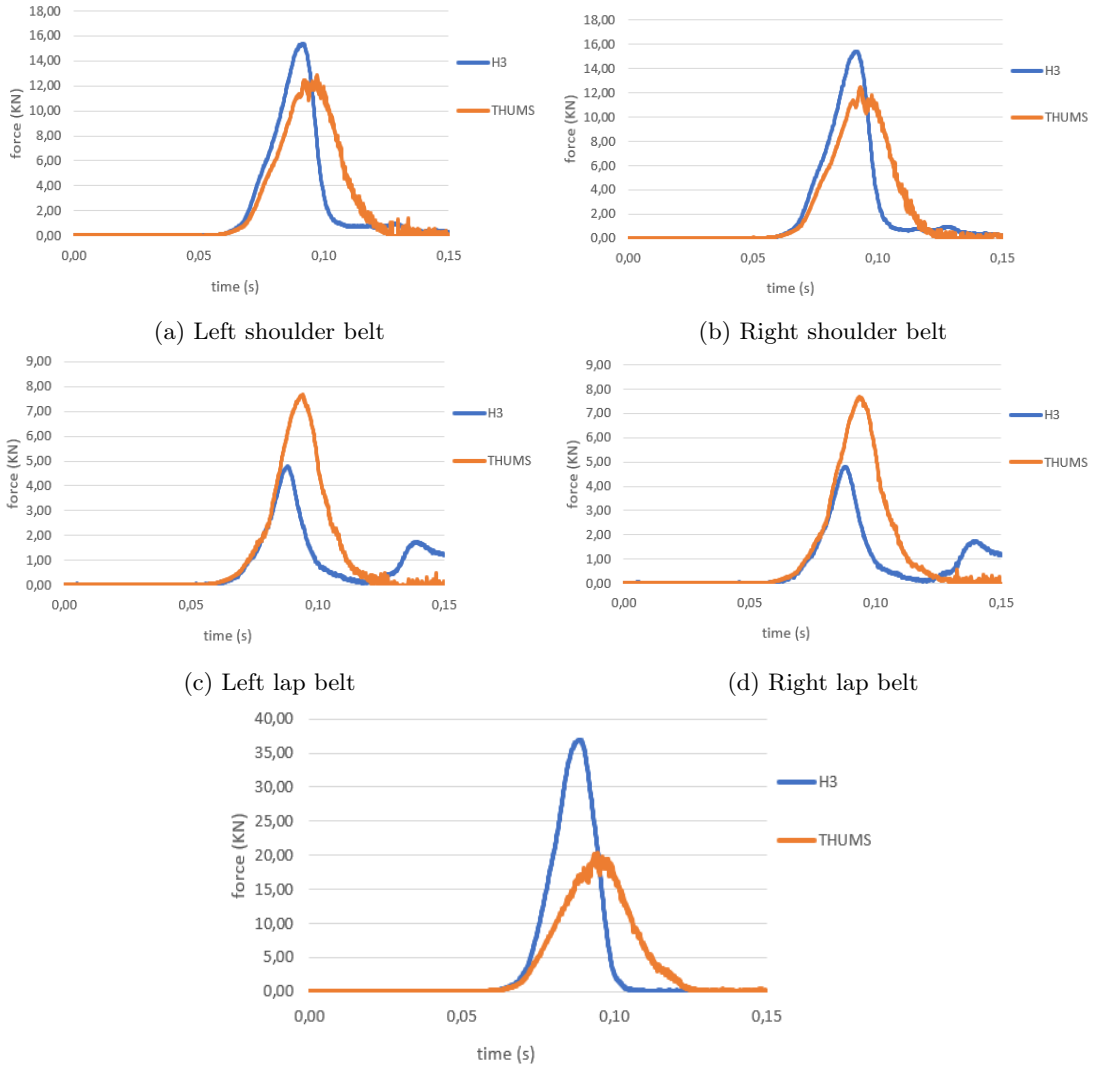

(a) Left shoulder belt

(b) Right shoulder belt

(c) Left lap belt

(d) Right lap belt

(e) Crotch belt

Figure 4.9: Comparison between magnitudes of seatbelt forces

4.2.4 Neck section loads comparison

As said before, the necks of the two models are very different from one another. The upper neck cross-section of Hybrid III can not be easily emulated in THUMS, the composition of the necks themselves is different, in particular the used materials and geometries. Hybrid III neck is made of plastic and steel meanwhile the THUMS neck simulates skin, bone and ligaments. Therefore it is almost impossible to directly compare forces and moments. However, it is still interesting to observe the behaviour of the two necks in order to find some similarity.

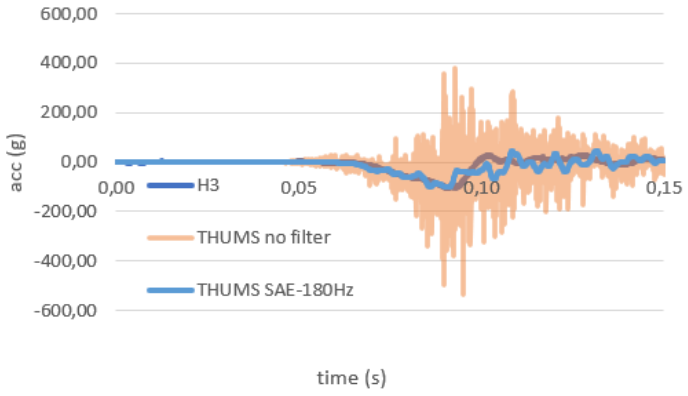

Figure 4.10: Comparison between magnitudes of chest acceleration in x, directions

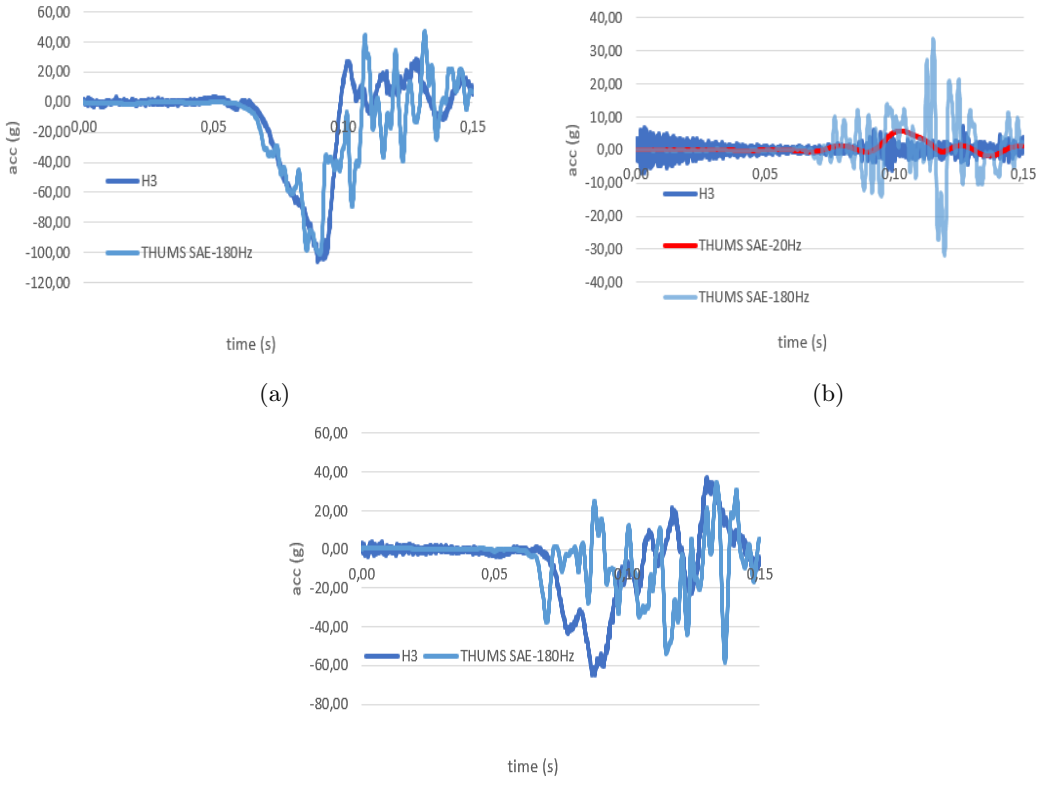

Figure 4.11: Comparison between magnitudes of chest acceleration in a) x, b) y and c) z directions

Other set cross-sections were defined on the Hybrid III FE model's neck at various height in order to observe the force and momentum trends. The sections are

showed in Figure 4.12 and are numbered from one to four starting from the closest to the head. With the sections, four coordinate systems were defined in order to correctly evaluate the loads on each sections.

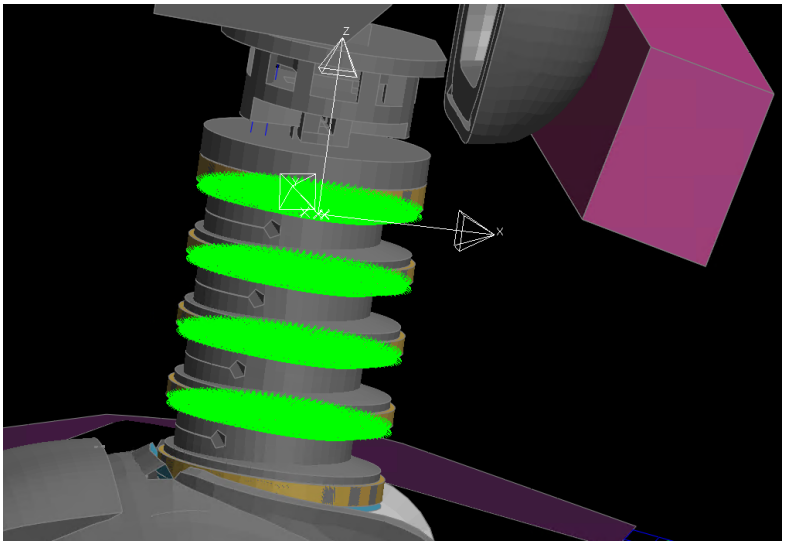

Figure 4.12: Hybrid III neck cross-sections and the reference system used for the first disk section

Vertebral cross-sections

On the other hand, fourteen cross-sections, two per cervical vertebra, were defined in the THUMS. The cross-sections of each vertebra were defined in two different ways, and so they differ in inclination and section cut height. The modality of definition were:

- section perpendicular to the spinal cord; section cut height that maximize the cross-section surface[1].
- section plane that cuts through the vertebra's spinous process and maximize the I_{yy} of the cross-section[2] (see Figure 5.4 for moment of inertia definition).

These cross-sections will be used later in this work for injury criteria definition, but are also useful for comparing the neck behaviour in the two models. Obviously, two reference systems per vertebra (one for each section type) have been defined in order to correctly evaluates the loads in each section. The x axis is directed toward the spinous process of the vertebra and the z axis is directed toward the head (the direction differs accordingly to the section inclination of course).

[1]This type of section is named section type A in this work
[2]This type of section is named section type B in this work

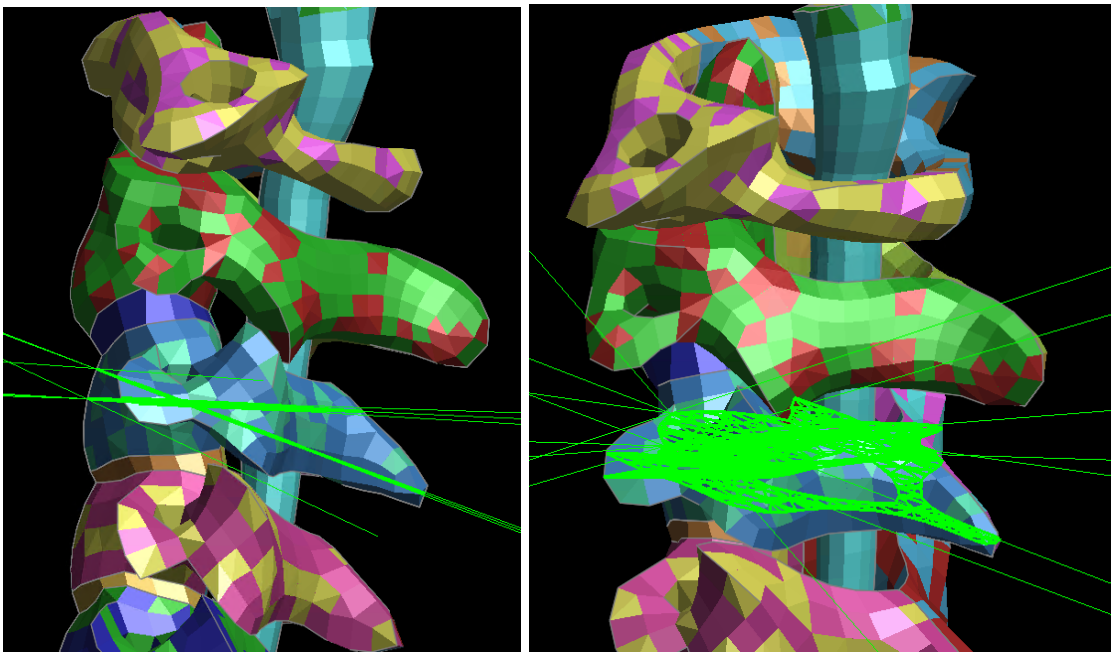

Figure 4.13: Cross-sections defined on C3

It is interesting to observe the curves' trends at different height of the neck. In particular, the M_y moment and the F_z force are analysed because they will be used later on.
In the Hybrid III FE model, the axial forces on the neck sections shows similar trends, the curves after the first $85ms$ almost seem to translate toward negative values and the traction force peaks tend to decrease when the distance from the head increases. In every section the peak force is reached at around $98ms$.
THUMS axial forces are shown in Figure 4.16. Again, it is possible to notice that the graphs tend to translate toward the x axis when section-head distance increases. Nevertheless, differently from the Hybrid III sections, THUMS cross-sections have different surface and orientation from each other, so this trend is not as accentuated as it is in the previous case. Moreover, axial forces differ also depending on the definition of the section considered, with C1, C6 and C7 forces that are the most varying in the considered section definition. It is interesting to notice that C1 doesn't follow the aforementioned trend but is the first and second least loaded vertebra in the first and second graph respectively. The peak time is reached later than in Hybrid III (around $2ms$) and the curves' slopes are less steep. It can be observed that in both Hybrid III and THUMS graphs, there is an initial compression peak. This time, the peak is reached later in the Hybrid III.
Regarding the moment, in Hybrid III cross-sections it presents a behaviour similar to the one previously discussed. The moment calculated on the occipital condyle has been described in Chapter 3.3: the graphs showed an initial extension moment

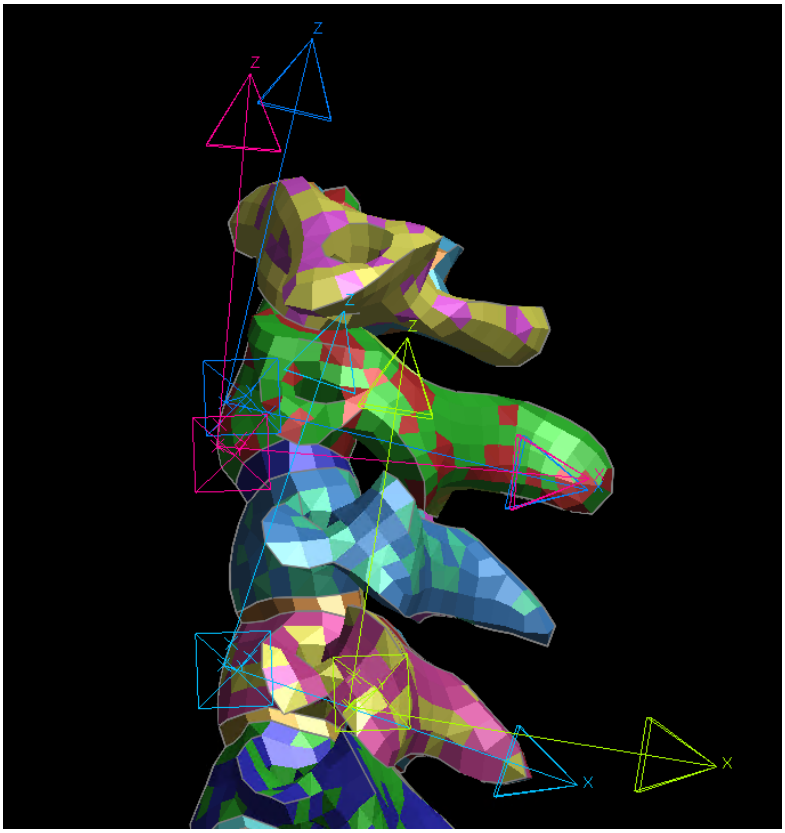

Figure 4.14: THUMS reference systems used for C2 and C4's sections

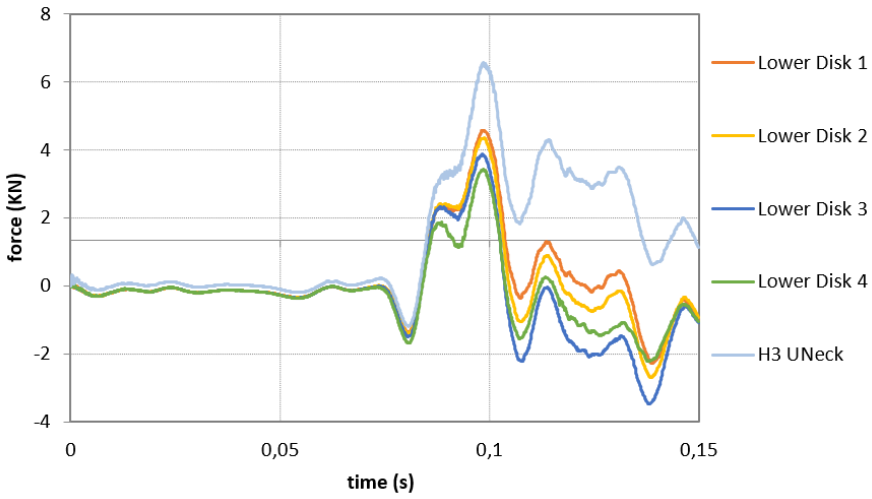

Figure 4.15: Hybrid III axial forces on neck cross-sections

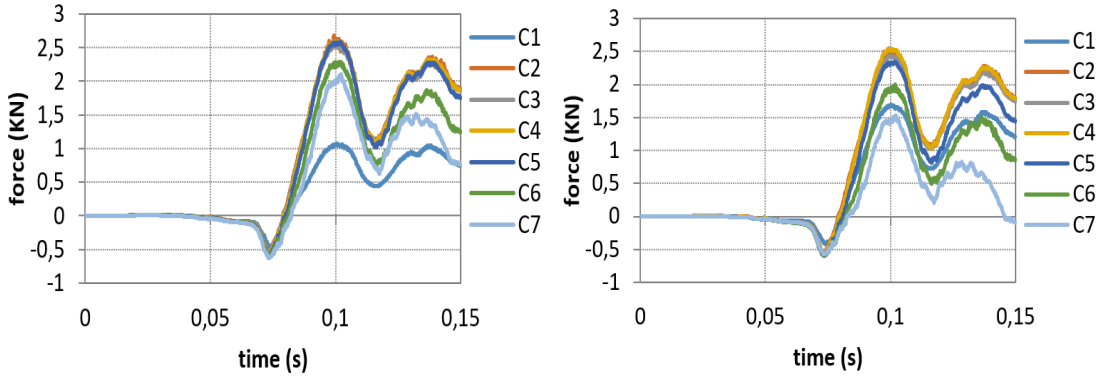

(a) Section type A

(b) Section type B

Figure 4.16: THUMS axial forces on neck cross-sections

peak that then transitioned in a flexion moment peak. If we look at the upper neck section (UNeck) that is above the occipital condyle, the curve is similar with a higher extension peak and a lower flexion peak. When descending along the neck the peak values tend to decrease, eventually transforming into a first flexion peak in Disk 3 and Disk 4. Meanwhile, the second peak (the flexion peak) value increases (see Figure 4.17). It is possible to assert that the upper part of the neck in characterized by load transition from extension to flexion, while the lower part of the neck is loaded only with flexion loads.

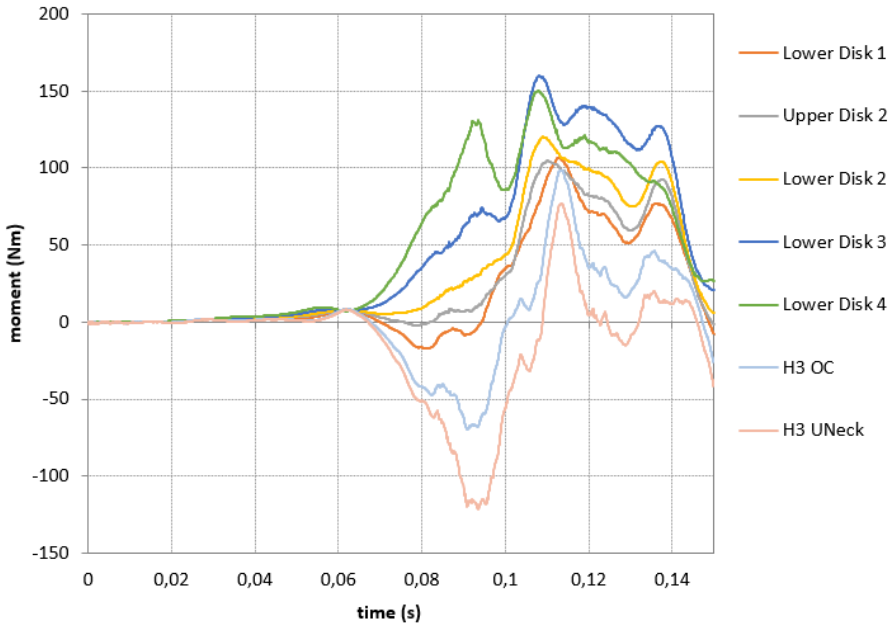

Figure 4.17: Hybrid III extension and flexion bending moments on neck cross-sections

The THUMS sections present, again, M_y curves that are initially loaded mainly with extension moments in the first vertebrae (C1-C3), C4 that has a extension-flexion load and then starting from C5 the vertebrae are loaded with flexion moments. The graphs present similar trends that tend to diverge in the final part of the simulation. Likewise what happen for the axial force, the loads on the two section type are different, especially on C1, C6 and C7. The curves' slopes are not directly comparable with the Hybrid III ones, but in both model is present the tendency to go from extension to flexion. Differently from axial force peak times, moment peak times differ in the vertebrae. The first peaks arrive earlier in the vertebrae that are nearer to the head, namely in succession from C1 to C7.

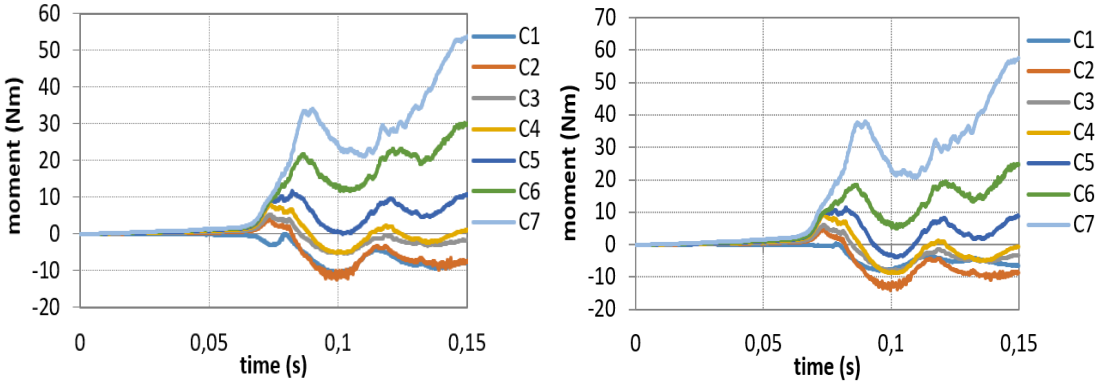

(a) Section type A

(b) Section type B

Figure 4.18: THUMS M_y moments on neck cross-sections

Figure 4.18 shows moment curves that have not reached a point of flex, but that are increasing. This indicates that probably the kinematic of the THUMS' neck and head is more damped than the Hybrid III one. This behaviour can be visualized by looking at the last simulation instant in both the numerical analysis. Figure 4.19 show a comparison between the head movements of the two models and is possible to notice that Hybrid III head has finished the forward rotation motion and is returning back, meanwhile the THUMS neck has not reached the end of its rotation.

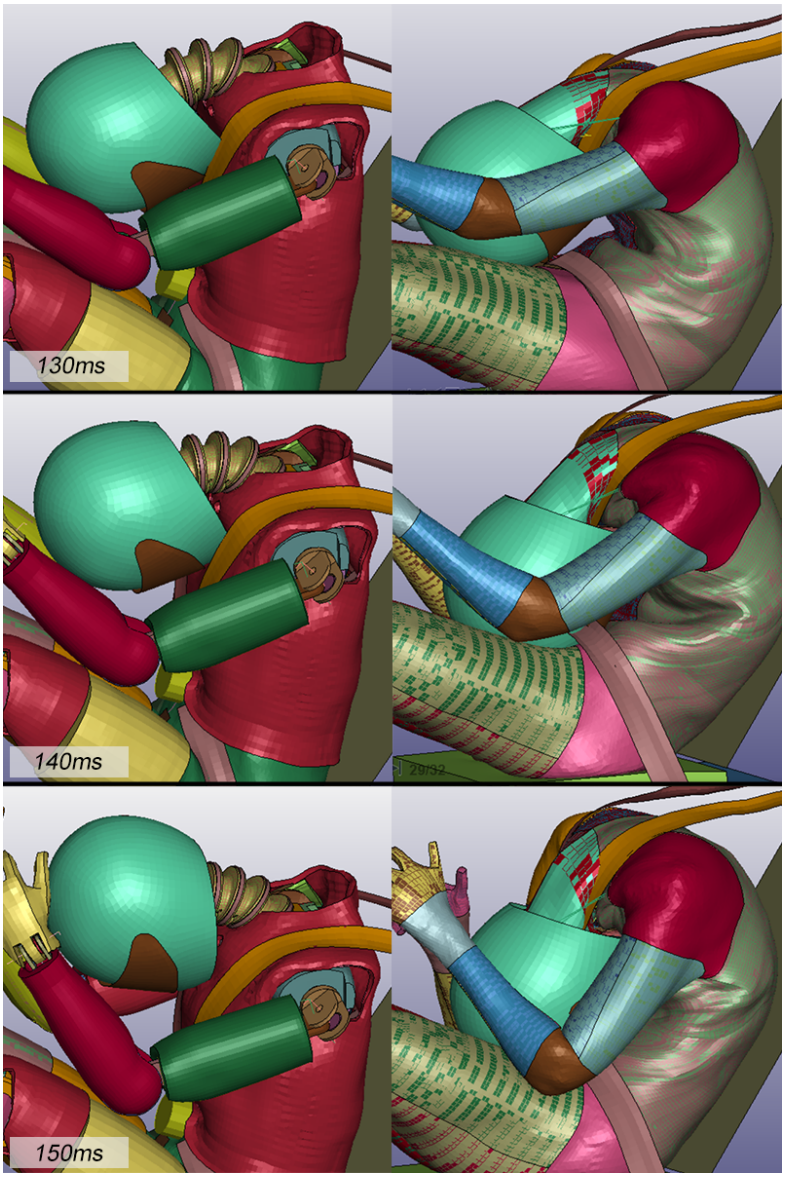

Figure 4.19: Comparison between the THUMS and Hybrid III head motion in the last 20ms of simulation

Chapter 5

Injury criteria development and assessment

In this chapter, some injury criteria are discussed and proposed. Firstly, we are going to define three limit loads (extension moment, flexion moment and traction force) for each vertebra by using the comparison between THUMS and Hybrid III models. In particular, the Nij criterion is used as a reference.
Then, the assessments of the RoM and of the plastic strain limit are performed. They were described in Chapter 1.

5.1 Limit load on vertebrae sections

In the previous chapter, we defined the cross-sections used for the calculation of loads in the middle of the vertebrae (see Figure 4.13). On the other hand, in Chapter 3.3 the Nij values have been calculated for Hybrid III. The purpose of this part of the work is to find a correlation between the two, thus to use the Nij value to theorize three limit loads for each vertebra section.
First of all, the Nij has to be calculated again, since we are confronting two simulation that are purely frontal, differently from the oblique pulse used when we calculated the Nij on Hybrid III FE model. The analysis on the Hybrid III model shows that the force on the upper neck cross-section is always a traction force. Meanwhile, the moment is initially extension moment and then a transition to flexion moment happens at around $100ms$. The peak of each physical quantity is respectively $6556N$, $69289Nmm$ and $98515Nmm$. The Nij graph is shown is Figure 5.2 and has a peak value of 1.16 at $97ms$. For this value, we have a probability of severe injury of 22% and a probability of serious injury of 28% according to the AIS curves for Nij criterion (see Chapter 1.3.1).
For defining the limit, it is essential to analyse the load curves of the vertebrae's cross-sections, too. All the vertebral sections are loaded with traction forces, as it happens in Hybrid III upper neck section. All the force curves have peak values at

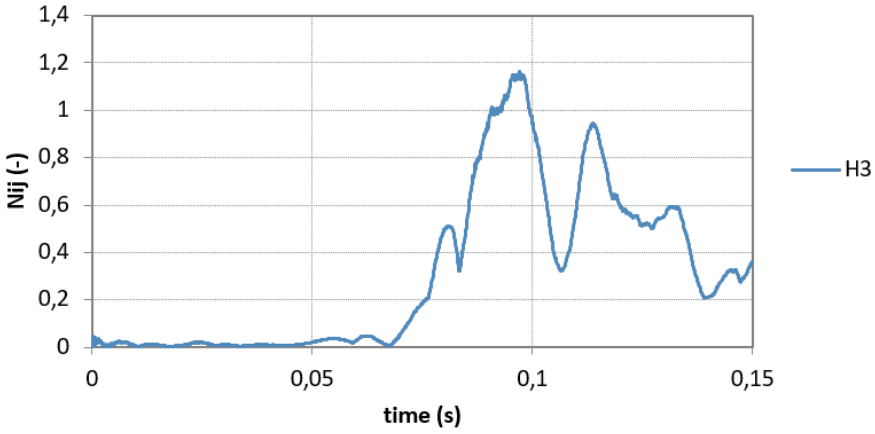

Figure 5.1: Hybrid III Nij graph

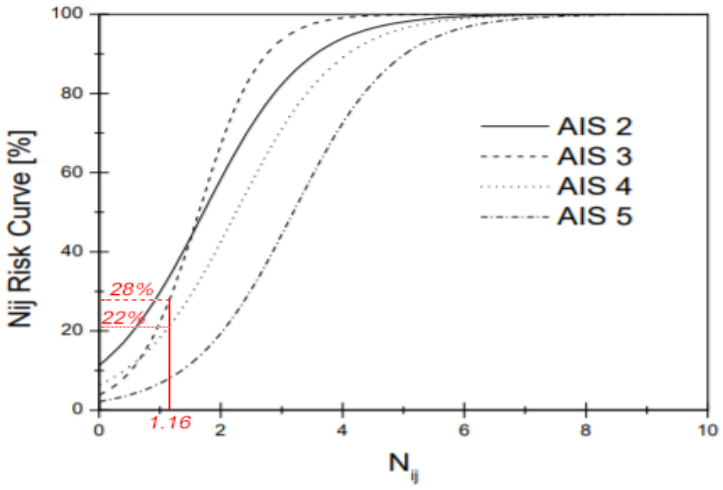

Figure 5.2: Probability of AIS 3 and AIS 4 for Nij equal to 1.16

around $100ms$. Meanwhile, the moment vary consistently from section to section. This behaviour is reasonable as it is compliant with the remarks done in Chapter 4.2.4. The first three vertebrae (from C1 to C3) present moments that are mainly extensional. C4 presents both extension and flexion. C5's loads are both extension and flexion with the latter that is dominant. On the contrary, C6 and C7 are only subjected to flexion loads.

Given the fact that the vertebrae are subjected to different loads, it is not reasonable to use the Nij value to calculate the limits on each vertebra without considering the loads on the vertebra itself. In fact, the Nij maximum value is reached in a traction-extension condition that is not suitable for the calculation of limits in C5,

C6 and C7. Let us consider the maximum value of traction, extension and flexion on the Hybrid III model. Then, we calculate the ratios between the maximum values of the loads and the load limits for Nij criterion (see Table 1.1), namely F_t^n, M_e^n and M_f^n.

$$F_t^r = \frac{F_{t,max}}{F_{t,lim}} \tag{5.1}$$

$$M_e^r = \frac{M_{e,max}}{M_{e,lim}} \tag{5.2}$$

$$M_f^r = \frac{M_{f,max}}{M_{f,lim}} \tag{5.3}$$

The results are listed in the Table 5.1.

	Maximum value	Maximum value time	Normalized load
F_t	$6556.14N$	$98.6ms$	0.963
M_e	$69288,9Nmm$	$91ms$	0.513
M_f	$98514.7Nmm$	$113.3ms$	0.318

Table 5.1: Maximum value for each load in Hybrid III upper neck cross-section

It is reasonable to use these normalized loads to calculate some initial limit load values for each vertebra. In particular, we assume that the limit loads in each vertebra are such that the ratios between the maximum load values and them are equal to the normalized loads calculated on the Hybrid III FE model, namely:

$$F_{t,lim}^{THUMS} = \frac{F_{t,max}^{THUMS}}{F_t^n} \tag{5.4}$$

$$M_{e,lim}^{THUMS} = \frac{M_{e,max}^{THUMS}}{M_e^n} \tag{5.5}$$

$$M_{f,lim}^{THUMS} = \frac{M_{f,max}^{THUMS}}{M_f^n} \tag{5.6}$$

The definition of the limits has been done considering the loading condition of each vertebra. For example, traction-extension limits have been formulated for vertebrae from C1 to C4 and traction-flexion limits have been formulated for vertebrae from C4 to C7. C4 presented a mixed behaviour so, it was the only vertebra that could be used for the definition of both extension and flexion moment limits. It has to be noted that the assumption that the ratios are equal in each vertebra and in Hybrid III's upper neck section is probably not compliant with what happens in reality. This is particularly true when moving away from the occipital condyle because the load distribution changes inevitably together with the neck structure. Nevertheless, this assumption is useful for finding some starting limit

values that will be modified later. The limits were calculated for both cross-section type defined in Chapter 4.2.4. Moreover, the fact that the bending moment has not reached its maximum in some vertebrae was highlighted in the same chapter. Hence, it was necessary to run a simulation 180ms long for finding these maximums. The results are shown in Figure 5.3.

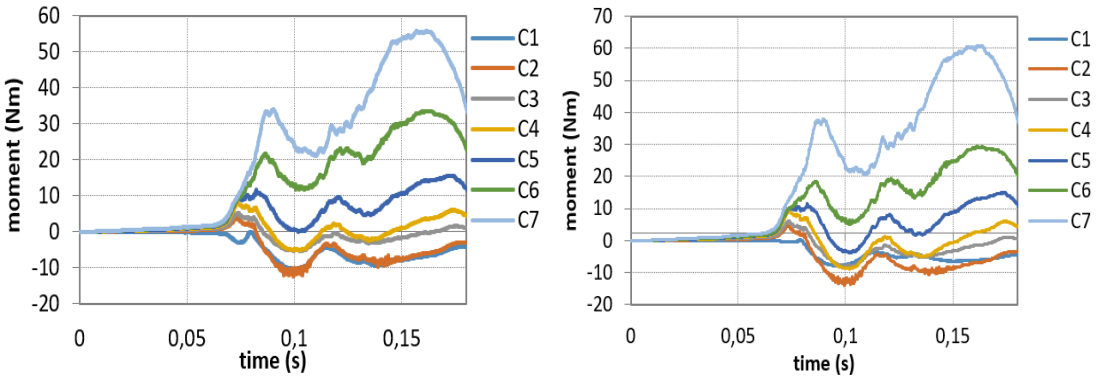

(a) Section type A

(b) Section type B

Figure 5.3: THUMS M_y moments on neck cross-sections, 180ms long FEA

Vertebra	$F_{t,max}$	$F_{t,lim}$	$M_{e,max}$	$M_{e,lim}$	$M_{f,max}$	$M_{f,lim}$
C1	1098.67	1140.55	3533.42	6884.39		
C2	2672.88	2774.74	12346.95	24056.4		
C3	2529.04	2625.42	5348.9	10421.6		
C4	2592.53	2691.33	5220.25	10171.0	7924.65	24936.8
C5	2581.15	2679.52			15557.32	48954.81
C6	2289.88	2377.15			33523.44	65315.87
C7	2099.62	2179.64			55687.65	175234.47

Table 5.2: Limit loads for each vertebra, forces expressed in N and moments expressed in Nmm; first values; cross-section type A

The values obtained are reported in Table 5.2 and 5.3. However, it is not possible to use the defined limits as they are because the assumption that the normalized loads are equal in each vertebra is very unlikely, as said before. Moreover, by looking at the data it is possible to notice that the limits don't represent correctly the actual size of the cervical vertebrae. For instance, it is unlikely that C1 can withstand more traction load than C7. These limits directly depend on the load

Vertebra	$F_{t,max}$	$F_{t,lim}$	$M_{e,max}$	$M_{e,lim}$	$M_{f,max}$	$M_{f,lim}$
C1	1690.03	1754.44	8010.04	15606.47		
C2	2545.9	2642.93	14092.34	27457.0		
C3	2436.07	2528.91	7975.33	15538.84		
C4	2543.16	2640.09	8806.86	17158.98	9180.82	28889.65
C5	2340.31	2429.50			14998.48	47196.28
C6	2008.13	2084.66			29255.09	92058.10
C7	1536.14	1594.68			60970.9	191859.47

Table 5.3: Limit loads for each vertebra, forces expressed in N and moments expressed in Nmm; first values; cross-section type B

curves of each vertebra and, moreover, we can not know which vertebra is the nearest to failure. For these reasons, the limits have been scaled by using physical quantities that are indicative of the vertebrae's sizes. In particular, the surface S of the cross-section has been used for the scaling of force limits and the moment of inertia I_{yy} has been used for scaling the moment limits. It has to be noted, that a conservative approach has been used. For instance, we considered the vertebra

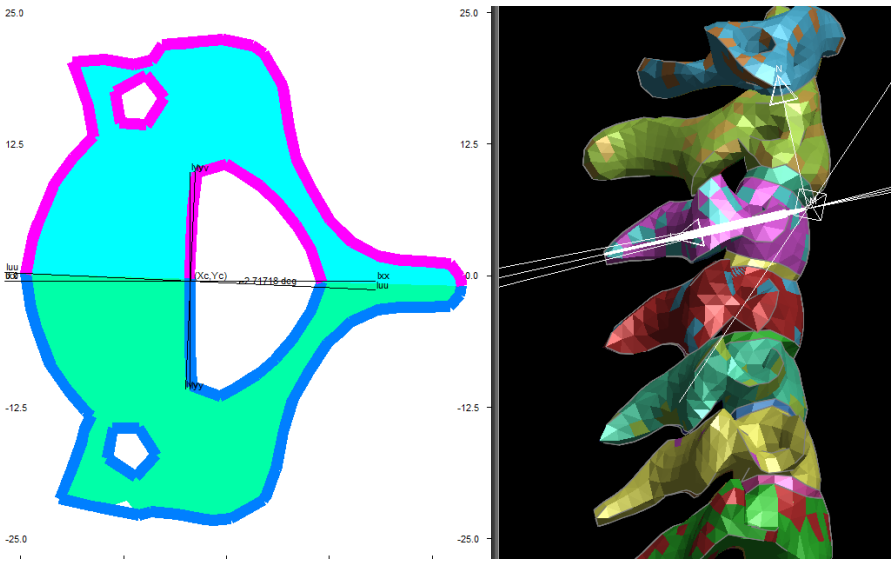

Figure 5.4: C3 cross-section geometry

with the lowest ratio between force limit and surface as the reference and we scaled all the other limits so that each vertebra's ratio was equal to the reference one.

Vertebra	$S\ [mm^2]$	$\frac{F_{t,lim}}{S}$	$I_{yy}\ [ton \cdot mm^2]$	$\frac{M_{e,lim}}{I_{yy}}$	$\frac{M_{f,lim}}{I_{yy}}$
C1	928.99	1.23	46843.26	0.44	
C2	1190.46	2.33	154241.8	0.16	
C3	1028.07	2.55	66118.23	0.16	
C4	1070.15	2.51	66028.98	0.15	0.38
C5	1067.51	2.51	61196.93		0.80
C6	1273.28	1.87	98167.89		1.07
C7	1155.1	1.89	87453.6		2.0

Table 5.4: Scaling ratios for THUMS' vertebrae limits; cross section type A

Vertebra	$S\ [mm^2]$	$\frac{F_{t,lim}}{S}$	$I_{yy}\ [ton \cdot mm^2]$	$\frac{M_{e,lim}}{I_{yy}}$	$\frac{M_{f,lim}}{I_{yy}}$
C1	1218.7	1.44	112318.7	0.14	
C2	1282.36	2.06	182790.6	0.15	
C3	1099.92	2.30	97842.43	0.16	
C4	1139.95	2.32	104700.0	0.16	0.28
C5	1173.68	2.07	105413.1		0.45
C6	1293.76	1.61	138812.8		0.66
C7	1270.16	1.25	244666.4		0.78

Table 5.5: Scaling ratios for THUMS' vertebrae limits; cross section type B

This process provided three reference ratios: one for traction force, one for extension moment and one for flexion moment. All the vertebrae were used for the definition of the first one, except C1, C6 and C7 because they were less loaded than the other vertebrae and they probably were not near to their respective traction limit loads (especially considering their surface). It has to be noted that this choice is actually not conservative. Vertebrae from C1 to C4 were considered for extension and vertebrae from C4 to C7 were considered for flexion. This is also compliant with what has been discussed before regarding the first limit load definition. By using the reference ratios, it is possible to define other load limits by

multiplying the ratios for the scaling dimensions of each vertebra. Moreover, it is actually possible to define flexion limits for the first three cervical vertebrae and extension limits for the last three cervical vertebrae this time. The three chosen minimum ratios are shown in Table 5.4 and 5.5, highlighted in green.
Table 5.6 and 5.7 provide the limits found by multiplying the chosen ratios by the section surface or moment of inertia.

Vertebra	$F_{t,lim}$	$M_{e,lim}$	$M_{f,lim}$
C1	2165.30	7215.63	17691.04
C2	2774.74	23759.05	58251.68
C3	2396.24	10184.7	24970.52
C4	2494.31	10170.95	24936.81
C5	2488.16	9426.63	23111.92
C6	2967.78	15121.56	37074.54
C7	2692.33	13471.15	33028.13

Table 5.6: Limit loads for each vertebra, forces expressed in N and moments expressed in Nmm; scaled values; cross section type A

Vertebra	$F_{t,lim}$	$M_{e,lim}$	$M_{f,lim}$
C1	2511.72	15606.47	30991.86
C2	2642.93	25398.41	50437.03
C3	2266.92	13595.02	26997.46
C4	2349.42	14547.87	28889.65
C5	2418.95	14646.95	29086.42
C6	2666.43	19287.78	38302.33
C7	2617.79	33995.94	67510.29

Table 5.7: Limit loads for each vertebra, forces expressed in N and moments expressed in Nmm; scaled values; cross-section type B

The limits contained in the aforementioned table were defined for two different section type. The cross-section were defined previously in order not to be arbitrary. It is also true that the two definition described in Chapter 4.1.2 were chosen in order to obtain a significant evaluation of loads. Particularly, the type A cross-sections were made for having some sections suitable for the evaluation of traction load parallel to the spinal cord. On the other hand, type B cross-sections were defined for maximizing the moment of inertia I_{yy} that can be defined as the indicator of a section's ability to resist to bending moment[1]. Due to these properties, the traction force limits were defined considering the type A cross-section and the extension and flexion moment limits were defined considering the type B cross-section. The results are contained in Table 5.8

Vertebra	$F_{t,lim}$	$M_{e,lim}$	$M_{f,lim}$
C1	2165.30	15606.47	30991.86
C2	2774.74	25398.41	50437.03
C3	2396.24	13595.02	26997.46
C4	2494.31	14547.87	28889.65
C5	2488.16	14646.95	29086.42
C6	2967.78	19287.78	38302.33
C7	2692.33	33995.94	67510.29

Table 5.8: Limit loads for each vertebra cross-section, forces expressed in N and moments expressed in Nmm; final values

The obtained values were acceptable, so other modification were not needed. Nevertheless, it is possible to notice that the C7's flexion limit value is very high if confronted with the limits of C2 and C6. The vertebrae have similar size, even if the moment of inertia of C7 is much higher because of the length of the spinous process. This consideration suggest that the actual limit could be lower, e.g. around $50000Nmm$.
If the obtained limits are used for calculating the Nij for each vertebra by replacing the standard Hybrid III's load limits, it is possible to compare the vertebral Nij curves with the Hybrid III one. The moment in THUMS' vertebrae has not to be referred to the occipital condyle because the limits were defined for each vertebra at the height of the respective section. The trends are mostly similar to the Hybrid III ones. These Nij curves have not an actual meaning in term of injury criteria definition because we defined the limits as they were independent from one another.

Nevertheless, it is interesting to compare them with Hybrid III Nij. Moreover, they permit to better understand how much the vertebrae are loaded when considering both forces and moments at the same time.

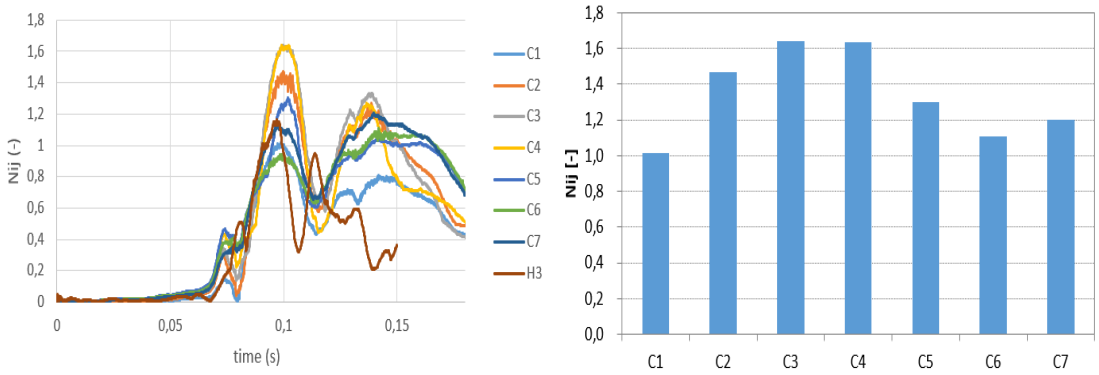

(a) (b)

Figure 5.5: Comparison of Nij for THUMS vertebrae and Hybrid III

According to the result shown in Figure 5.5, vertebrae from C2 to C5 are the most likely to be in a critical condition, when considering forces and moments at the same time. In particular, C3, C4 and C5 has a maximum traction load that exceed the defined limit traction load. So a fracture is expected in these vertebrae. On the other hand, fracture is not expected in any vertebra when moment limits are considered (both extension and flexion) alone because all the maximum values are lower than their respective limits. These prediction are made by considering only one load at a time. Actually, the load combination has to be considered when assessing failure. Both force and moments contributes to stress that is responsible for fractures. The Nij calculated in Figure 5.5 can be used for considering the combination of loads. In this case Nij is higher than 1 in every vertebra. Therefore the chance of moderate, serious and/or severe injury is higher than 20% in every vertebra, if AIS curves for Nij are considered. However the this AIS curves are defined for Nij criterion, indeed, and can be different for the limits defined in this chapter.

5.1.1 Limit definition with scaled crash pulses

The obtained limits have been found for given boundary conditions, crash pulse and cross-section definitions. The boundary conditions are somehow standard for this type of crash test and the cross-sections where defined following a procedure as rigorous as possible. It is interesting to scale the crash pulse for verifying if the same load limits are obtained for some different deceleration (i.e. crash at different speed). Two scaled crash pulse were considered. The first one had a peak of $58g$ and a second had a peak of $52g$.

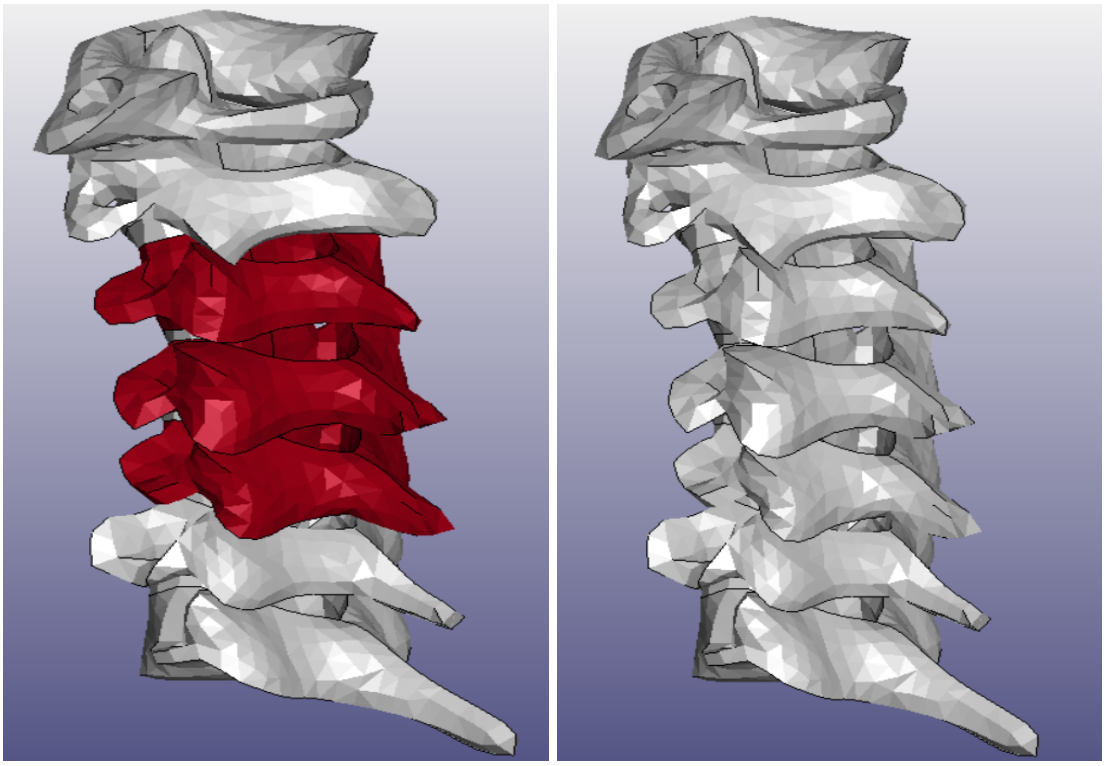

(a) Force limits (b) Moments limits

Figure 5.6: Vertebral expected fracture (highlighted in red) according to vertebral section limit loads

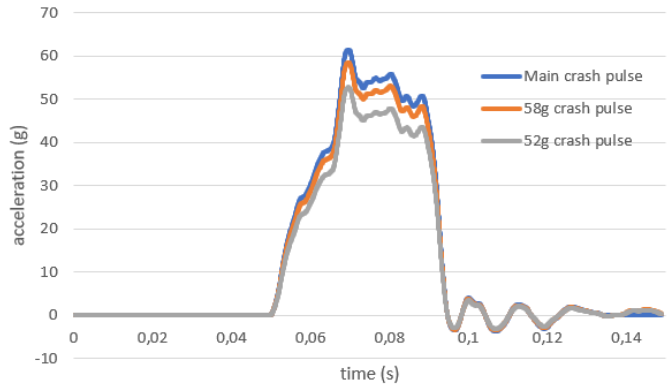

Figure 5.7: Scaled crash pulses

58g peak scaled crash pulse

A Hybrid III FEA for a peak of 58g was conducted. Moments and forces contribute to a Nij that reached values higher than 1 during the simulation. The upper neck

cross-section detects a traction force peak of $6000N$ at $100ms$. The M_y moment has an extension peak at $90ms$ ($68000Nmm$) and a flexion peak at $120ms$ (around $88000Nm$). The maximum Nij is equal to 1.05.

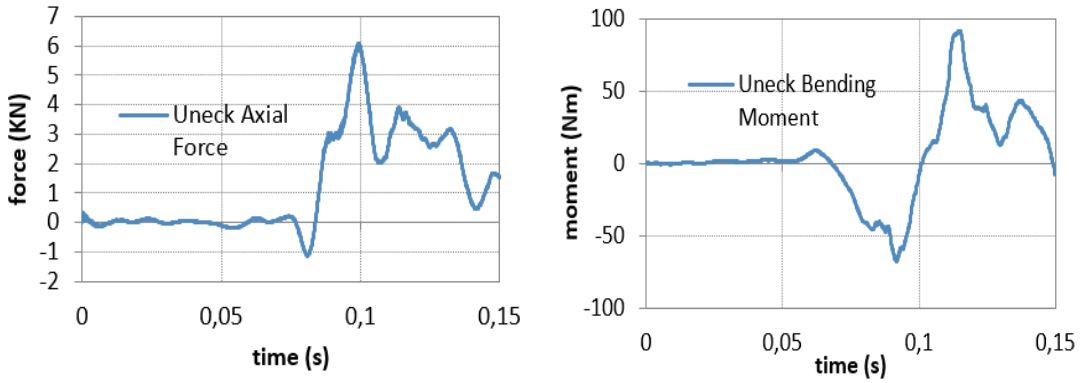

(a) (b)

Figure 5.8: Hybrid III data for 58g peak scaled crash pulse

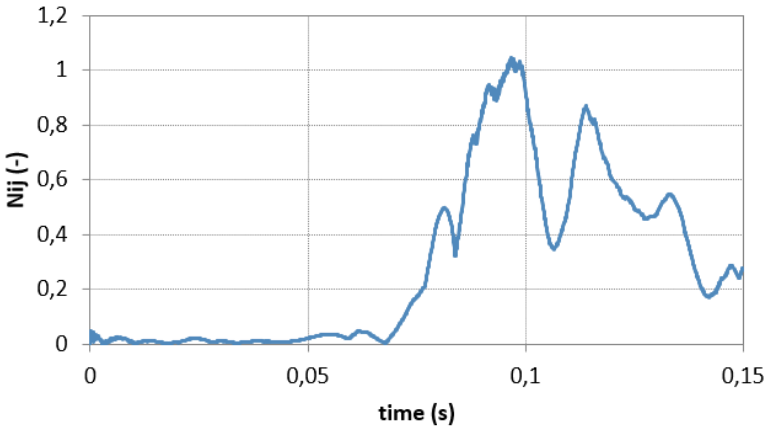

Figure 5.9: Hybrid III Nij for 58g peak scaled crash

A FEA with THUMS was than performed. The axial forces on the section are lower than the forces of the main numerical simulation. The peak differences are all around $250N$. On the contrary, the M_y moment peaks are similar to the one of the main numerical simulations. The peaks are reached later ($1.5ms$ of delay) but their magnitude is almost the same. This indicates that the cervical spine probably undergoes a similar motion but with different acceleration and speed.
The same steps described previously in this chapter have been used for the subsequent calculation of the limits. First values were calculated with the ratios between Hybrid III maximum and limit loads. Then the limits were scaled using geometry properties of the sections. Finally the limits were chosen depending on the more

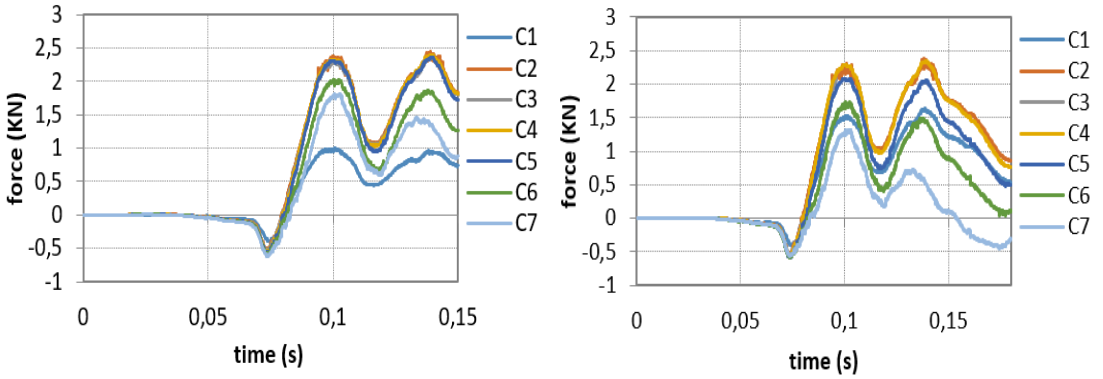

(a) Section type A (b) Section type B

Figure 5.10: THUMS F_z force for 58g peak scaled crash

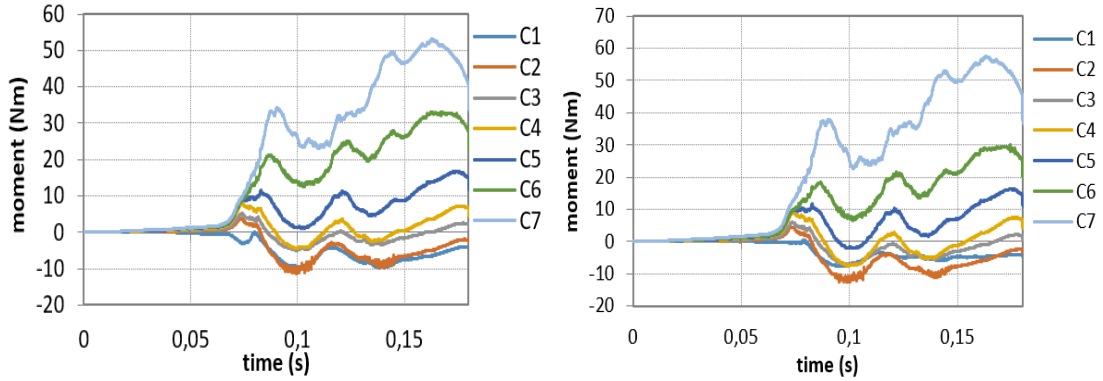

(a) Section type A (b) Section type B

Figure 5.11: THUMS M_y moment for 58g peak scaled crash

appropriate section type. The final results are reported in Table 5.9.

52g peak scaled crash pulse

A Hybrid III FEA for a peak of 52g was conducted. Moments and forces contribute to a Nij inferior to 1 throughout the entire simulation. So this time the Hybrid III conditions are not critical, even if close to be it. The upper neck cross-section detects a traction force peak of 5000N at 100ms. The M_y moment has an extension peak at 90ms (60000Nmm) and a flexion peak at 120ms (around 70000Nm). The maximum Nij is equal to 0.86.
A FEA with THUMS was than performed. The axial forces on the section are lower than the forces of the main numerical simulation. The peak differences are all around 500N. On the contrary, the M_y moment peaks are similar to the one of the main numerical simulations. The peaks are reached later (2ms of delay) but

Vertebra	$F_{t,lim}$	$M_{e,lim}$	$M_{f,lim}$
C1	2145.83	15429.28	32901.36
C2	2749.79	25110.04	53544.59
C3	2374.69	13440.06	28660.85
C4	2471.88	14382.69	30669.62
C5	2465.78	14480.65	30878.51
C6	2941.09	19068.78	40662.24
C7	2668.12	33609.95	71669.78

Table 5.9: Limit loads for each vertebra cross-section, forces expressed in N and moments expressed in Nmm; final values for 58g peak scaled crash pulse

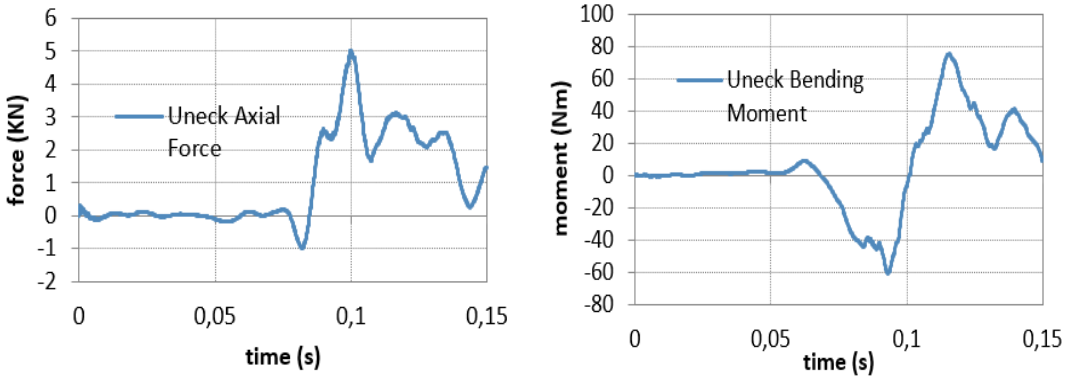

(a) (b)

Figure 5.12: Hybrid III data for 52g peak scaled crash pulse

their magnitude is almost the same. Again, this indicates that the cervical spine probably undergoes a similar motion but with different acceleration and speed.

Again, the same steps described previously in this chapter have been used for the subsequent calculation of the limits. First values were calculated with the ratios between Hybrid III maximum and limit loads. Then the limits were scaled using geometry properties of the sections. Finally the limits were chosen depending on the more appropriate section type. The final results are reported in Table 5.10.

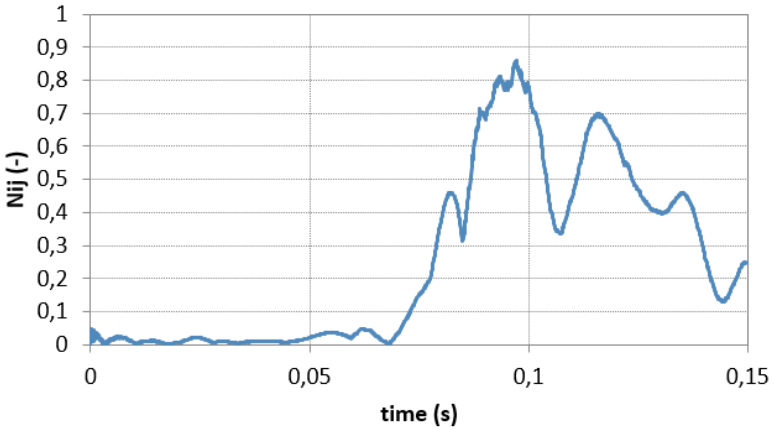

Figure 5.13: Hybrid III Nij for 52g peak scaled crash

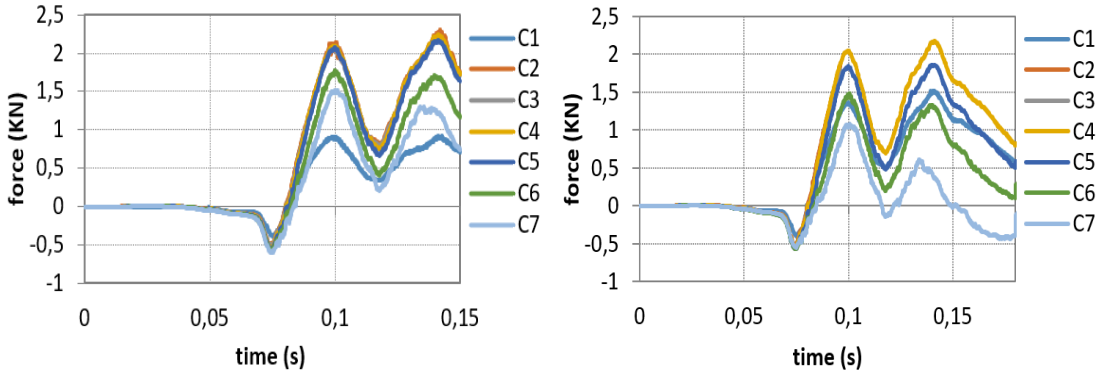

(a) Section type A

(b) Section type B

Figure 5.14: THUMS F_z force for 52g peak scaled crash

Comparison of the limits

The limits previously calculated for the three different crash pulse are not identical. Table 5.11 contain the differences between the limits calculated for the main crash pulse and the limits calculated for the other two crash pulse. A percentage error has been calculated:

$$\frac{L_{lim}^{main} - L_{lim}^{scaled}}{L_{lim}^{main}} \tag{5.7}$$

where L_{lim}^{main} indicates the limit loads for the main crash pulse simulation and L_{lim}^{scaled} indicates the limit loads for the scaled crash pulse simulations.
It has to be noted that the percentage error is equal in all the vertebrae for a given load and crash pulse because of the geometrical scaling that has been done for defining the limits. In fact, the limits are defined by multiplying surfaces or moment of inertia for a reference ratio (see Chapter 5.1).

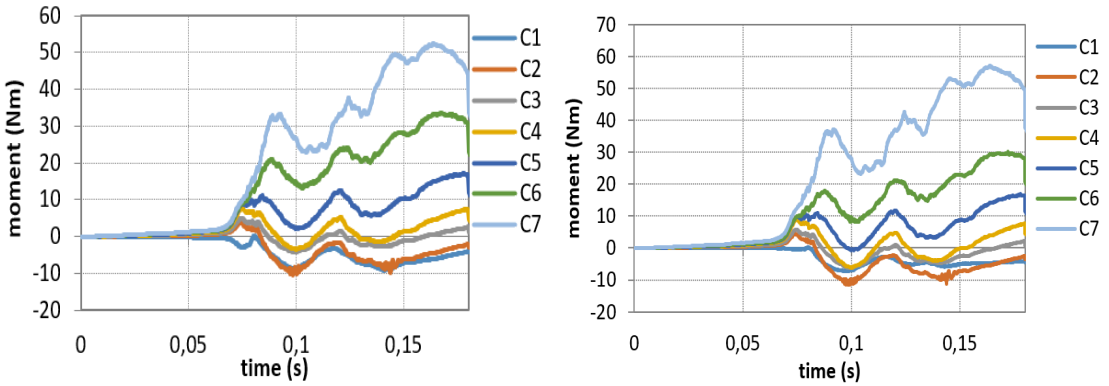

(a) Section type A

(b) Section type B

Figure 5.15: THUMS M_y moment for 52g peak scaled crash

Vertebra	$F_{t,lim}$	$M_{e,lim}$	$M_{f,lim}$
C1	2445.72	14636.58	39635.43
C2	3134.09	23819.98	64503.81
C3	2706.57	12750.13	34526.99
C4	2817.33	13643.77	36946.92
C5	2810.39	13736.69	37198.55
C6	3352.13	18089.11	48984.76
C7	3041.0	31883.20	86338.77

Table 5.10: Limit loads for each vertebra cross-section, forces expressed in N and moments expressed in Nmm; final values for 52g peak scaled crash pulse

The extension limits are similar in every simulation and are probably the most precise. Meanwhile, traction limits are very close for the main crash pulse and the $58g$ scaled one but the limits for the $52g$ scaled pulse are 13% greater than the main ones. The same happen for the flexion limits. As regard traction, the limits of the main simulation identify failure in C3, C4 and C5 but it is shown later that this should not actually happen. Meanwhile, the limits of the $52g$ scaled crash pulse simulation don't identify failure for traction load any every vertebra. This is coherent with the Nij equal to 0.86. This indicates that probably the traction limits of the main case are too conservative. Regarding flexion, the fact that the maximum loads in all the simulation are equal indicates that probably Hybrid

Limits		C1	C2	C3	C4	C5	C6	C7
$58g$	F_t difference	19.47	24.95	21.55	22.43	22.37	26.69	24.21
	M_e difference	117.20	288.38	154.36	165.18	166.30	219.00	385.99
	M_f difference	−1909.49	−3107.57	−1663.39	−1779.97	−1792.10	−2359.91	−4159.50
	F_t err%	0.9%	0.9%	0.9%	0.9%	0.9%	0.9%	0.9%
	M_e err%	1.14%	1.14%	1.14%	1.14%	1.14%	1.14%	1.14%
	M_f err%	−6.16%	−6.16%	−6.16%	−6.16%	−6.16%	−6.16%	−6.16%
$52g$	F_t difference	−280.42	−359.34	−310.33	−323.02	−322.23	384.35	−348.67
	M_e difference	969.89	1579.43	844.89	904.10	910.26	1198.67	2112.74
	M_f difference	−8643.56	−14066.68	−7529.54	−8057.26	−8112.14	−10682.44	−18828.48
	F_t err%	−12.95%	−12.95%	−12.95%	−12.95%	−12.95%	−12.95%	−12.95%
	M_e err%	6.21%	6.21%	6.21%	6.21%	6.21%	6.21%	6.21%
	M_f err%	−27.89%	−27.89%	−27.89%	−27.89%	−27.89%	−27.89%	−27.89%

Table 5.11: Difference between the limit load calculated for the difference crash pulses; forces expressed in N and moments expressed in Nmm

III normalized flexion load is not close to THUMS normalized vertebral flexion loads (assumption made for limit calculation see Chapter 5.1). The former should probably be greater in order to obtain lower limits as it is shown later.

5.1.2 Method's limitation

Load limits have been defined in this chapter for each cervical vertebra. The used procedure permitted to obtain some reasonable values that can be applied in numerical simulation injury assessment. Nevertheless, it is important to remark that the described method is affected by some intrinsic problem and limitation that could condition the results. Some of the limitation have already been pointed out. The limitation are here listed below:

- The limit loads are directly dependent on the loads measured on the vertebrae, this problem has been partially solved by scaling the first found limits, nevertheless the issue remain.
- Directly related to the first limitation: the measured loads (i.e. the limit loads) obviously depend on the boundary conditions and on the crash pulse.
- The limits are defined on specific cross-section that are not easy to identify. Moreover, they are not possible to be reproduced in other HBM or in THUMS versions that have different vertebral mesh.
- The definition of a cutting plane for C1's cross-section (type A) can be done at two different height: in the superior part of the vertebra (as it was done

in this work) and in the inferior part of the vertebra.

- The assumption that the normalized loads are equal in Hybrid III upper neck section and in THUMS cervical vertebrae is not realistic (especially moving away from the occipital condyle), even if it was partially solved by scaling the first found limits.

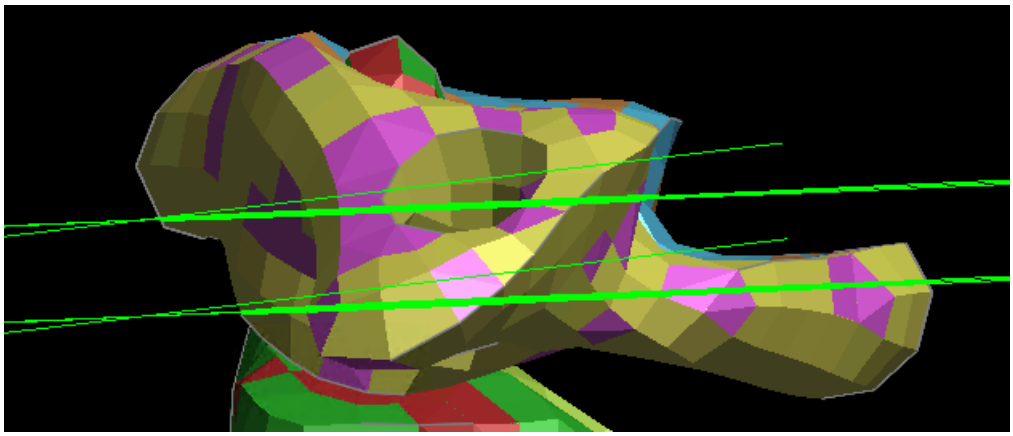

Figure 5.16: Different definition of C1's cross-section plane

5.2 Vertebral range of motion assessment

In Chapter 1.3.2 the mobility of head and neck was discussed. In particular, FSUs' range of motion has been defined and listed in Table 1.3. FEAs are very useful because they permit to evaluate the displacement and the rotation of a chosen node with respect to a reference frame of choice. THUMS is a very accurate HBM and it features accurate reproductions of vertebrae. Therefore, the numerical assessment of RoM permits to take advantage of both the aforementioned features. It is possible to define a reference frame in the model and then to calculate displacements and rotations of a vertebral node. Hence, we can calculate relative movements of vertebrae.
Practically, one reference system was defined in each vertebra and one node was chosen as representative of each vertebra. The reference frames defined for cross-sections type B was used for simplicity. The movement of each vertebra's reference node with respect to another vertebra's reference frame (hence the movement of a vertebra with respect to another vertebra) was requested as an output by using the card DATABASE_HISTORY_NODE[16]. Again, it is important that each reference frame moves with the vertebra during the simulation and that the node movement evaluation is referred to the moving reference frame. So the correct

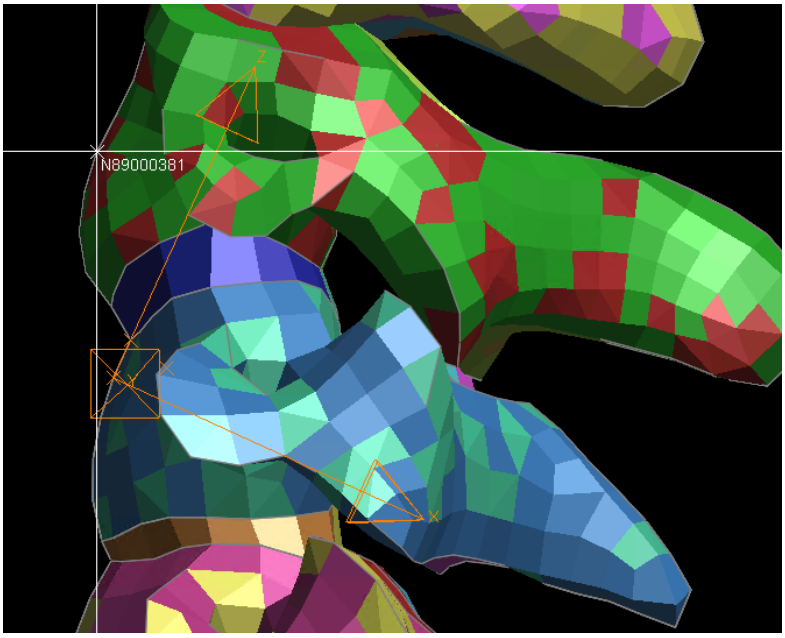

Figure 5.17: Reference frame and node used for relative movement C2-C3 evaluation

	θ_y limit [deg]	$\sigma[deg]$	Maximum θ_y [deg]
C0-C1	13.6	±5.9	-18.15
C1-C2	9.2	±4.4	-4.28
C2-C3	5.6	±2.4	-5.76
C3-C4	8.2	±3.05	6.71
C4-C5	8.55	±2.65	9.03
C5-C6	9.35	±3.35	12.2
C6-C7	7.95	±2.45	16.71
C0-C2	22.6	±7.4	-20.67
C2-C7	40.75	±9.45	44.16
C0-C7	58.45	±10.1	30.49

Table 5.12: θ_y rotation maximum values and limits (σ is the standard deviation)

parameters have to be set in the cards. Figure 5.18 shows the reference frame chosen for C3 and the node used for describing the movement of C2.
Moreover, it is possible to identify a node for describing the occipital condyle, even if its geometry is not reproduced accurately. So, it is possible to evaluate the relative movement between the occipital condyle and the vertebrae.

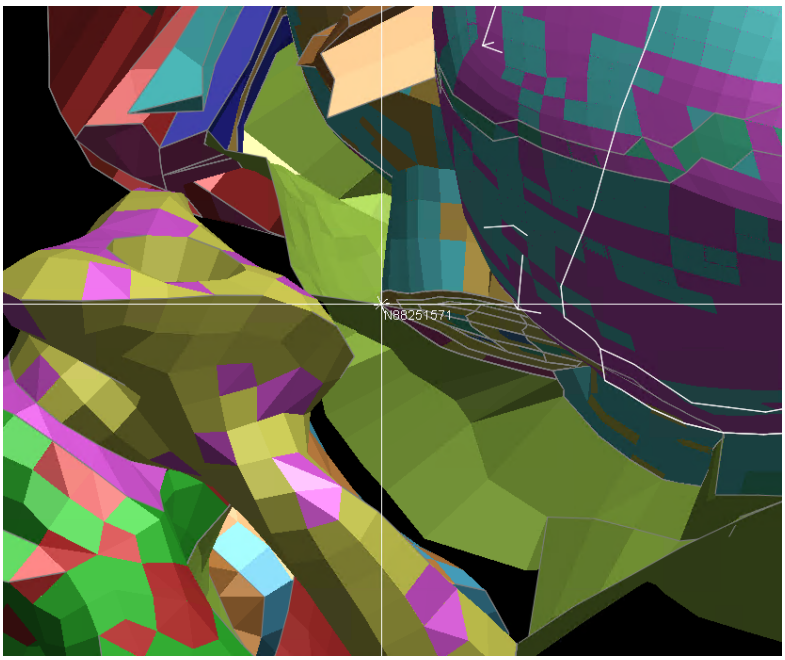

Figure 5.18: Node used for evaluation of C0 movements

Here the main results of the movement evaluation are discussed. Figure 5.19 shows examples of displacement component in the x, y and z directions (complete graph can be found in Appendix A.2).
It has to be noted that the y axis of every reference frame is parallel to the y axis of the global reference frame by definition. It is possible to notice that the y displacements are almost negligible if confronted with the displacement in the other directions. This indicates that the total rotation almost consist only of rotation in the sagittal plane (θ_y), as it is expected from a frontal impact simulation. Some example of θ_y graphs are reported in Figure 5.20. The complete set of graphs can be found in Appendix A.2.
The RoMs defined in the first chapter refer to rotations. The graphs showed that torsion and lateral flexion are almost negligible in the simulation. Hence θ_y rotation is considered. The assessment has been done by confronting the maximum value of each θ_y graph with the limit rotation defined in Table 1.3. However, the values contained in the aforementioned table refer to the total angular displacement in the sagittal plane, i.e. they are the angles between the limit positions of flexion and extension. The specific rotation limits for flexion and extension are not defined.

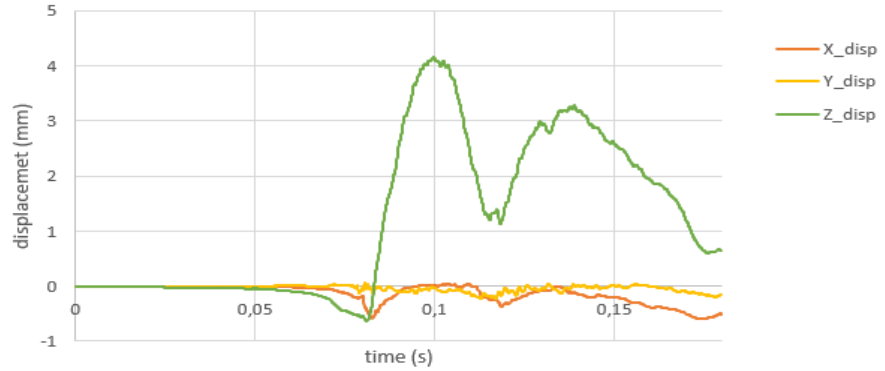

(a) Relative displacements C2-C3

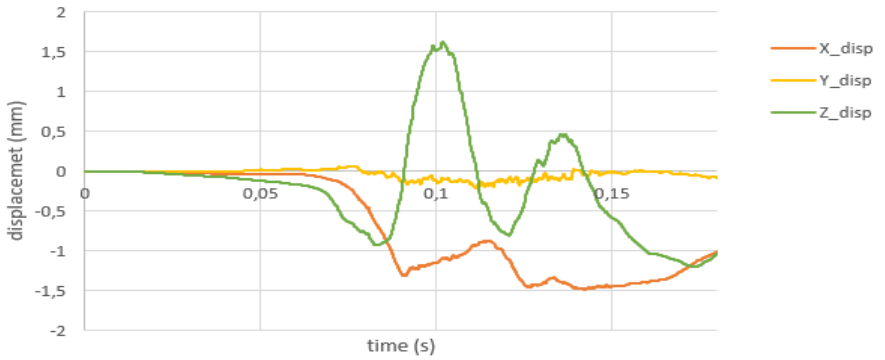

(b) Relative displacements C4-C5

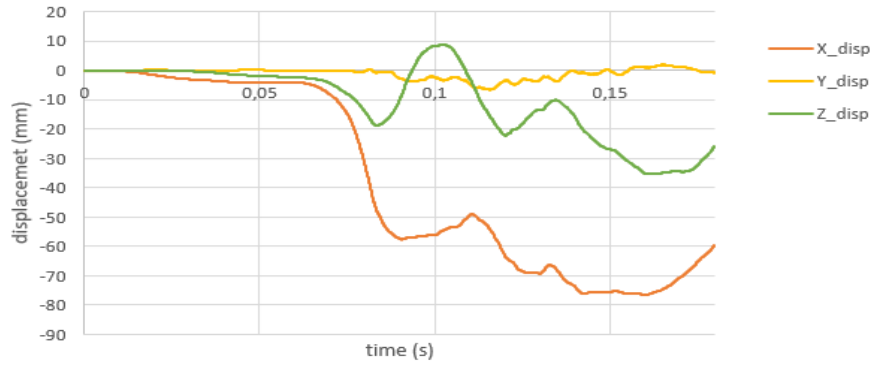

(c) Relative displacements C0-C7

Figure 5.19: Example of relative movement graphs

B.Watier studied the RoM of the cervical spine in his work *"Etude expérimentale du rachis cervical: comportement mécanique in-vitro et cinématique in-vivo"*[2] and the ration between flexion and extension rotation limits were around 1:1 in subjects from 30 to 50 year-old. Niewiadomski et al. studied RoM in their work *"Experimental assessment of cervical ranges of motion and compensatory strate-*

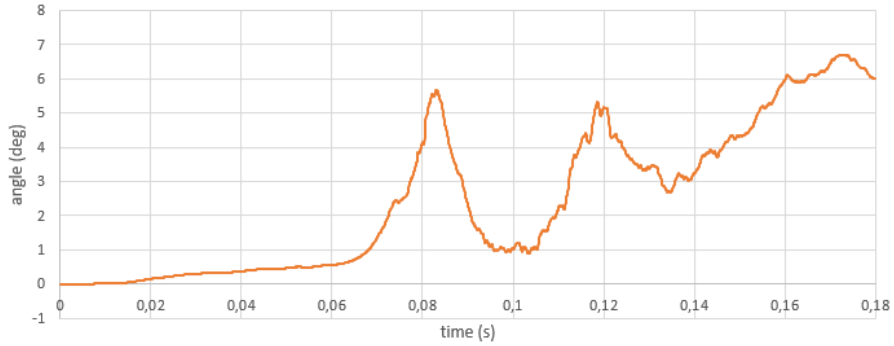

(a) Relative rotation; C2-C3

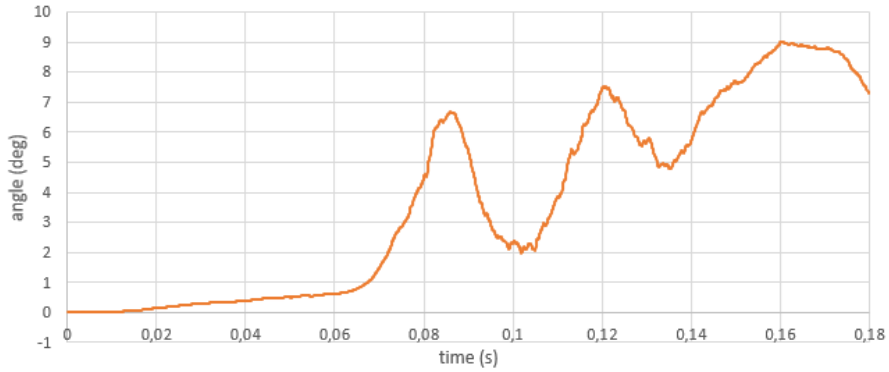

(b) Relative rotation; C4-C5

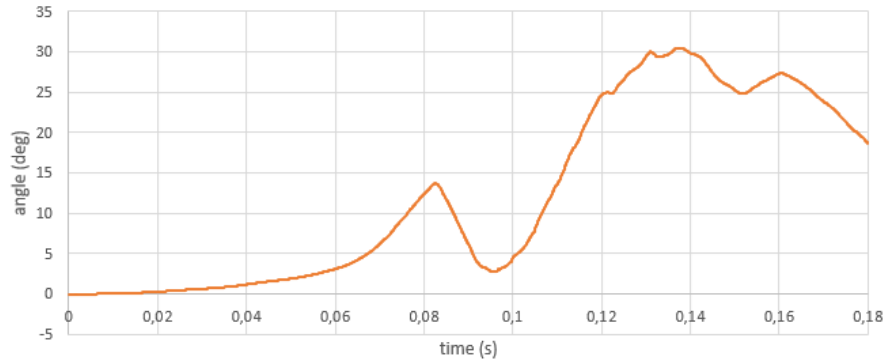

(c) Relative rotation; C0-C7

Figure 5.20: Example of relative rotation θ_y graphs

gies"[4] and found similar results. The flexion limit this time was a little higher than the extension limit with a ratio of 11:10. The study was done on subjects seated on an experimental chair. The bust of the subjects was straight. In this study, THUMS seated position already shows an initial neck flexion with respect to a straight bust configuration because the seat is inclined. Taking this into account, it is reasonable to consider the flexion/extension amplitude ratio as 1:1. Therefore,

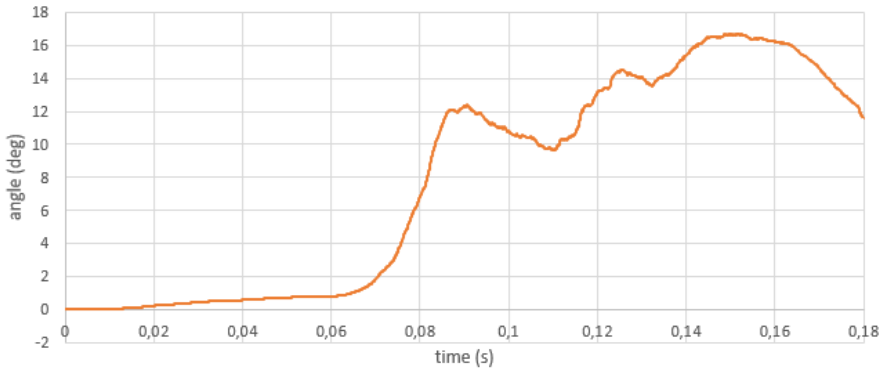

Figure 5.21: Relative rotation θ_y; C6-C7

we considered half the limits of Table 1.3 for both extension and flexion. This is obviously an approximation because the rotation limit ratio between flexion and extension probably varies for each FSU.
The displacement evaluations and graphs were not directly used in injury assessment but were useful for comprehending the behaviour of the vertebrae and for verifying that they move compliantly to what is expected for a frontal impact.
Figure 5.23 shows the maximum angles and the upper and lower limits of each FSU (calculated with standard deviation). C1-C2 is the only FSU where the maximum angle is lower than the lower limit; C2-C3 and C4-C5 rotations are slightly greater that their relative reference limit (see Table 5.12). C5-C6 and C6-C7 rotations are both greater than their reference limits with C6-C7 that exceed the upper limit. Therefore, it is very likely that fracture will happen in these vertebrae. Figure 5.22 shows the vertebrae that are expected to fracture with colors from yellow to red (increasing probability of fracture).
These results are not coherent with the ones found previously. Therefore, the next section is going to be useful to understand which criteria is more accurate and which one has to be modified.

5.3 Plastic deformation on cervical vertebrae

Lately, several studies correlated plastic strain levels with bones fracture. These studies can be applied in crashworthiness, for injury assessment. In fact, FE model are capable of evaluating the plastic strain in every part of the model at each time step. Therefore, it is possible to take advantage of this feature by visualizing the vertebral plastic deformation during the crash numerical simulation. The plastic strain values (ϵ) are confronted with a limit value that has been chosen equal to 2% as disclosed in the Chapter1.3.3. The criteria refers to the cortical part of the bones.
Because of the fact that the focus of this chapter will be vertebral plastic strain,

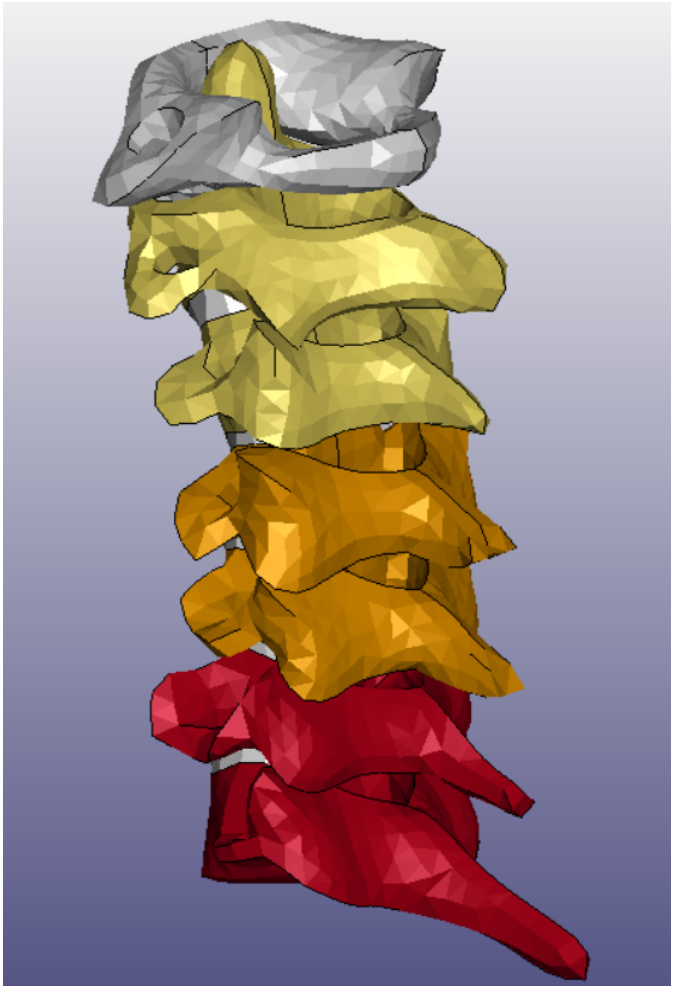

Figure 5.22: Vertebral expected fractures according to RoM

here below are reported the main feature of the FE model of the cervical bones. Each vertebra is composed of four part; two parts are composed of solid elements (one part for the left half and one part for the right half of the vertebra) and two parts are composed of shell elements and cover the surfaces of the solid parts. Given that the assessment has to be performed on the cortical bone, the focus has to be on the shell elements. The main feature of the shell parts are listed below:

- The section card is: SECTION_SHELL with ELFORM=16[16] (fully integrated shell element)
- Density equal to $2e^{-9}ton\backslash mm^3$
- Young modulus equal to $1.302e^4MPa$
- Yield stress equal to $80MPa$

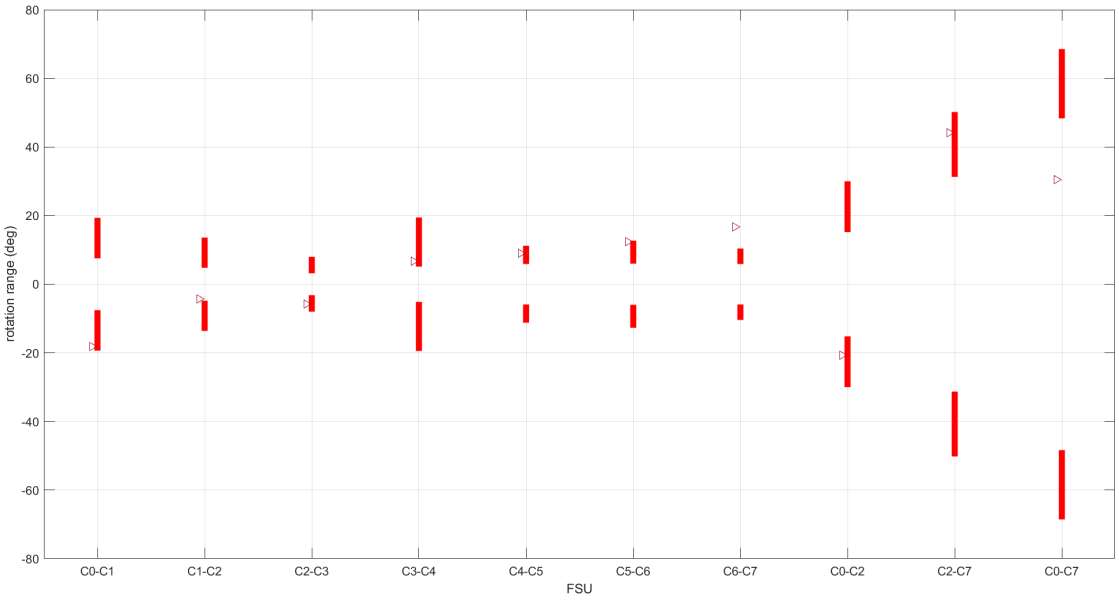

Figure 5.23: Range of motion bar chart with maximum measured values (purple triangles)

- Second plastic strain of 0.003 corresponding to a second yield stress of $110MPa$
- Third plastic strain of 0.015 corresponding to a second yield stress of $120MPa$
- strain rate parameter C equal to 360.7[17]
- strain rate parameter P equal to 4.605[17]

The effective plastic strain have been visualized in the post-processing environment where the strain values can be visualized through element coloration. The maximum of the fringe range has been set to 0.02 because it is the strain value that should cause bone fracture. In Figure 5.24 are shown two examples (complete set of figure in Appendix A.3).
This type of visualization permit us to do an overall evaluation of the strain throughout the entire simulation. Nevertheless, it is not very practical. It is not possible to analyse data by just looking at the figures. In order to obtain other information such as the number of elements that pass the threshold, a MatLab® script has been implemented. This script analyses an ASCII output file that contains elements' ID and elements' plastic strain. Then, it provide the following graphs:

- Maximum plastic strain
- Percentage of elements that exceeded the threshold
- Percentage of plasticised elements

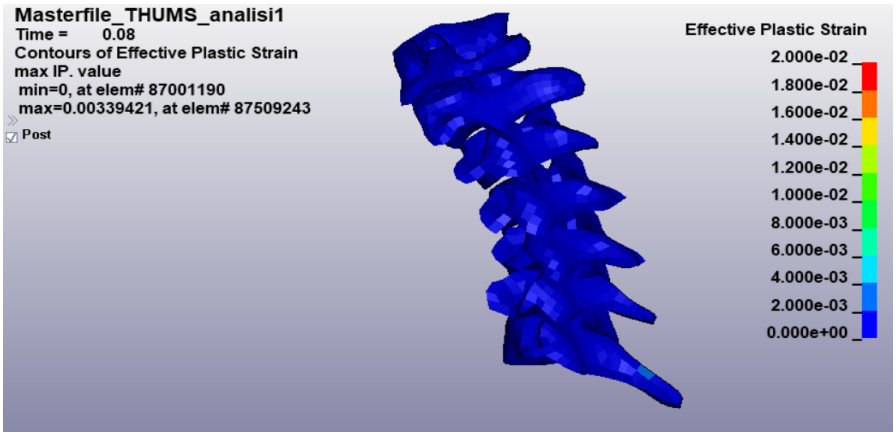

(a) Plastic strain at 80ms

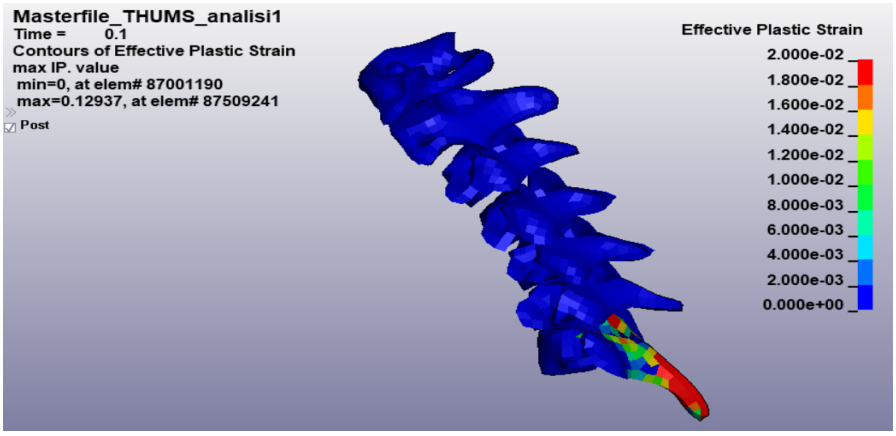

(b) Plastic strain at 100ms

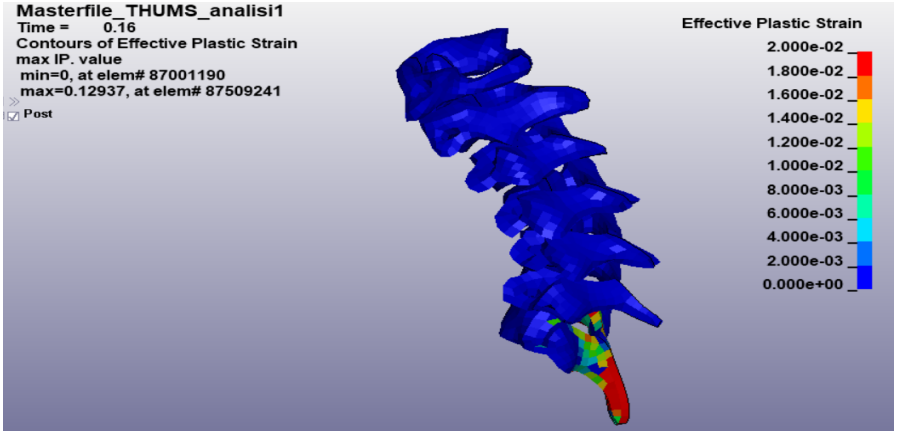

(c) Plastic strain at 160ms

Figure 5.24: Effective plastic strain of the cervical vertebrae visualized in the post-processing environment

- Average strain of plasticised element
- Average strain on each vertebra

The MatLab script can be found in Appendix B. Some example of the aforementioned graphs are reported in Figure 5.25. The first time instance that is here shown is $80ms$.
Figure 5.24 does not display any element with a plastic strain superior to 2%. In fact, the maximum plastic strain is equal to 0.34% and is measured on C7. Therefore, in this case there is not fracture on the vertebrae. The percentage of plasticised elements is quite low 8% and the average strain of the plasticised element is under 1%. Hence, it is possible to assert that the vertebrae are not very loaded at $80ms$.
Figure 5.25 shows that some element of C7 have passed the strain limit at $100ms$. It is interesting to notice that θ_y reaches an angle of 12 degrees at around $90ms$. This angle is higher than the limit angle defined in the RoM (if the standard deviation is considered). Therefore, we expect that some element of C7 have passed the threshold at $90ms$. The graphs are shown in Figure 5.26.
As was expected, some element of C7 passed the limit strain. The maximum ϵ of C7 is around 10%. The percentage of element that passed the threshold is around 7% in C7. It interesting to notice that some element of C6 became plasticised at $90ms$ as it is possible to see by looking at the graphs.
In the previous chapter, we found out that also the relative rotation between C5 and C6 almost reaches the upper limit values of RoM. This happens at around 160ms. Hence, it is interesting to look at the graphs for the time-step of interest and check if a fracture happens as expected. The graphs are reported in Figure 5.27.
As was expected, fracture is found in C6, too. The percentage of elements that have failed is low (2%) in C6. The ϵ has reached its maximum value in C7 and the number of failed element is high (13%). It is interesting to notice that all the vertebrae, except C1, has plasticised elements. In particular, C7 has more than a half elements that are plasticised.
Overall, a good correlation have been found between the RoM and the plastic strain injury criteria. On the other hand, some of the limit loads found for vertebral sections seems too conservative or not enough conservative. For instance, C7 is expected to fracture at $160ms$, because the limit flexion moment is almost reached at that time. Nevertheless, it fractures at $90ms$ in both RoM and plastic strain injury criteria. Therefore, a more suitable value for the limit load should be, for instance, around $50000Nmm$. On the contrary, the axial load limits indicates that a fracture should happen in C3, C4 and C5, but that is not shown plastic strain. Therefore, as said before, traction load limits are probably too conservative.

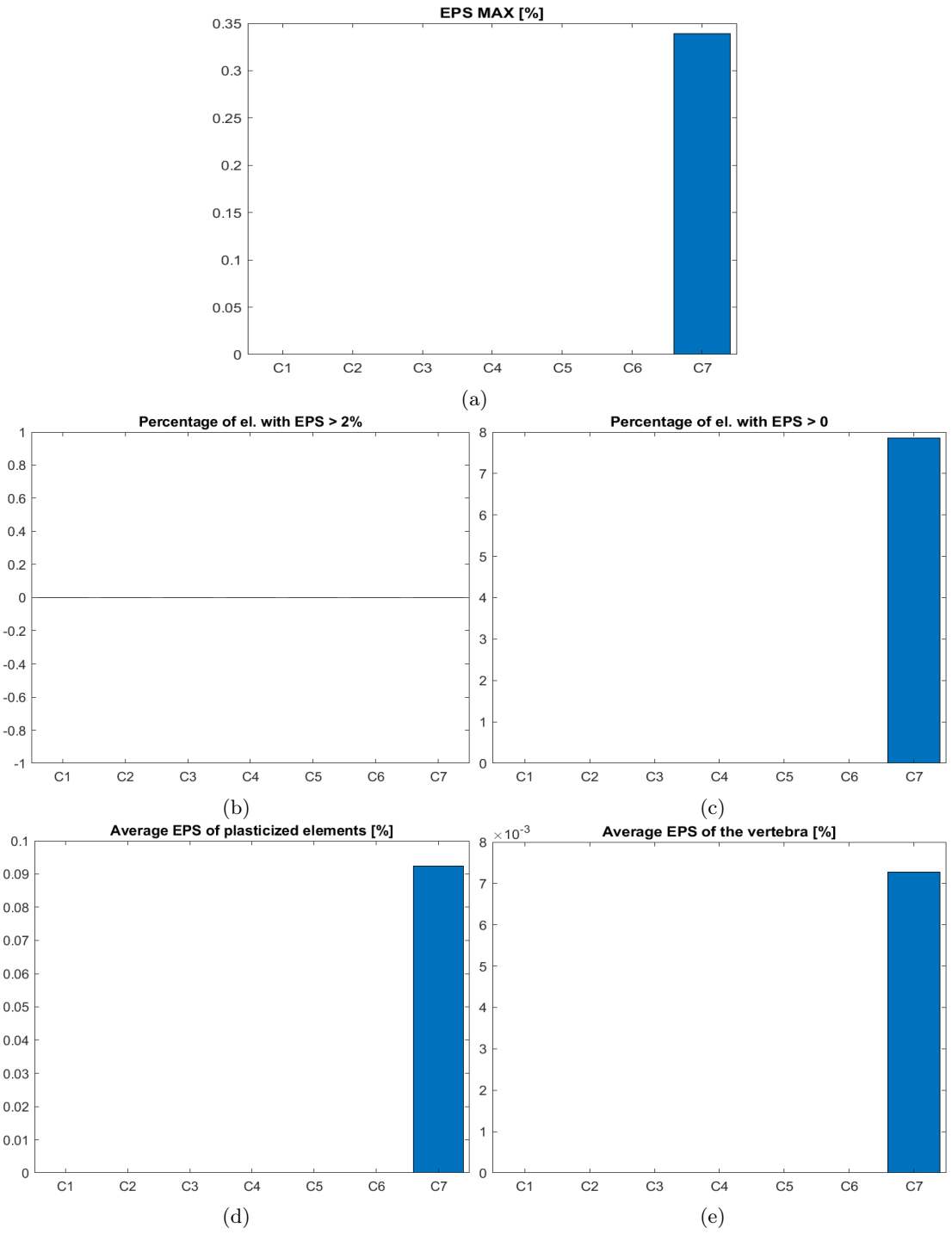

Figure 5.25: Plastic strain on vertebrae graphs; $80ms$

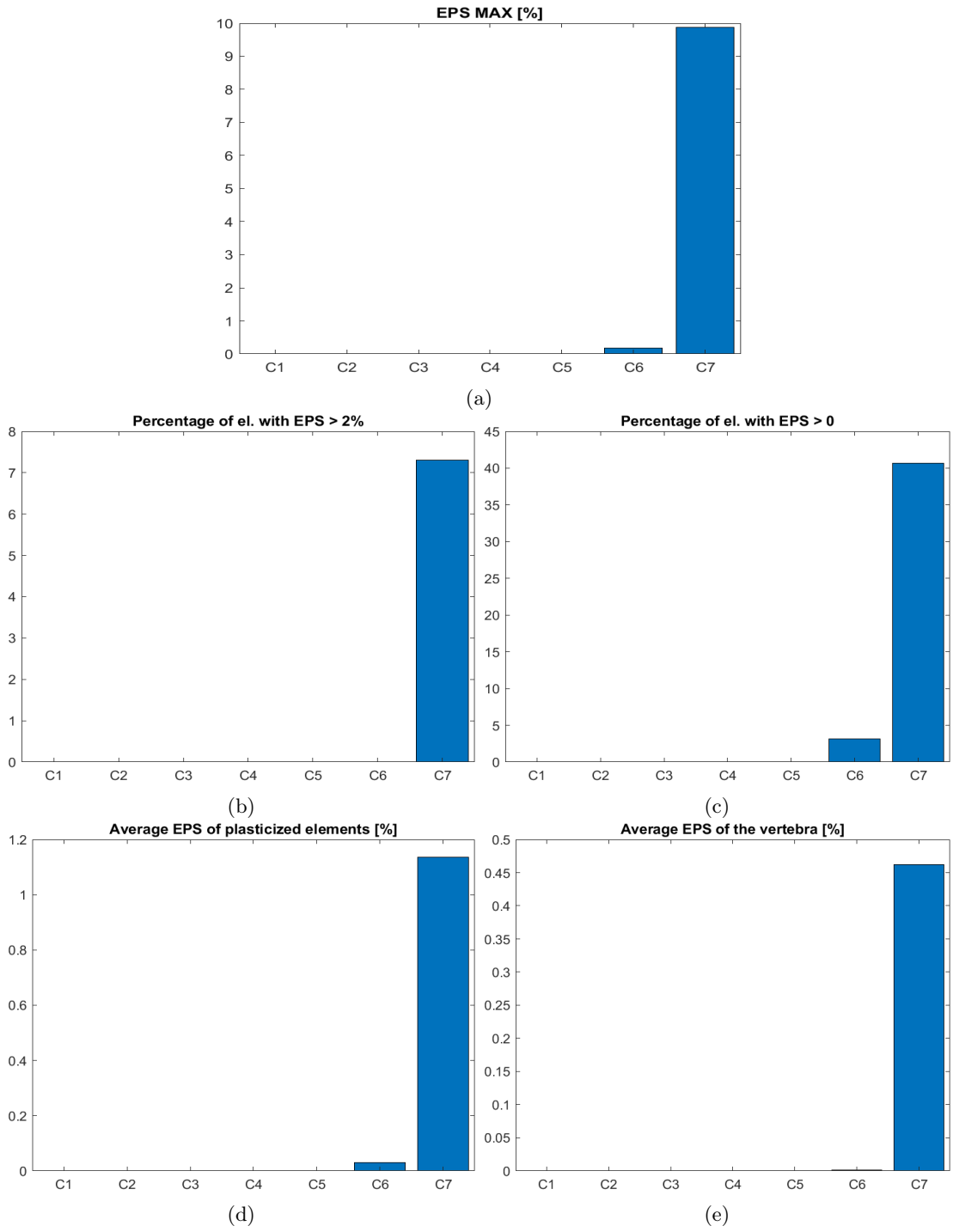

Figure 5.26: Plastic strain on vertebrae graphs; $90ms$

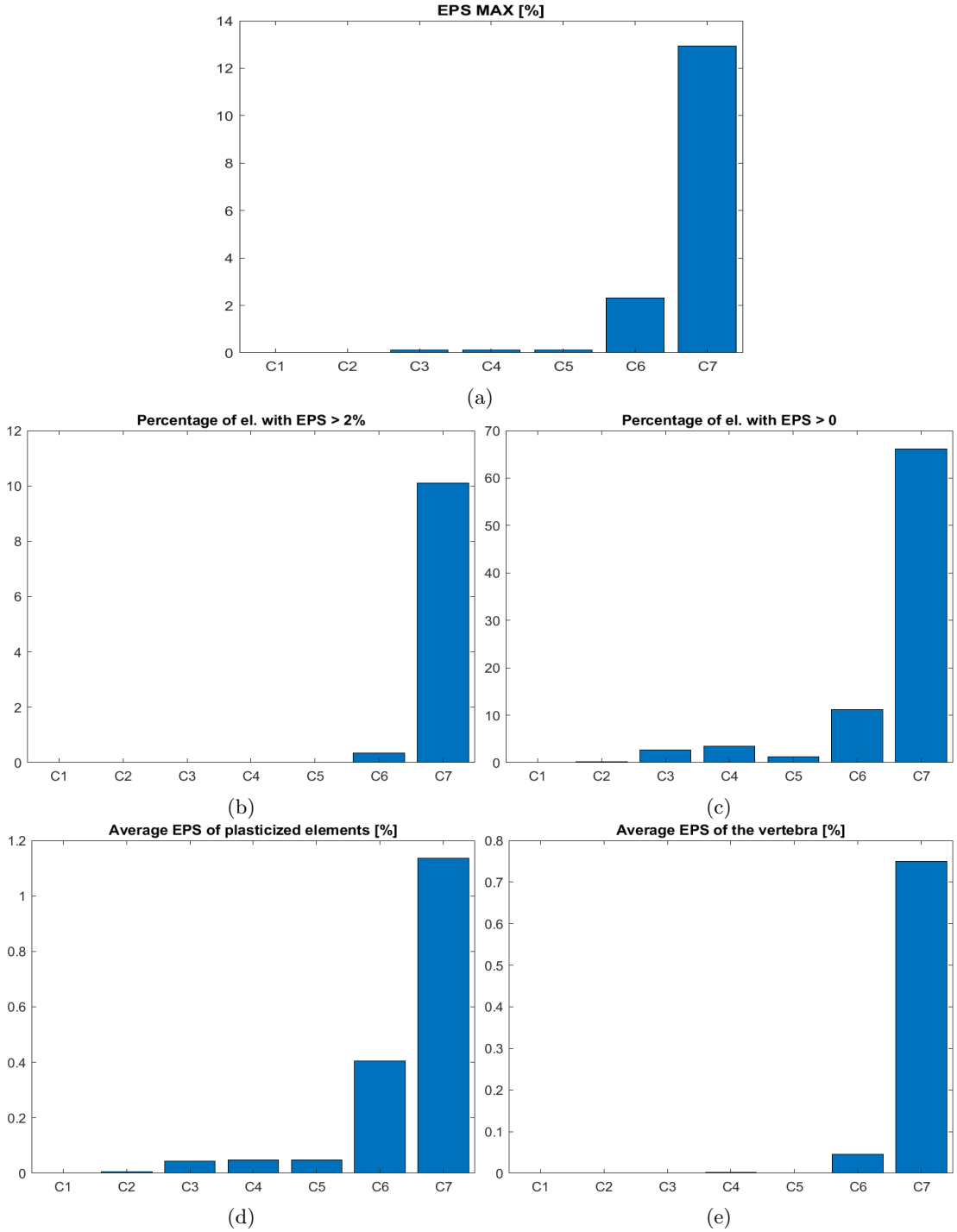

Figure 5.27: Plastic strain on vertebrae graphs; 160ms

Figure 5.28: Vertebral expected fracture (highlighted in red) according to plastic strain limit

Chapter 6

Conclusion and future development

6.1 Conclusion and discussion

This thesis was focused on developing feasible methods to assess neck injury on THUMS for frontal impact crashes in particular. The considered crash test simulated a possible car crash in motor sport (e.g. rally). However in the last chapter were analysed procedures for assessment of injury in every type of crash.
In Chapter 4.2.4 the fact that Hybrid III's neck is stiffer than THUMS' neck[14] has been confirmed. The force on Hybrid III upper neck section was almost twice the forces measured on the THUMS' vertebral sections. The extension moment was five time greater than the extension moment measured on C1-C4 and the flexion moment was two-three times the flexion moment moment on C6-C7. Moreover, we found information on the load distribution between the different neck part. THUMS is a HBM so the results that it provides are obviously different from the Hybrid III's and have to be compared with some scale factor.
THUMS biofidelity is higher than Hybrid III. That is why it is important to find criteria for performing injury assessment directly on it. In the first part of Chapter 5 we however attempted to find three limit loads per vertebra (traction, extension and flexion) by using the Nij criterion and Hybrid III loads as a reference. The found limits were satisfying to a certain degree. Nevertheless, the used method is affected by several limitation, with the most important that are related to the fact that the two compared model are very different, indeed. Moreover, the found limits are dependent on boundary conditions and cross-sections definition. The THUMS' different crash speed simulations suggest that the vertebral forces are linked to the head acceleration, meanwhile the moments are mostly linked to the head motion as the peaks are reached later in time, but have similar magnitude.
In the second part of the aforementioned chapter, the focus was the injury assessment through medicinal and human biology studies. Two criteria were analysed (RoM and effective plastic strain limit) and provided coherent results. Some of the previously defined vertebral load limits were confirmed by these later results.

The modification of other limits were proposed because they were too conservative (traction) or the contrary (flexion in C7). In fact, the vertebral limit loads assessed injury on C3, C4 and C5, but RoM assessed probable fractures on C6 and C7, with fracture in C3, C4 and C5 that were less probable. Finally, effective plastic strain evaluation assessed fractures in C6 and C7.
This work highlighted the importance of taking advantage of FEA's features such as the possibility to measure physical quantities in all the model at every time-step. Therefore, criteria based on measurement of strain and stress on entire parts or on the calculation of relative movement are the most suited for HBM injury assessment.
THUMS biofidelity is very important for studying the human body behaviour during crashes. However, it has to be noted that the version 4.02 of THUMS that we used behave as a human cadaver and not as an alive human being. There is no muscle activation given by human reaction to the incoming crash. Nevertheless, THUMS permits to measure physical quantities that are not measurable during PSHS test.

6.2 Future development

Even considering the method limitation, the limit loads found for vertebral section was satisfying, but could be further refined. For example, it could be interesting to perform different analysis while changing several parameter and then re-define the limits using statistical tool. As regard RoM, it would be interesting to define rotation limit for both extension and flexion that were not approximation in order to be more precise in the injury assessment.
THUMSv4.02 is not provided with muscles activation, so the numerical simulation described in this thesis are similar to PMHS tests. The muscular activation is necessary for simulating the actual behaviour of the occupant during a car crash. However, muscular activation time and forces are difficult to evaluate correctly. In fact, the occupant response to crash depend on several factor such as reflexes, attention etc. THUMSv5 and following versions have the possibility to implement muscle activation and should be studied for better understanding the human body behaviour during car accident.
Despite the improvement of numerical simulation and HBMs, it is unlikely that experimental test and certification test won't be performed in future. Nevertheless, it is not feasible to perform tests on volunteer as in the early work of Col. Stapp and nowadays most popular mannequin, Hybrid III, is not totally comparable to a human body. So it would be interesting to develop ATDs with higher degrees of biofidelity.

Appendix A

Numerical simulations' graphs and figures

In this appendix are collected all the graphs of the numerical simulation used in:

- Hybrid III validation
- RoM assessment
- Vertebral plastic strain limit assessment

A.1 Hybrid III validation graphs

Hybrid III FEA2.4

The simulation was used in Hybrid III validation. The crash pulse is equal to the pulse of the experimental crash test performed by FIA on 06/04/2017. The lap belt angle is equal to 82°.

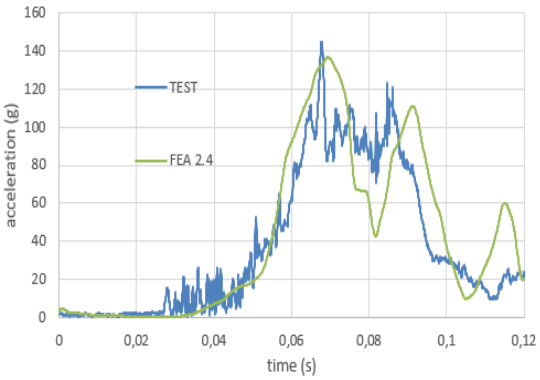

(a) Total acceleration

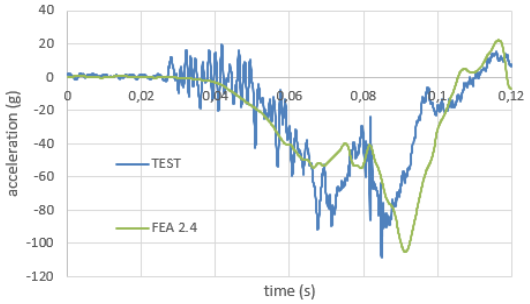

(b) X acceleration

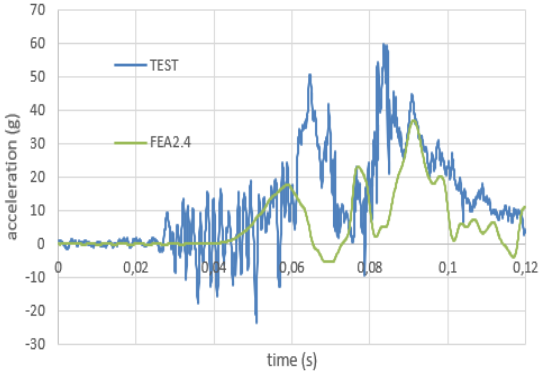

(c) Y acceleration

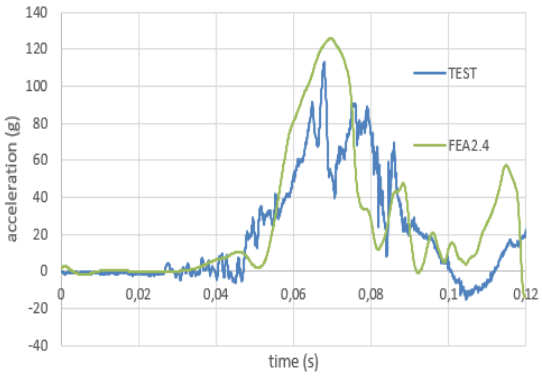

(d) Z acceleration

Figure A.1: Head acceleration magnitude; FEA2.4

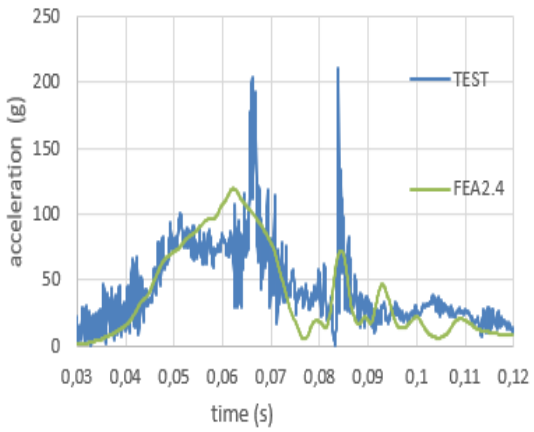

(a) Total acceleration

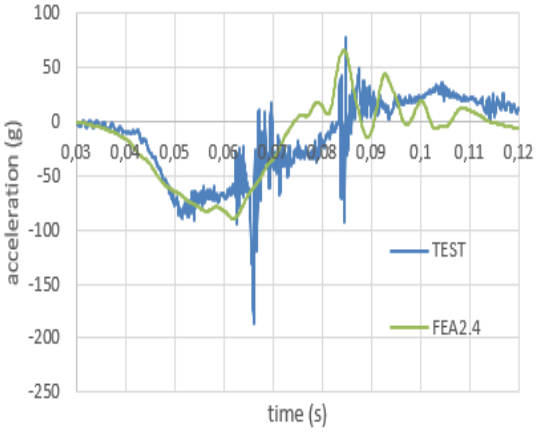

(b) X acceleration

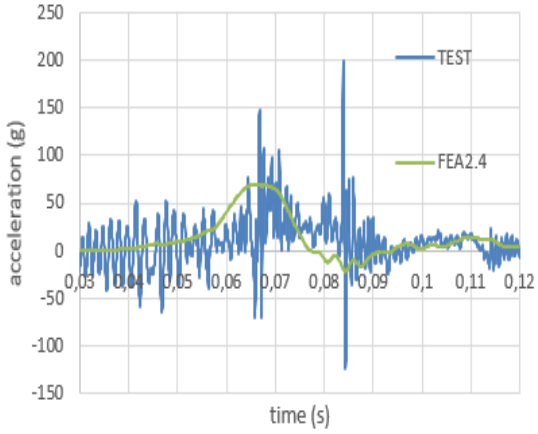

(c) Y acceleration

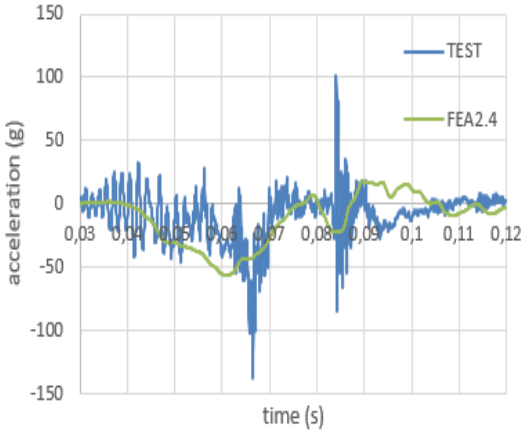

(d) Z acceleration

Figure A.2: Chest acceleration magnitude; FEA2.4

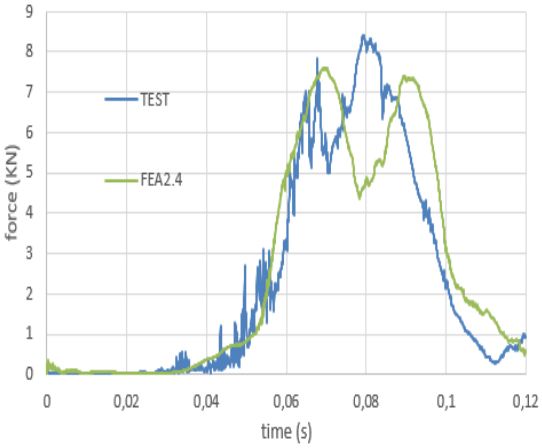

(a) Total force

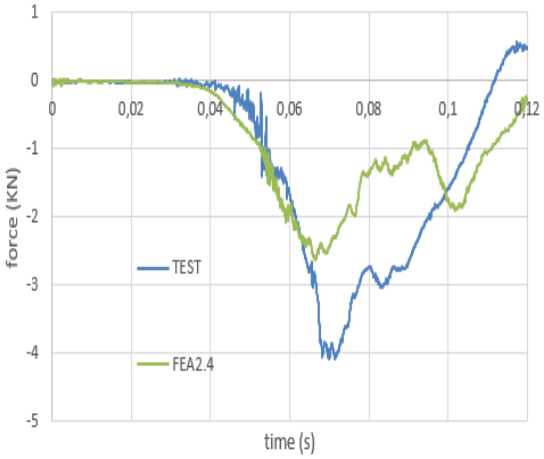

(b) X force

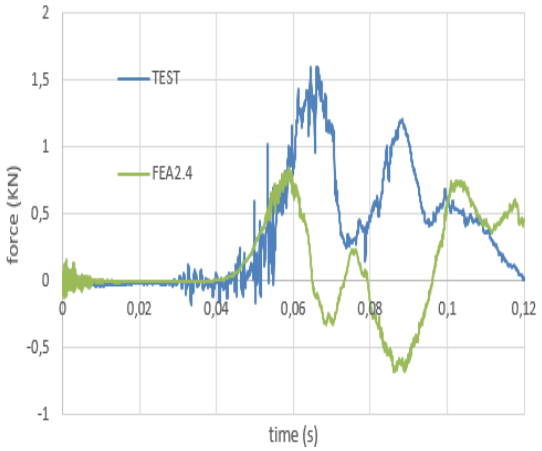

(c) Y force

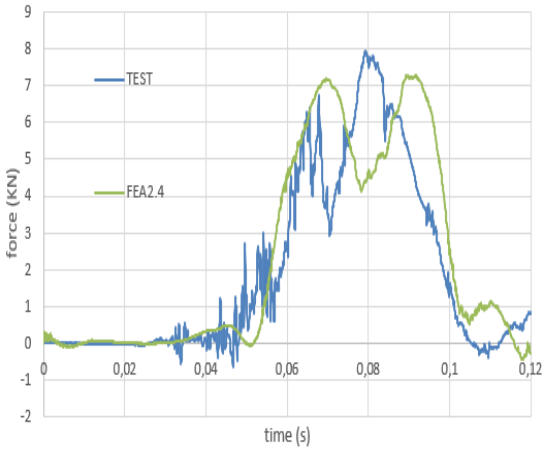

(d) Z force

Figure A.3: Upper neck section; force magnitude; FEA2.4

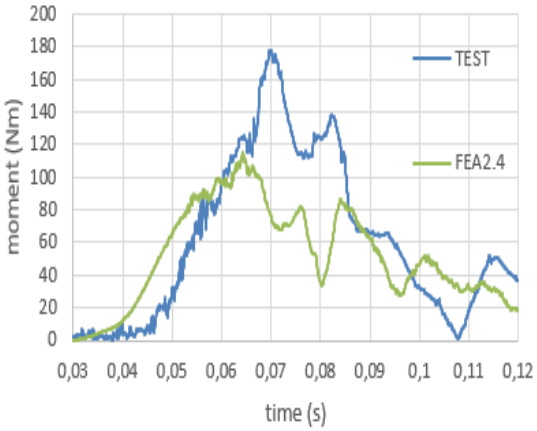

(a) Total moment

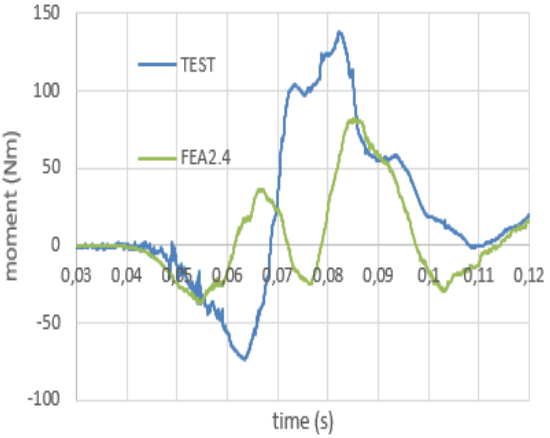

(b) X moment

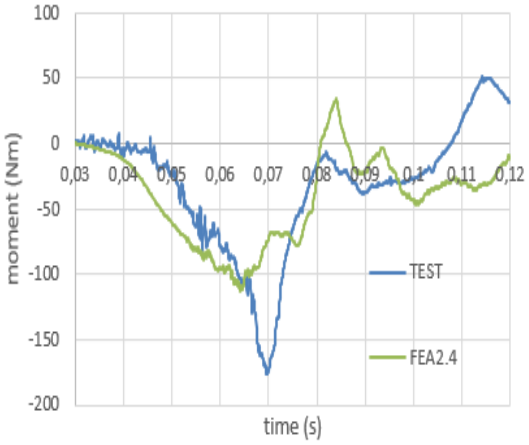

(c) Y moment

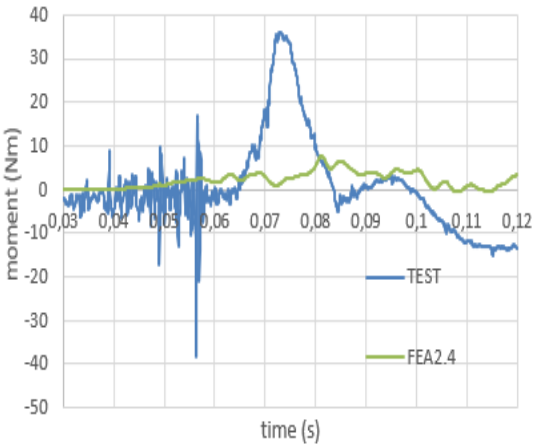

(d) Z moment

Figure A.4: Upper neck section; bending moment magnitude (sagittal plane); FEA2.4

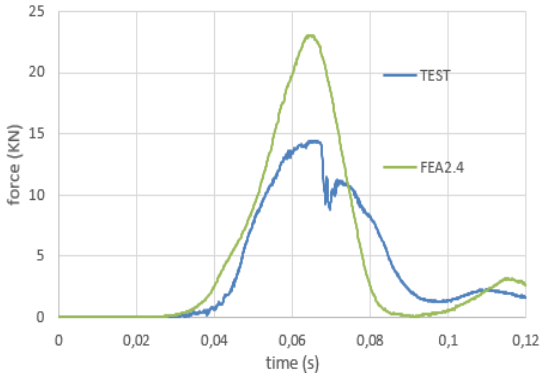

(a) Left shoulder force

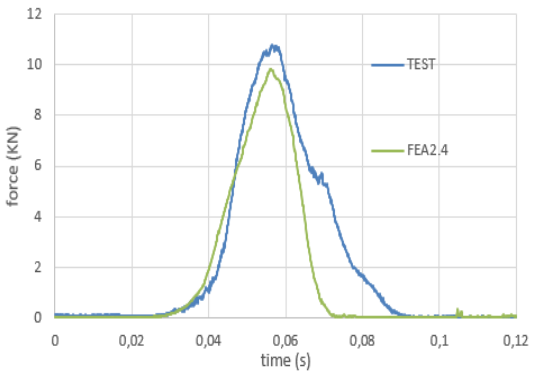

(b) Right shoulder force

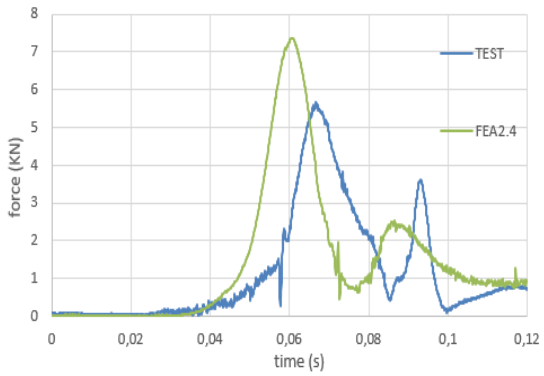

(c) Left lap force

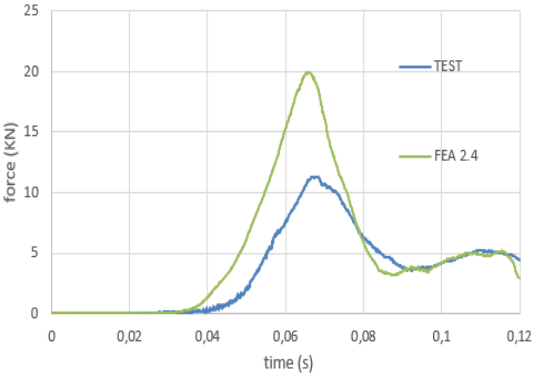

(d) Right lap force

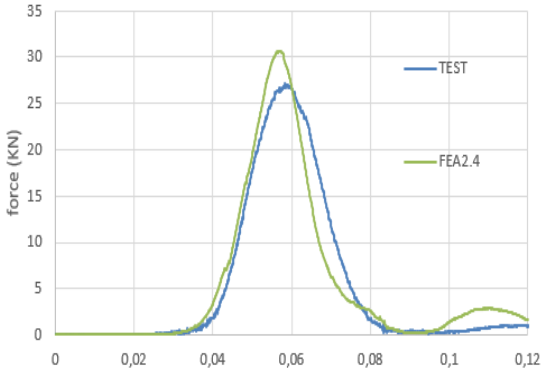

(e) Crotch force

Figure A.5: Seatbelts force magnitude; FEA2.4

Hybrid III FEA2.5

The simulation was used in Hybrid III validation. The crash pulse is equal to the pulse of the experimental crash test performed by FIA on 06/04/2017. The lap belt angle is equal to 50°.

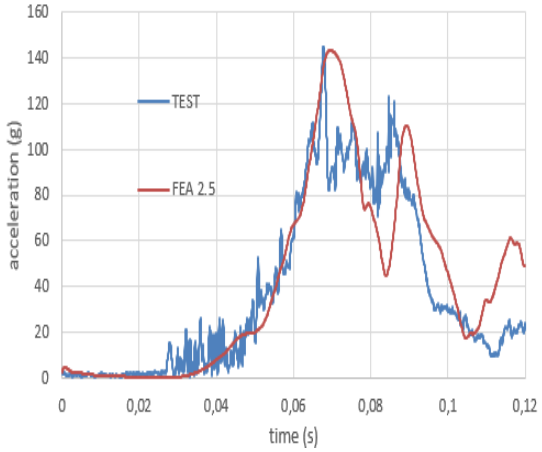

(a) Total acceleration

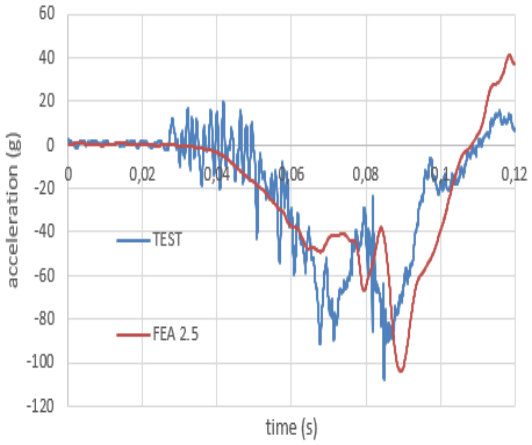

(b) X acceleration

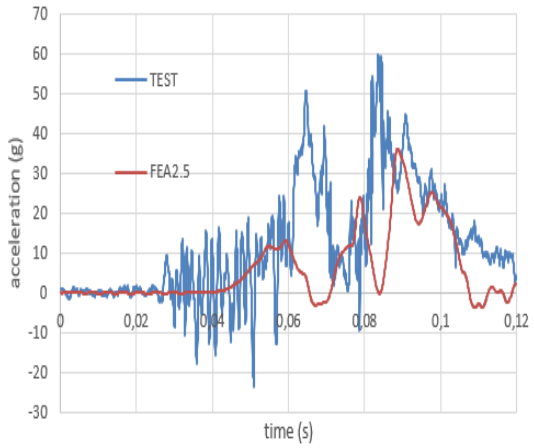

(c) Y acceleration

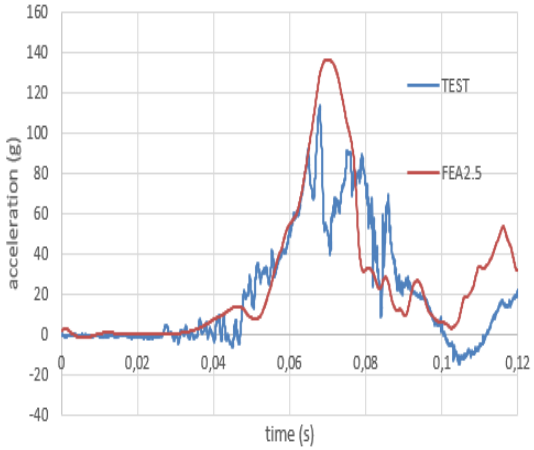

(d) Z acceleration

Figure A.6: Head acceleration magnitude; FEA2.5

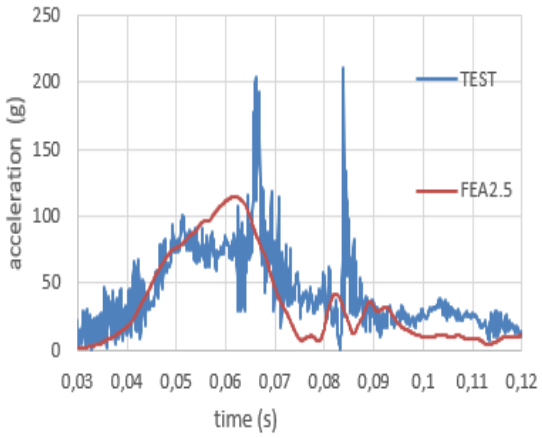

(a) Total acceleration

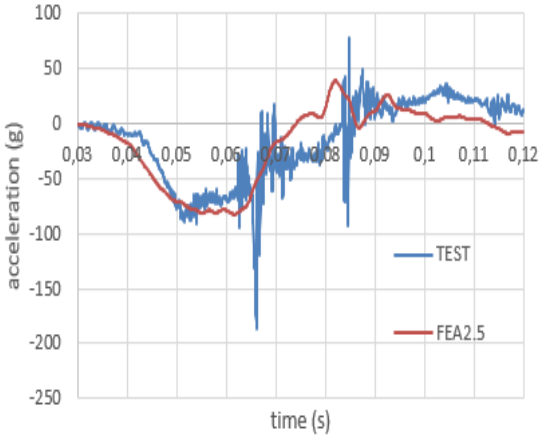

(b) X acceleration

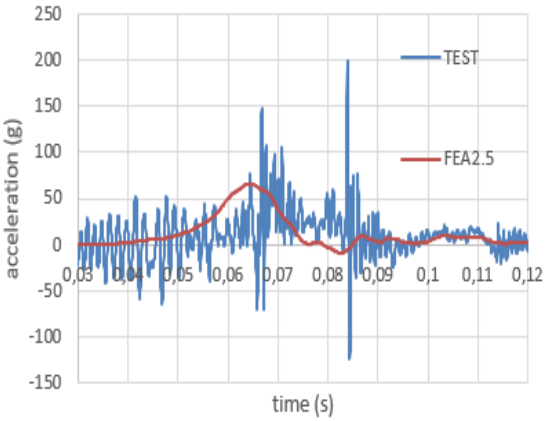

(c) Y acceleration

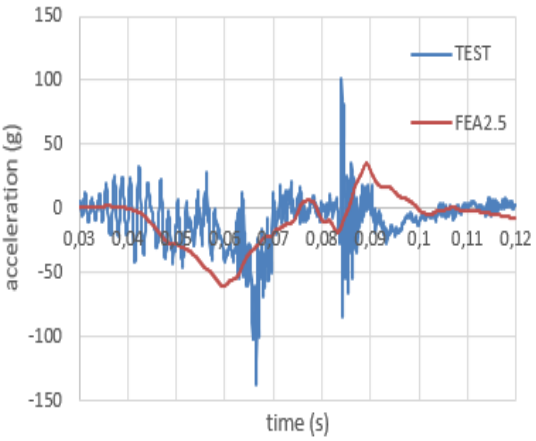

(d) Z acceleration

Figure A.7: Chest acceleration magnitude; FEA2.5

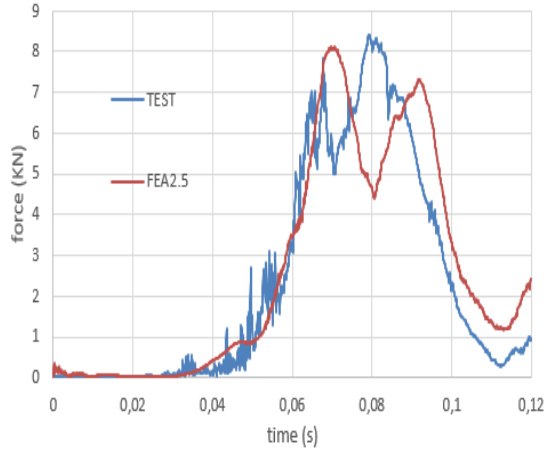

(a) Total force

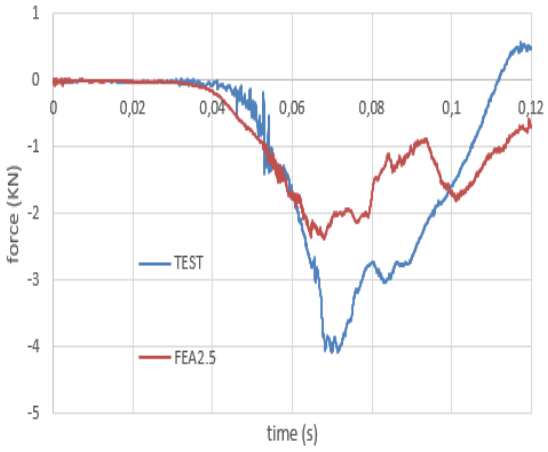

(b) X force

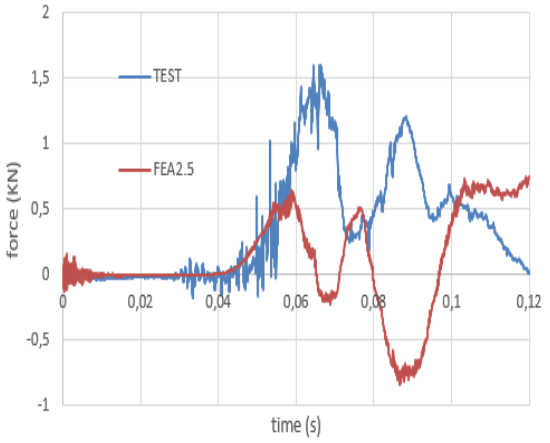

(c) Y force

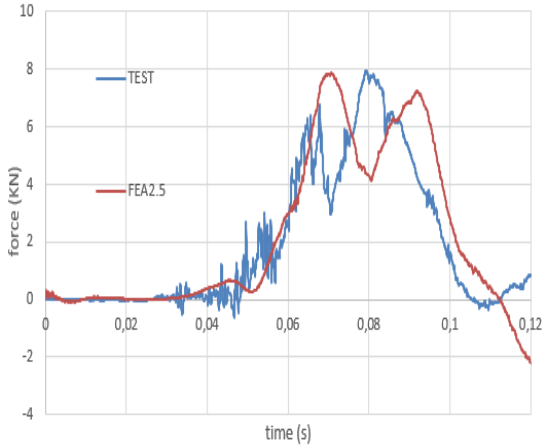

(d) Z force

Figure A.8: Upper neck section; force magnitude; FEA2.5

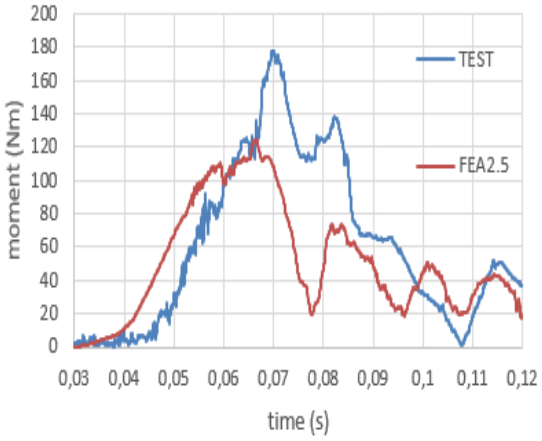

(a) Total moment

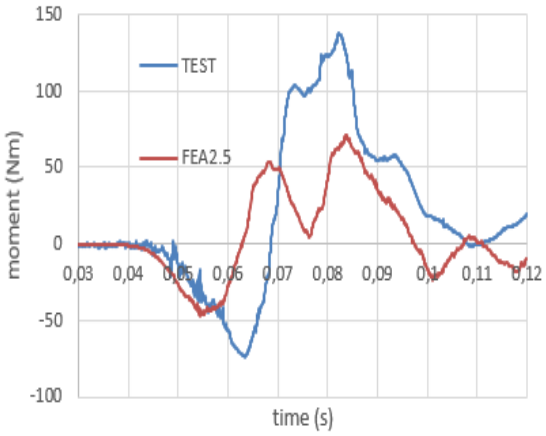

(b) X moment

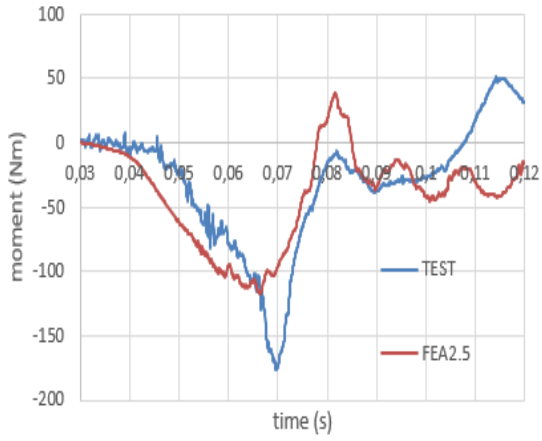

(c) Y moment

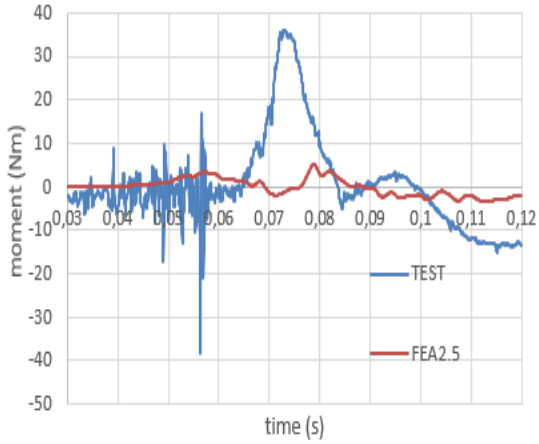

(d) Z moment

Figure A.9: Upper neck section; bending moment magnitude (sagittal plane); FEA2.5

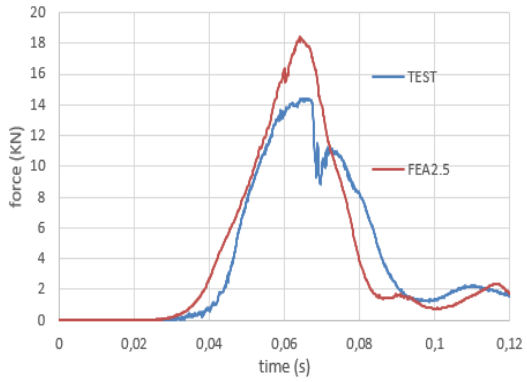

(a) Left shoulder force

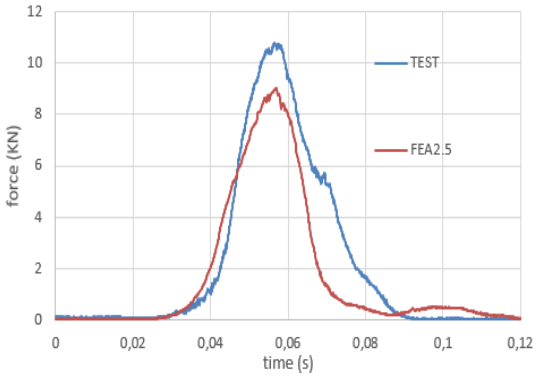

(b) Right shoulder force

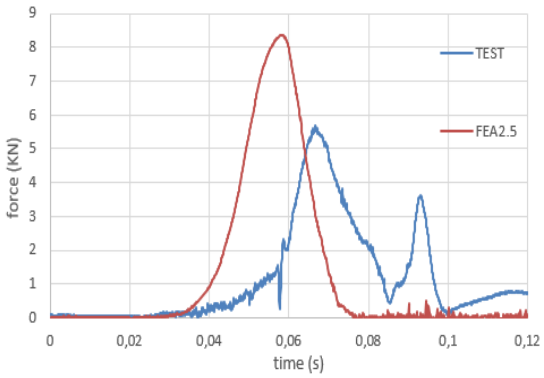

(c) Left lap force

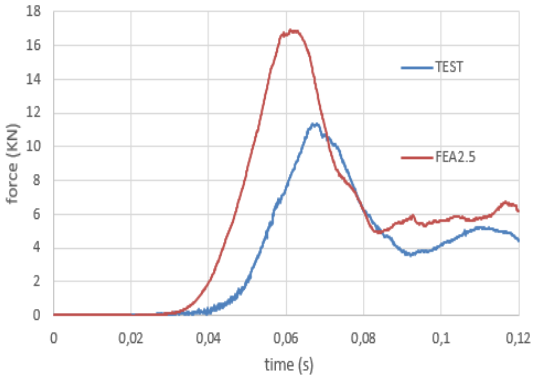

(d) Right lap force

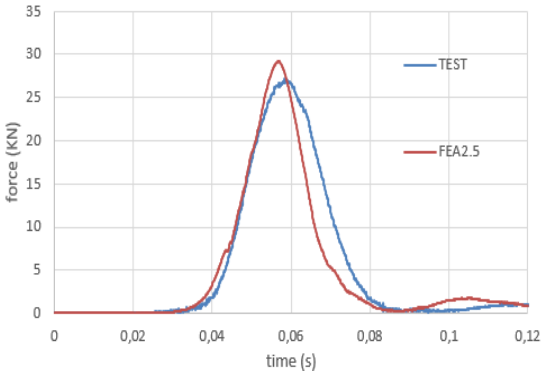

(e) Crotch force

Figure A.10: Seatbelts force magnitude; FEA2.5

Hybrid III FEA3.3

The simulation was used in Hybrid III validation. The crash pulse is equal to the pulse of the experimental crash test performed by FIA on 06/04/2017. The lap belt angle is equal to 82°. The length of the lap belt is increased of 10mm.

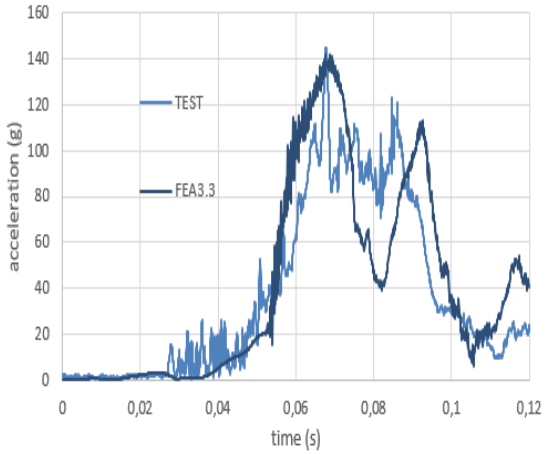

(a) Total acceleration

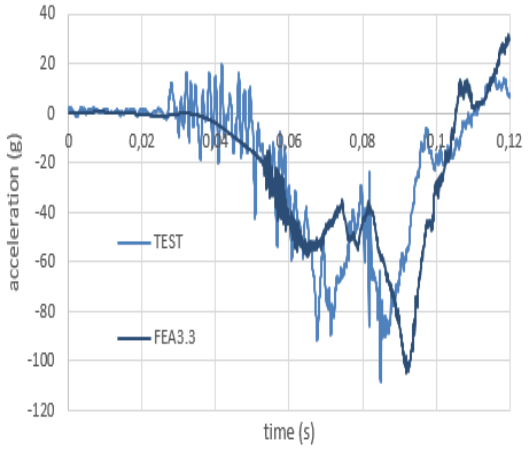

(b) X acceleration

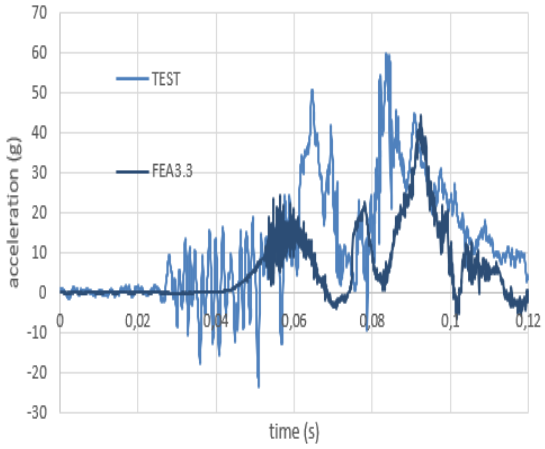

(c) Y acceleration

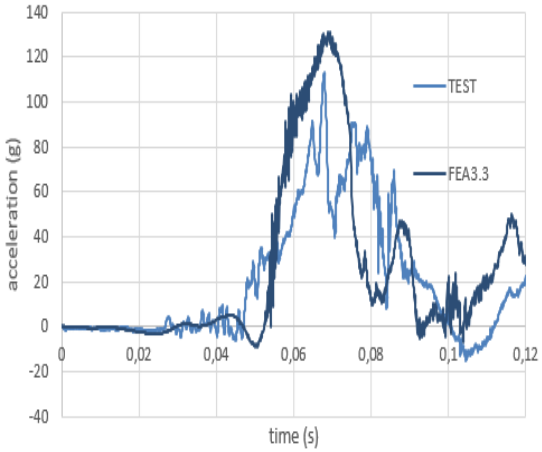

(d) Z acceleration

Figure A.11: Head acceleration magnitude; FEA3.3

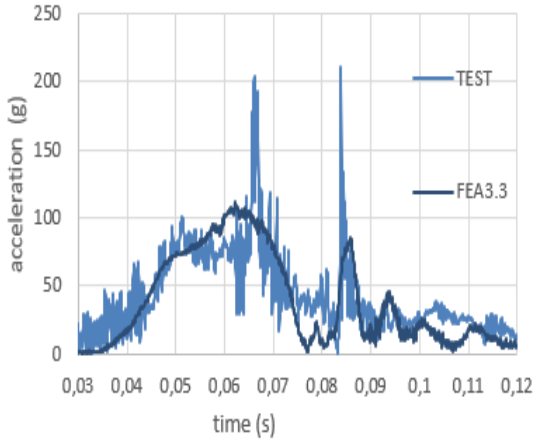

(a) Total acceleration

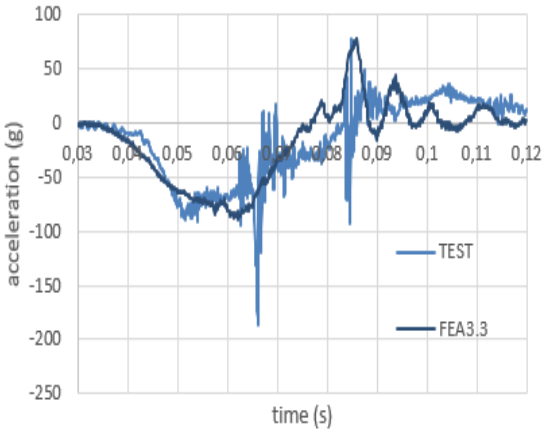

(b) X acceleration

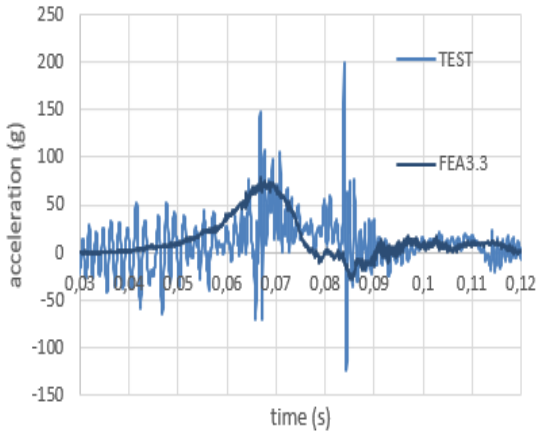

(c) Y acceleration

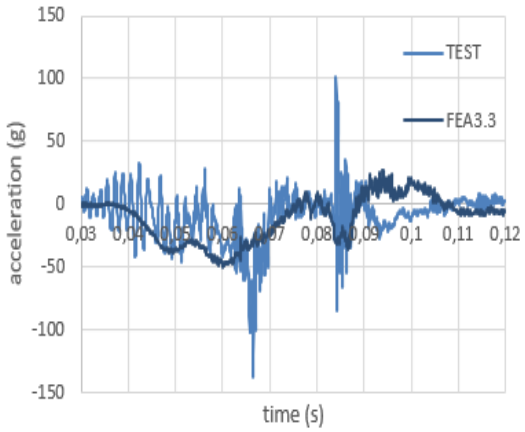

(d) Z acceleration

Figure A.12: Chest acceleration magnitude; FEA3.3

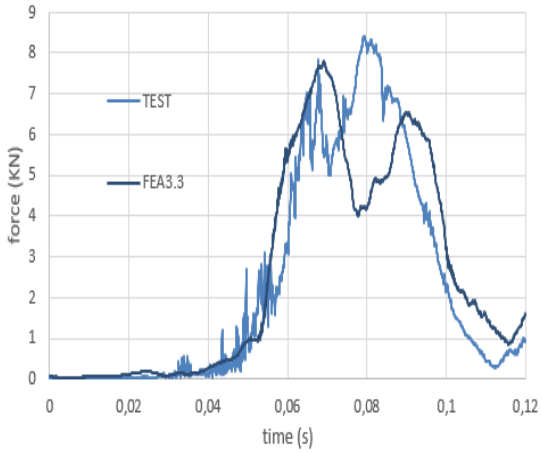

(a) Total force

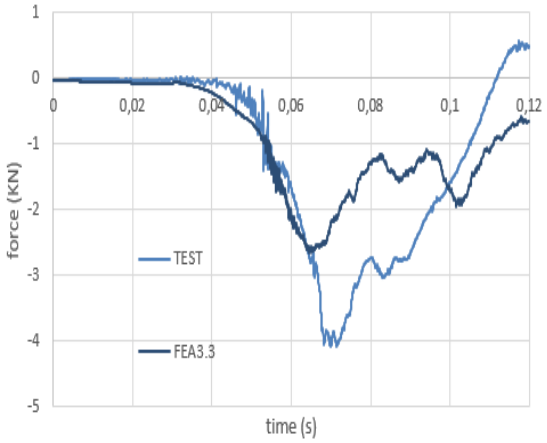

(b) X force

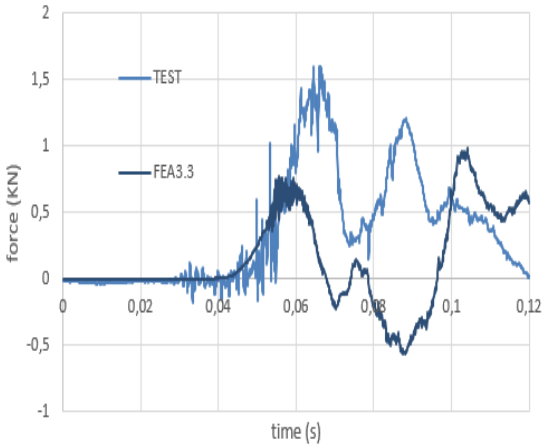

(c) Y force

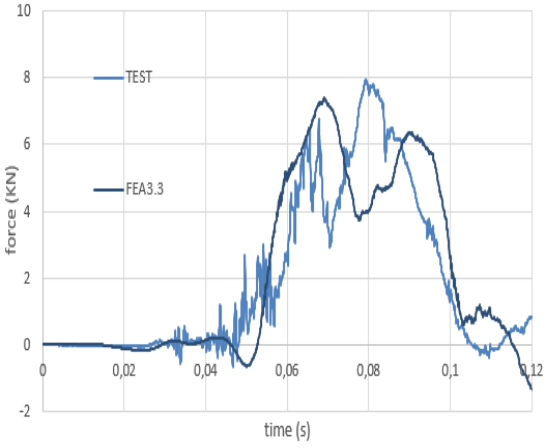

(d) Z force

Figure A.13: Upper neck section; force magnitude; FEA3.3

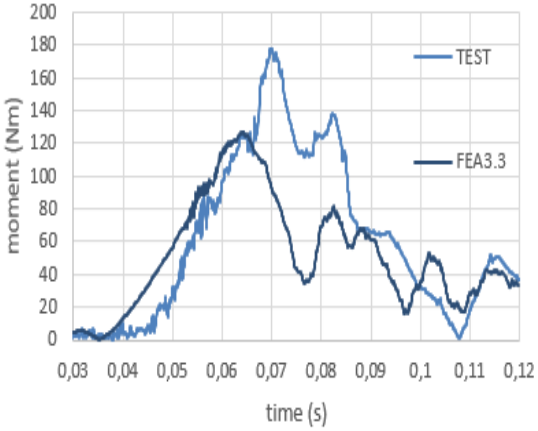

(a) Total moment

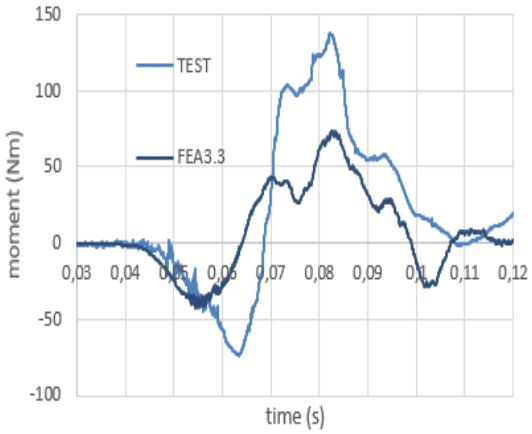

(b) X moment

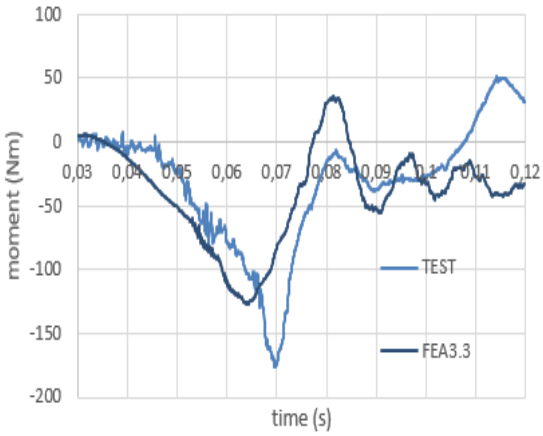

(c) Y moment

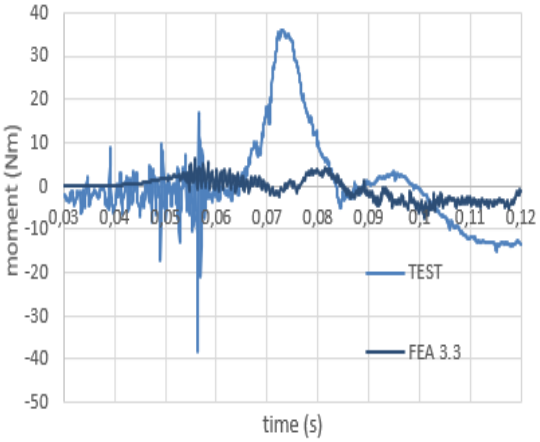

(d) Z moment

Figure A.14: Upper neck section; bending moment magnitude (sagittal plane); FEA3.3

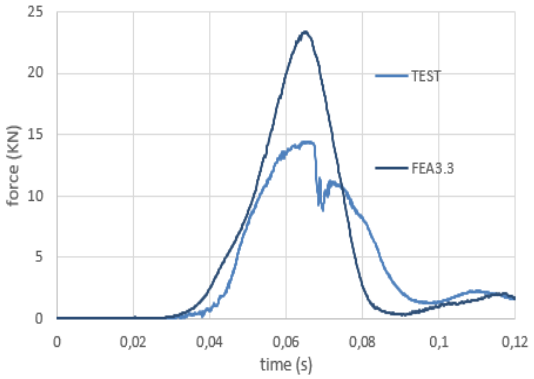

(a) Left shoulder force

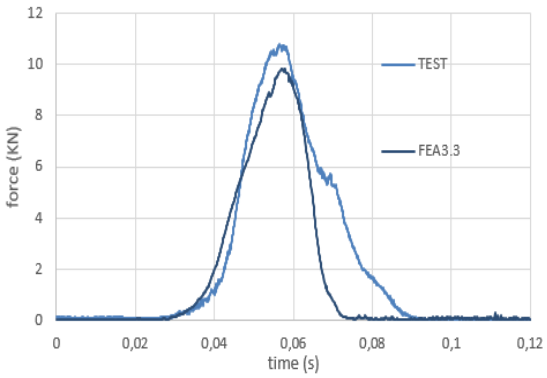

(b) Right shoulder force

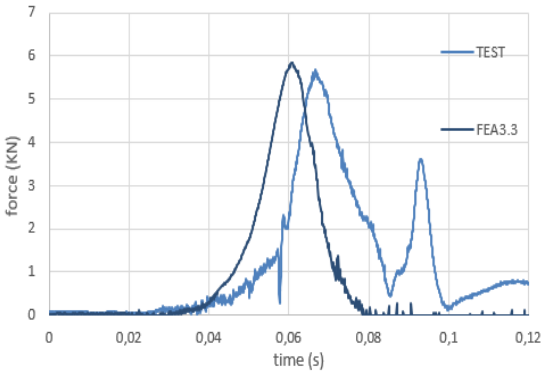

(c) Left lap force

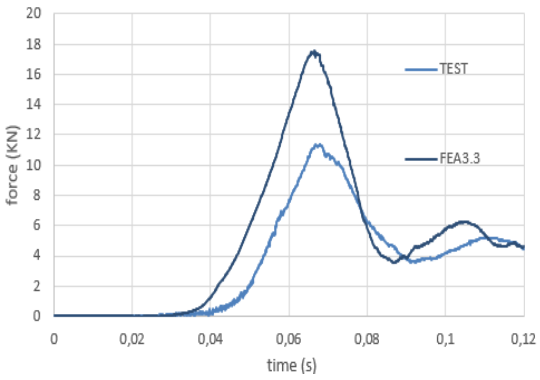

(d) Right lap force

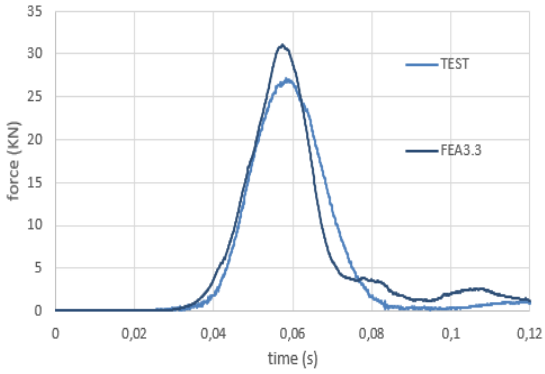

(e) Crotch force

Figure A.15: Seatbelts force magnitude; FEA3.3

Hybrid III FEA3.3LaST

The simulation was used in Hybrid III validation. The crash pulse is equal to the pulse of the experimental crash test performed by FIA on 06/04/2017. The lap belt angle is equal to 82°. The length of the lap belt is increased of 10mm. Neck model modified with LaST parameters.

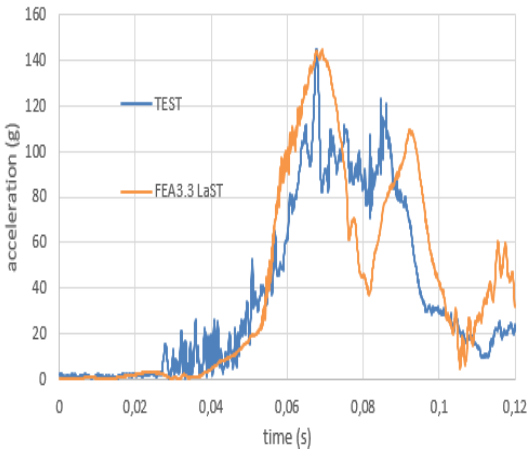

(a) Total acceleration

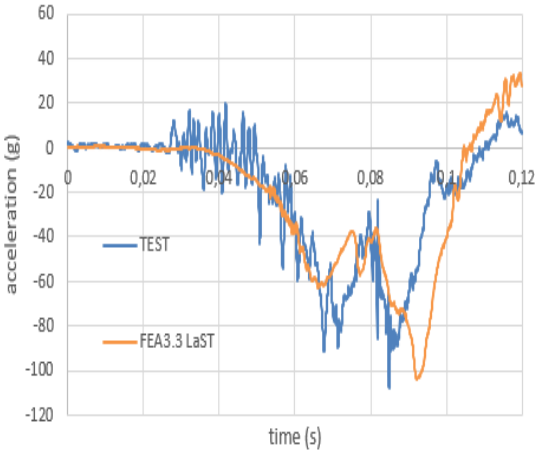

(b) X acceleration

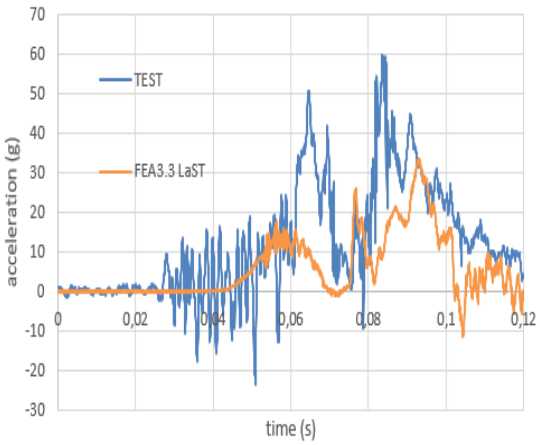

(c) Y acceleration

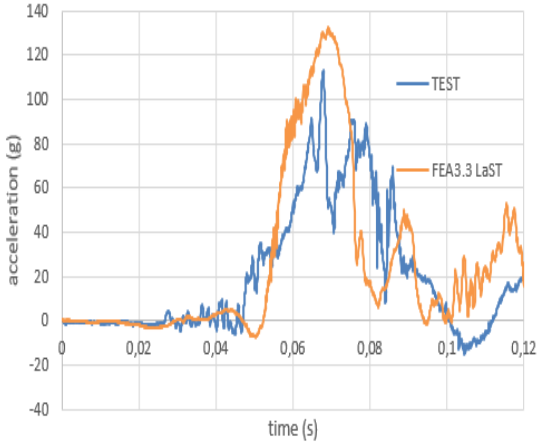

(d) Z acceleration

Figure A.16: Head acceleration magnitude; FEA3.3LaST

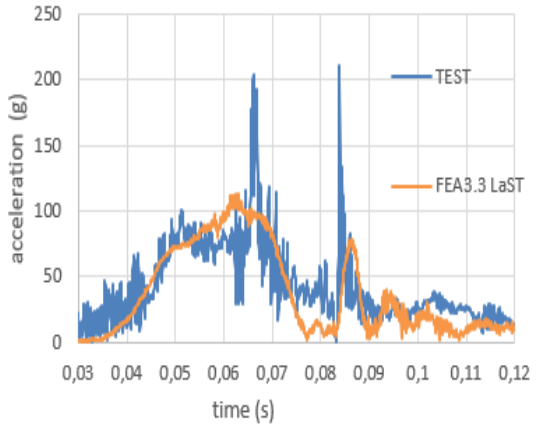

(a) Total acceleration

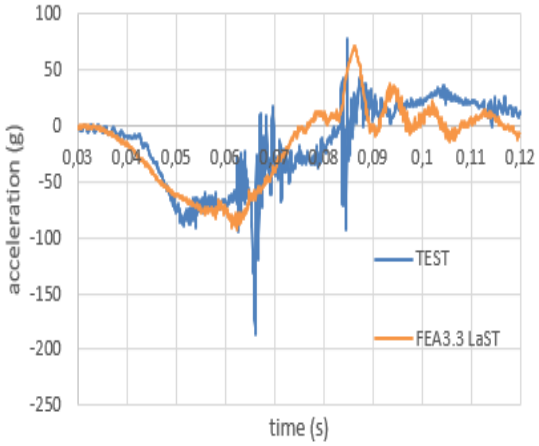

(b) X acceleration

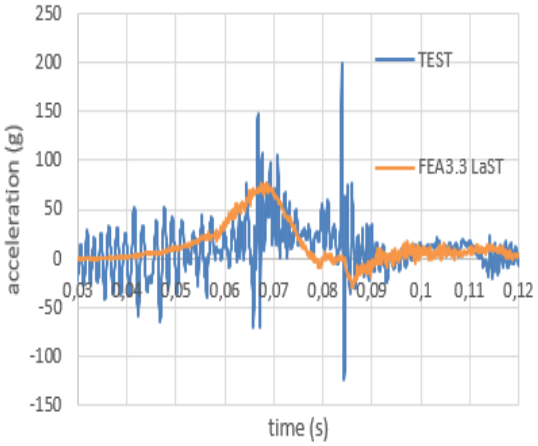

(c) Y acceleration

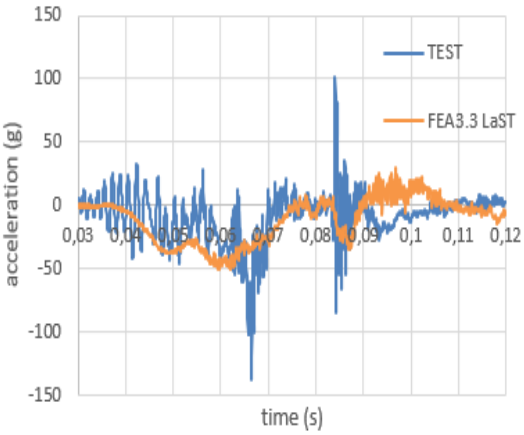

(d) Z acceleration

Figure A.17: Chest acceleration magnitude; FEA3.3LaST

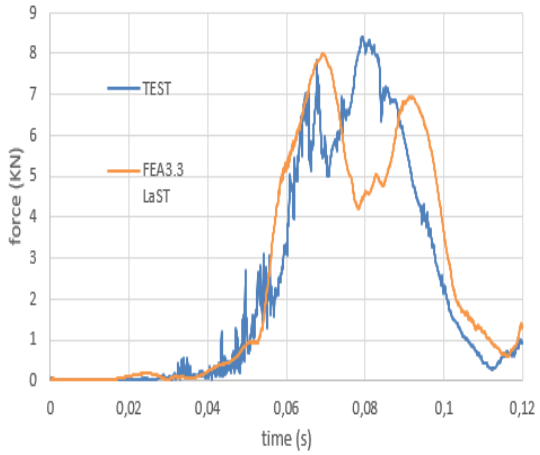

(a) Total force

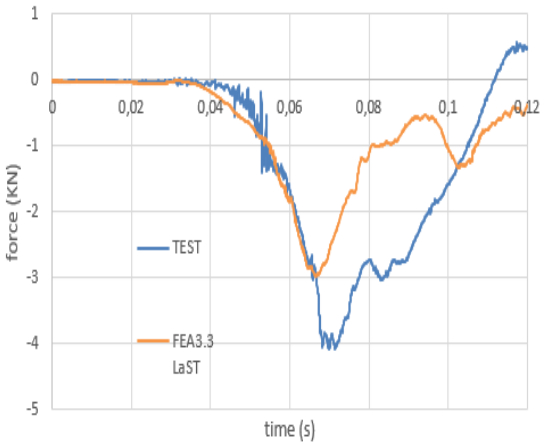

(b) X force

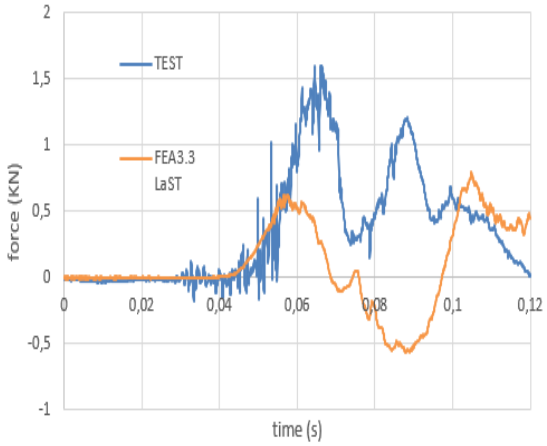

(c) Y force

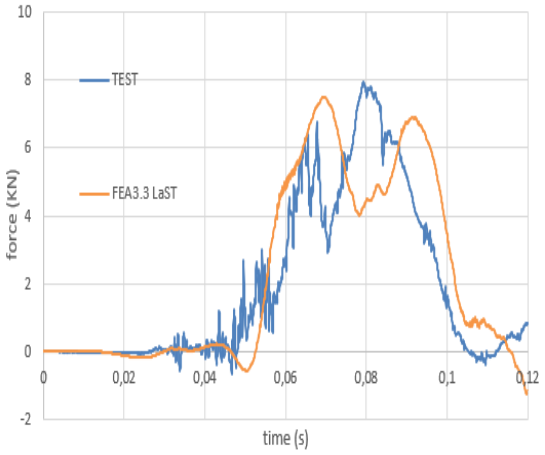

(d) Z force

Figure A.18: Upper neck section; force magnitude; FEA3.3LaST

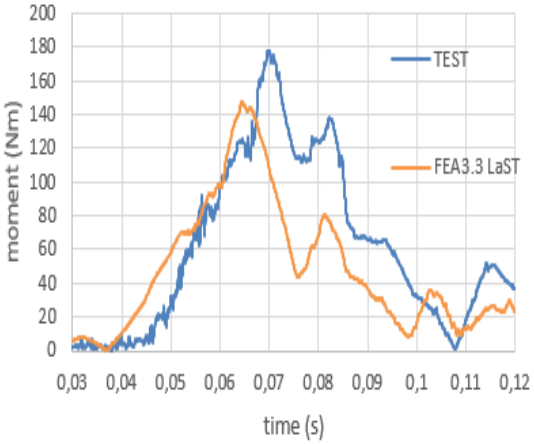

(a) Total moment

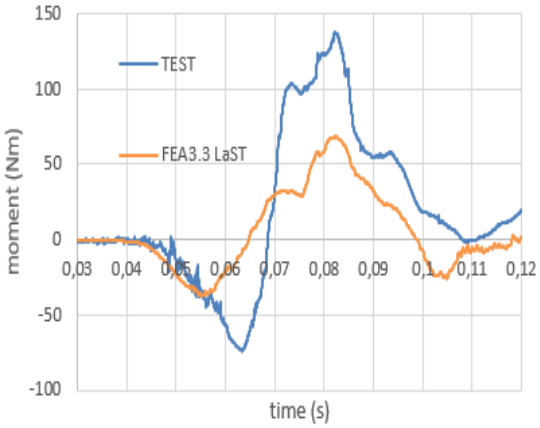

(b) X moment

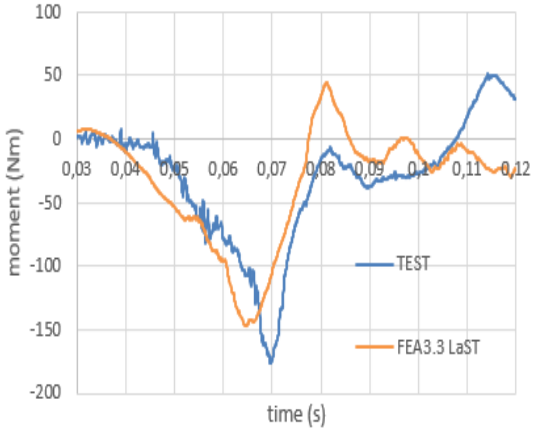

(c) Y moment

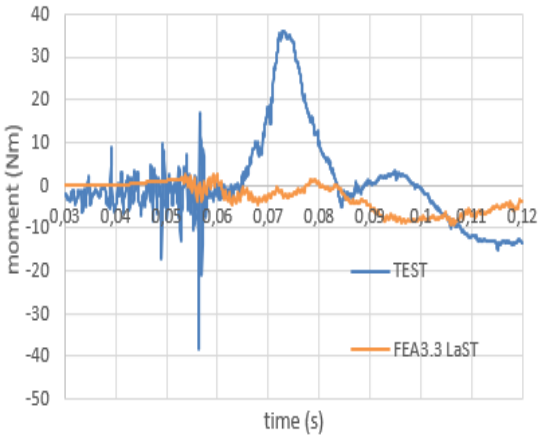

(d) Z moment

Figure A.19: Upper neck section; bending moment magnitude (sagittal plane); FEA3.3LaST

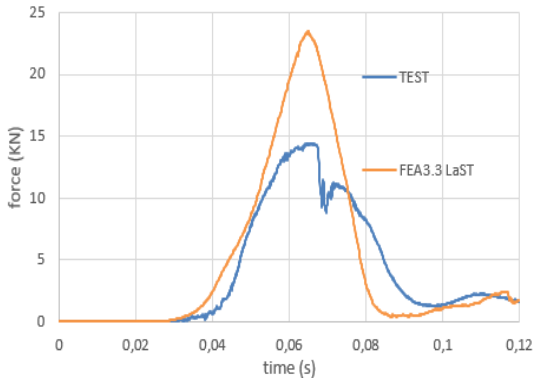

(a) Left shoulder force

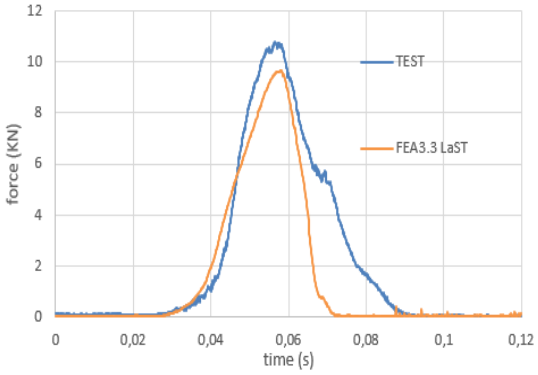

(b) Right shoulder force

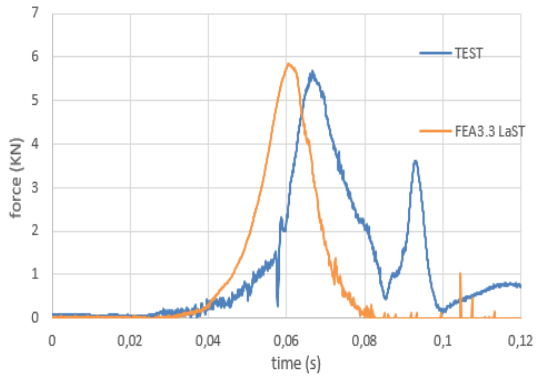

(c) Left lap force

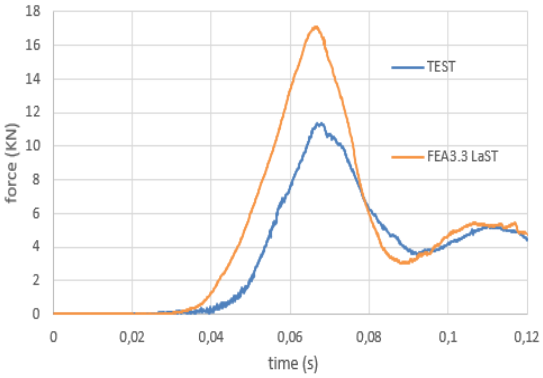

(d) Right lap force

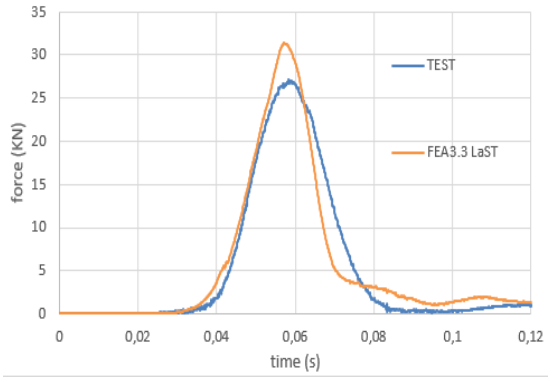

(e) Crotch force

Figure A.20: Seatbelts force magnitude; FEA3.3LaST

A.2 RoM assessment graphs

Vertebral relative displacement

Vertebral relative displacements measured in THUMS simulation with $50ms$ of adjustment and termination time equal to $180ms$.

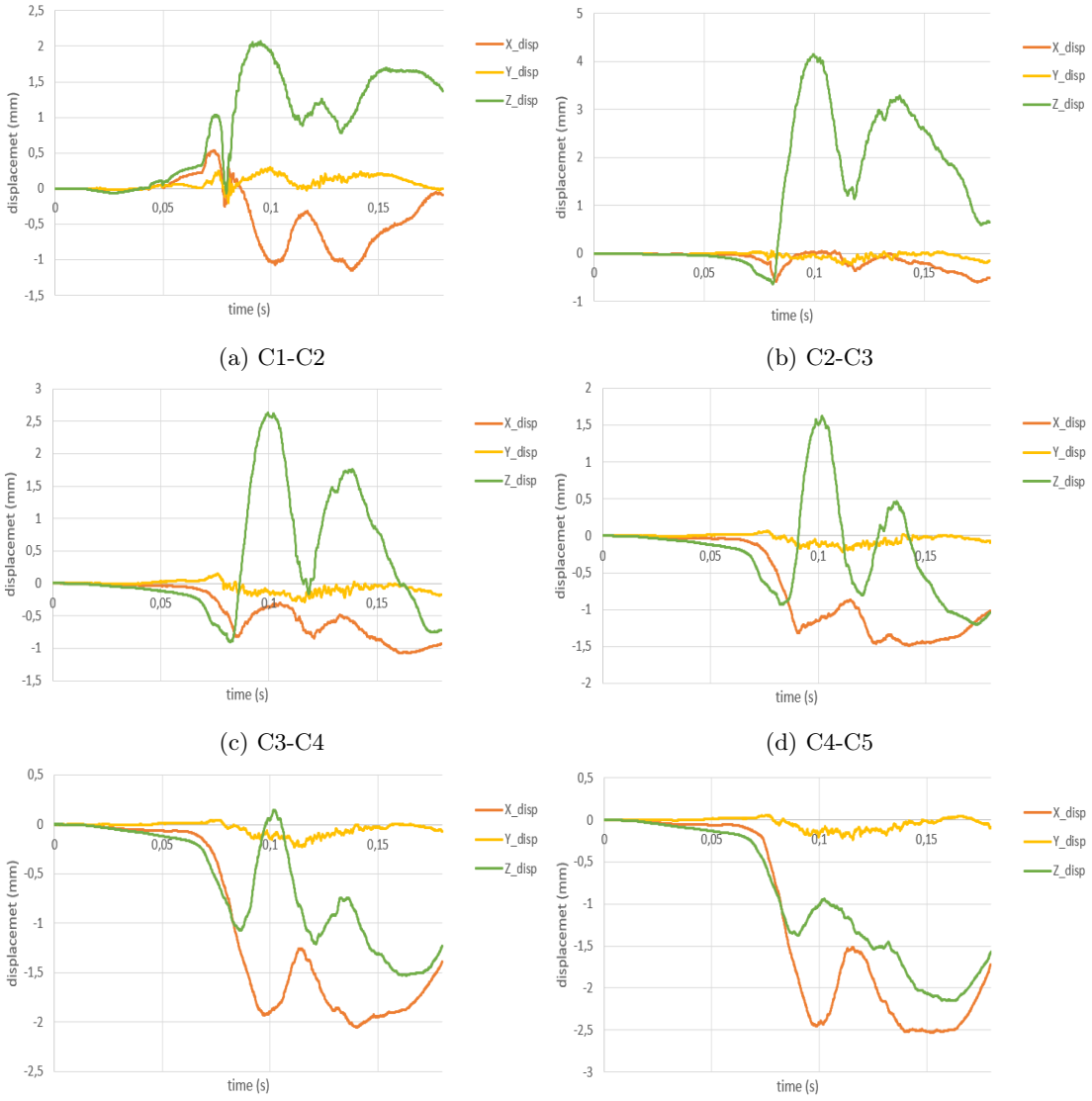

(a) C1-C2

(b) C2-C3

(c) C3-C4

(d) C4-C5

(e) C5-C6

(f) C6-C7

Figure A.21: Functional Spinal Units relative displacements

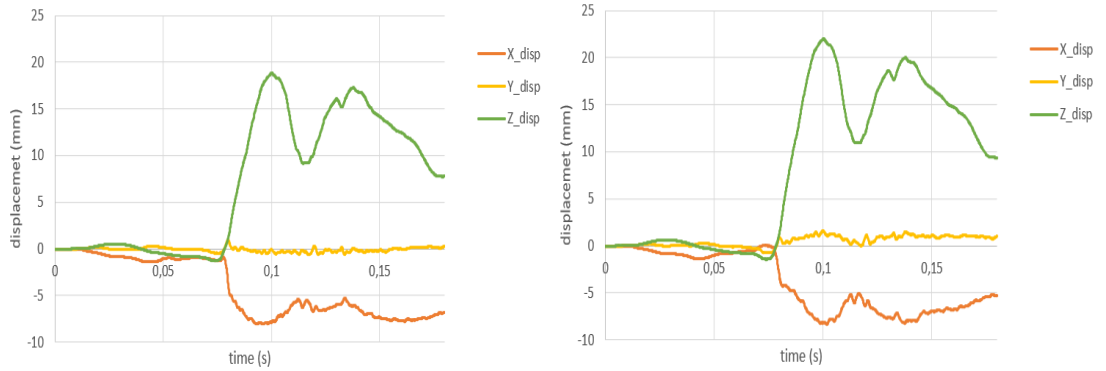

(a) C0-C1

(b) C0-C2

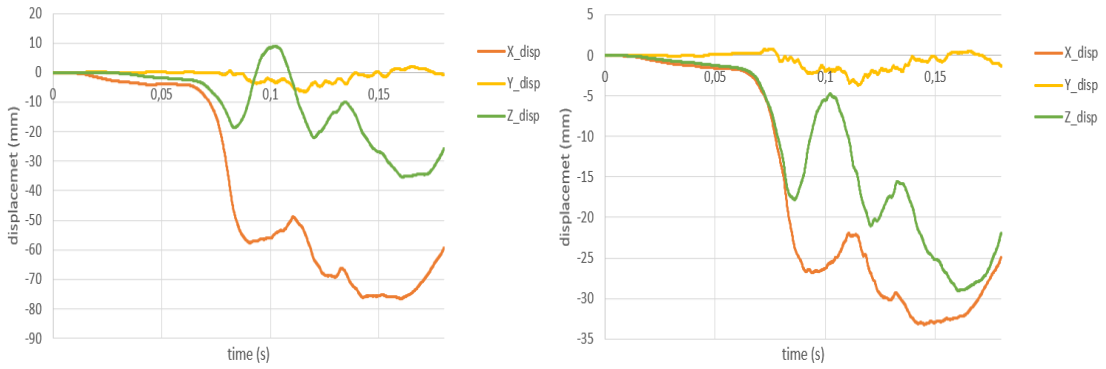

(c) C0-C7

(d) C2-C7

Figure A.22: Upper cervical and lower segments relative displacement

Vertebral rotation

Vertebral rotations measured in THUMS simulation with $50ms$ of adjustment and termination time equal to $180ms$.

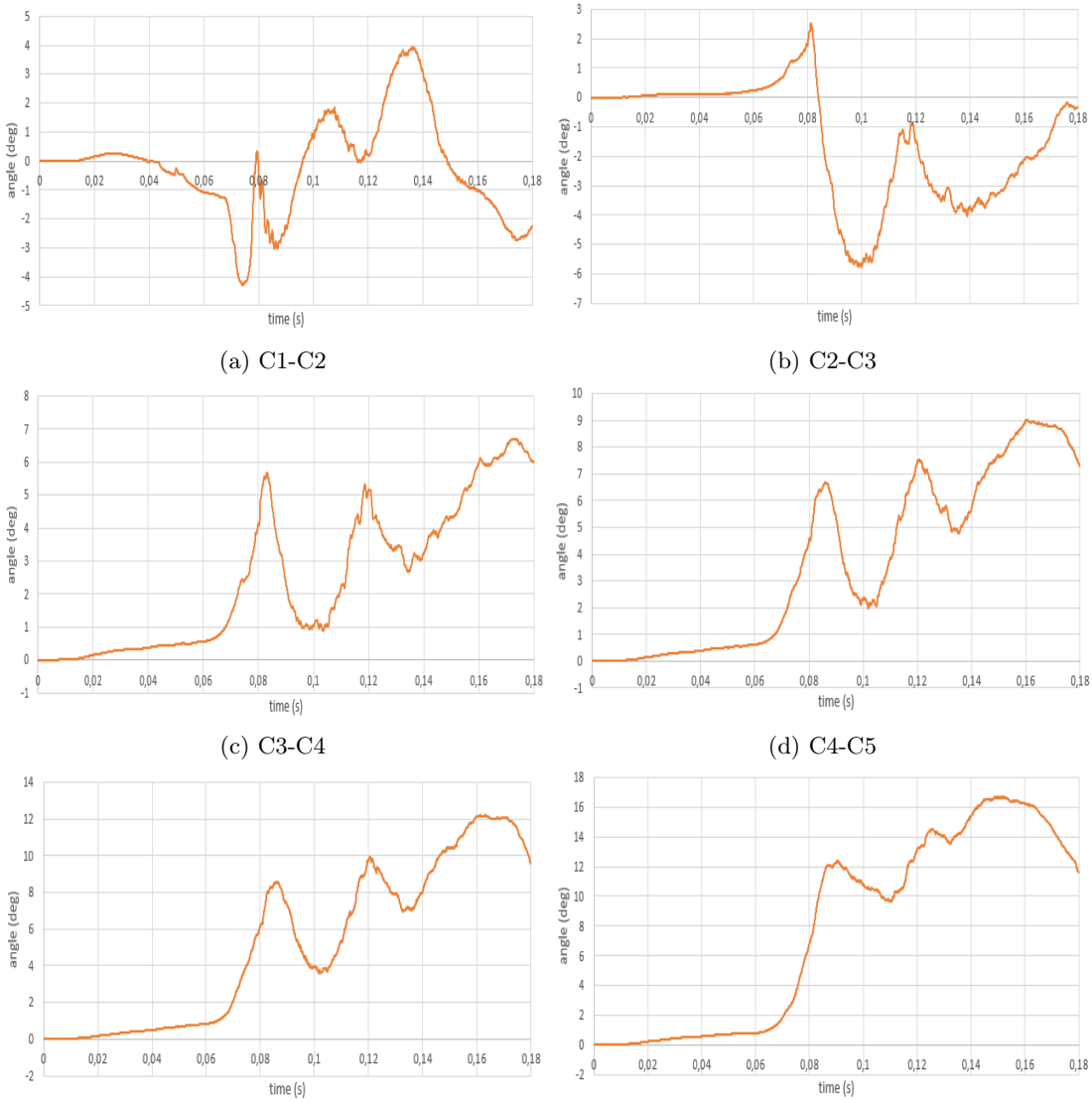

(a) C1-C2

(b) C2-C3

(c) C3-C4

(d) C4-C5

(e) C5-C6

(f) C6-C7

Figure A.23: Functional Spinal Units rotations

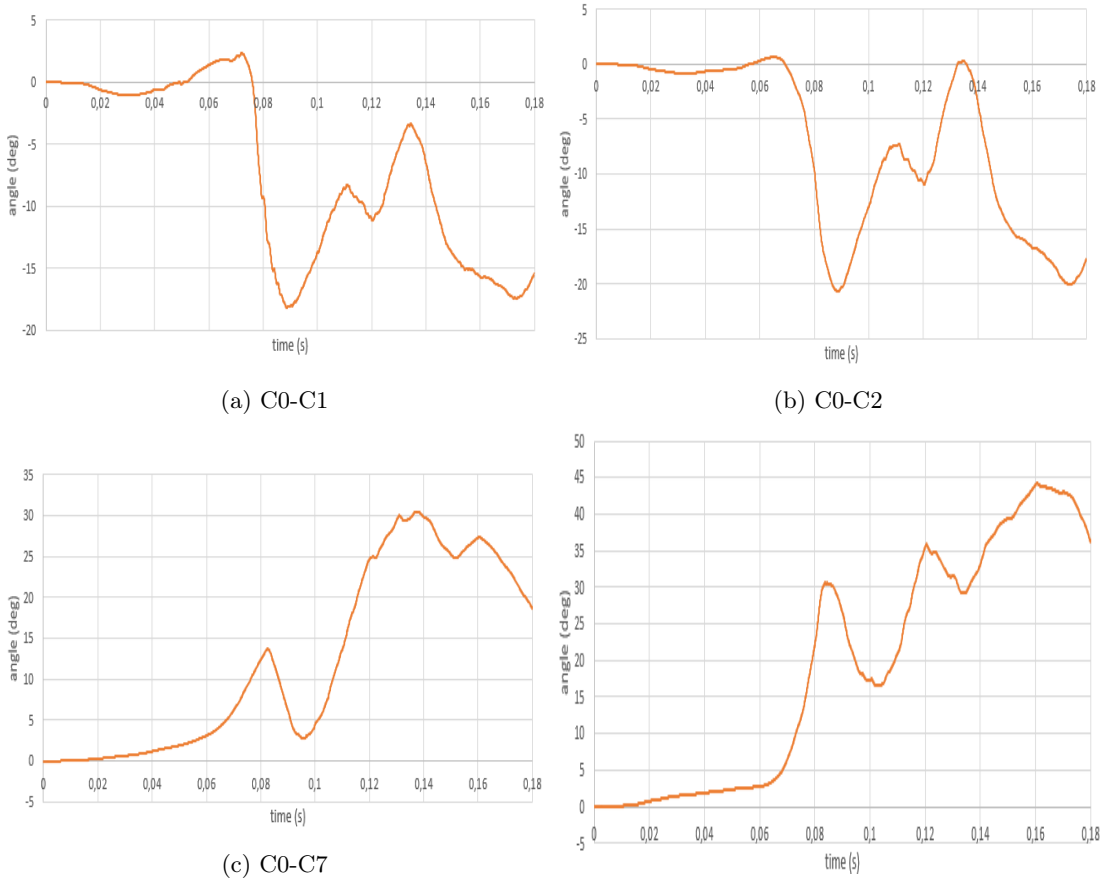

(a) C0-C1

(b) C0-C2

(c) C0-C7

(d) C2-C7

Figure A.24: Upper cervical and lower segments rotations

A.3 Vertebral plastic strain assessment graphs and figures

Effective plastic strain graphs

Effective plastic strain graphs for THUMS simulation with $50ms$ of adjustment and termination time equal to $180ms$.

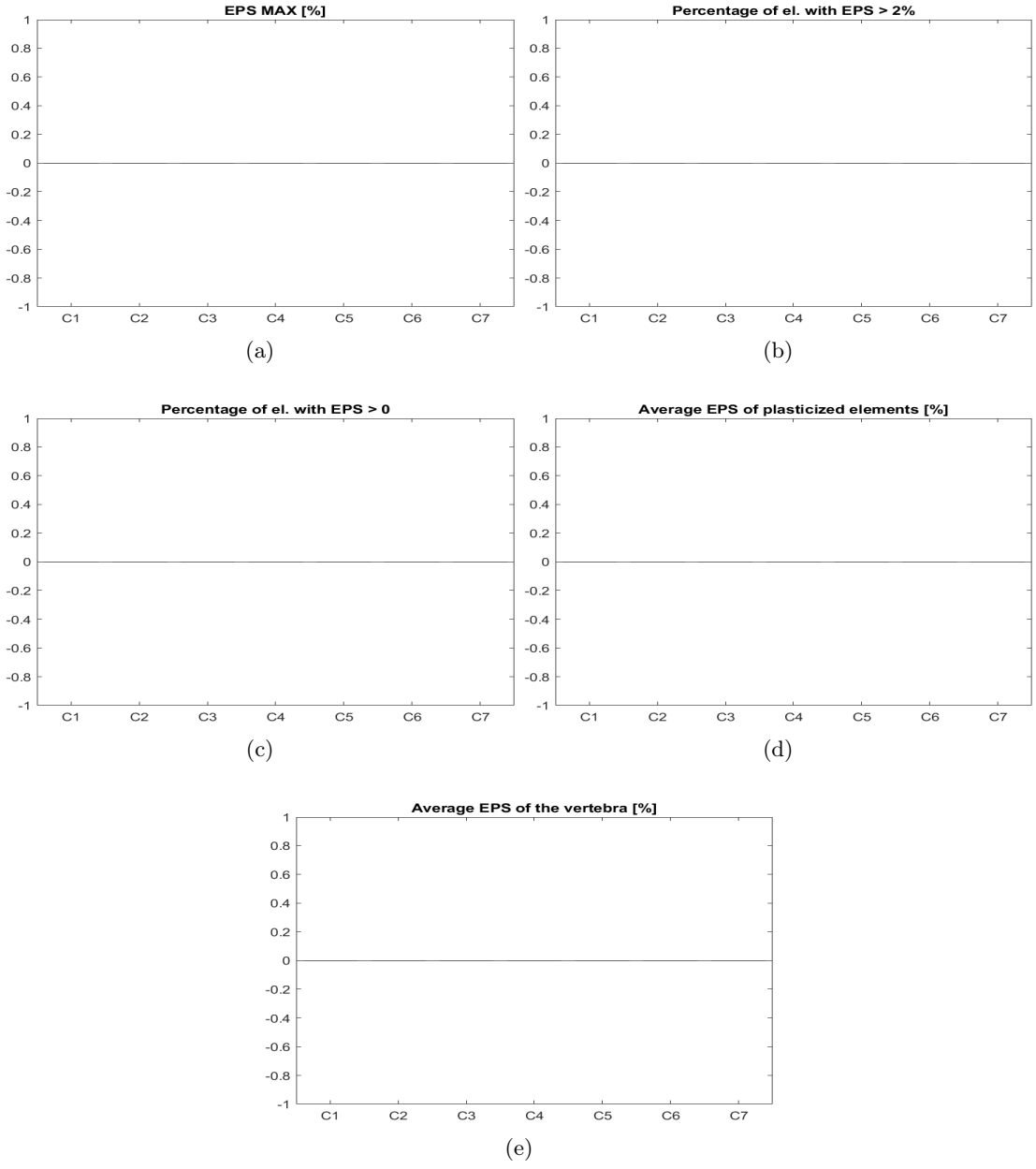

(a) (b) (c) (d) (e)

Figure A.25: Plastic strain of vertebrae; graphs; 70ms

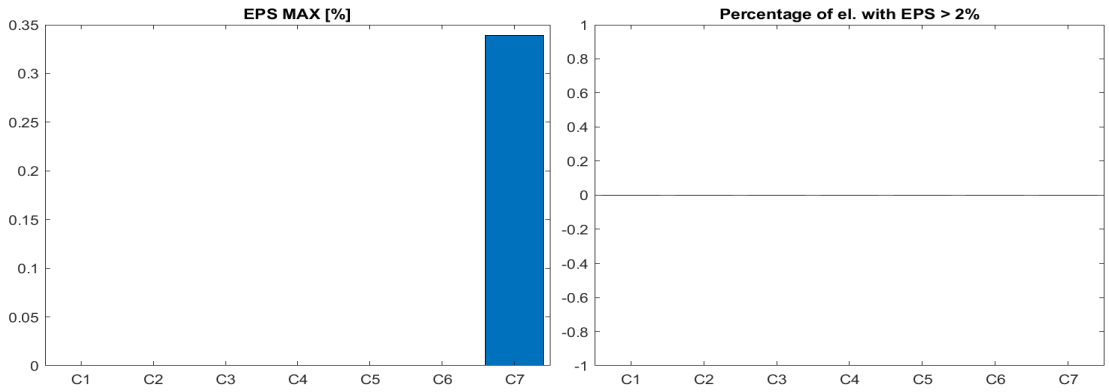

(a)

(b)

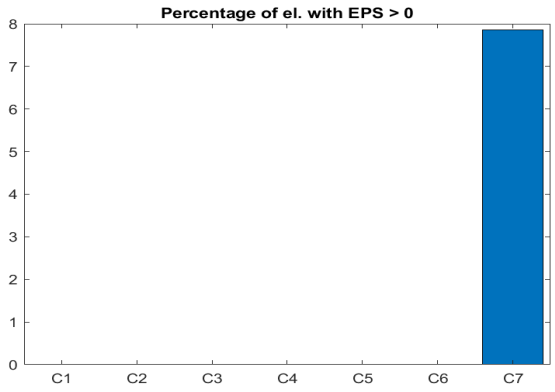

(c)

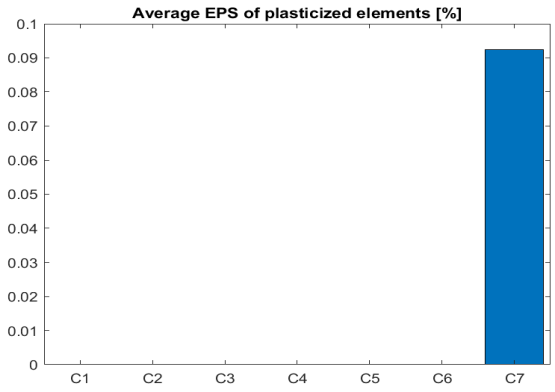

(d)

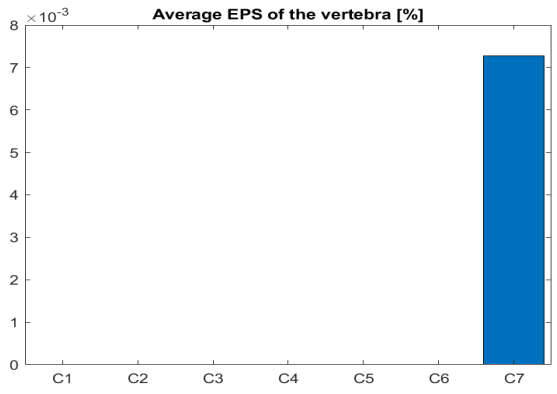

(e)

Figure A.26: Plastic strain of vertebrae; graphs; 80ms

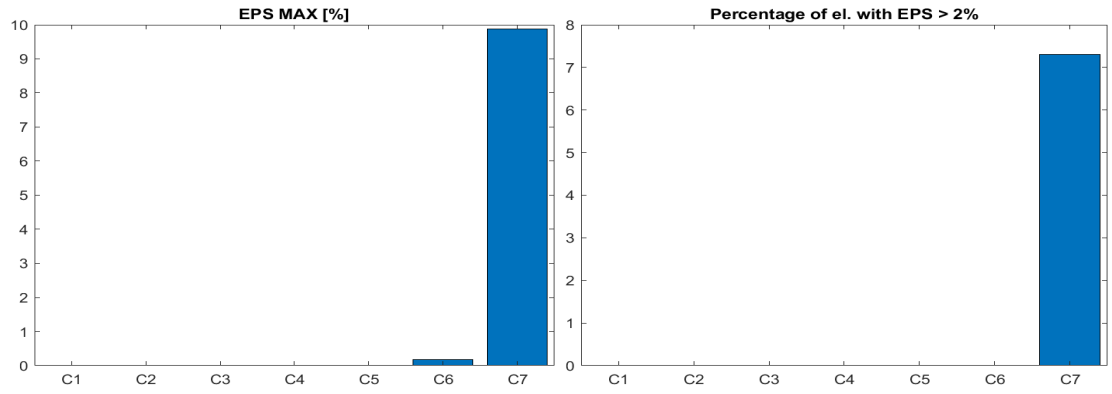

(a)

(b)

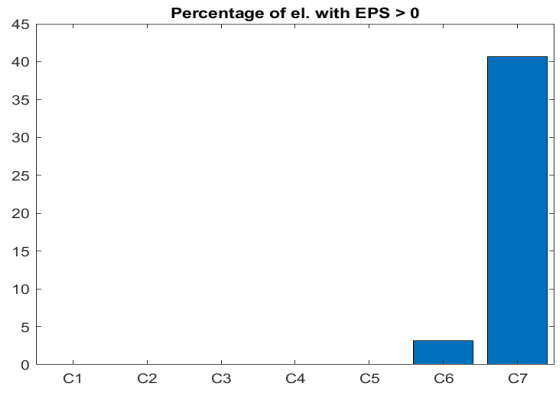

(c)

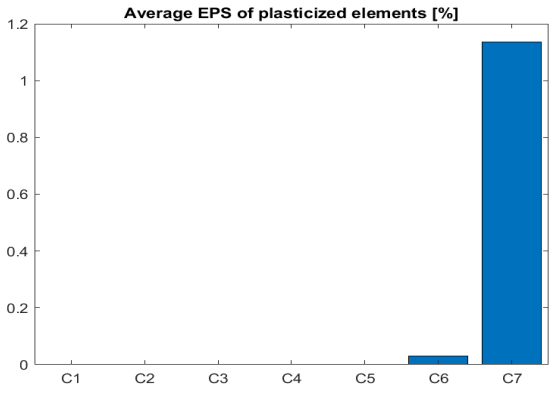

(d)

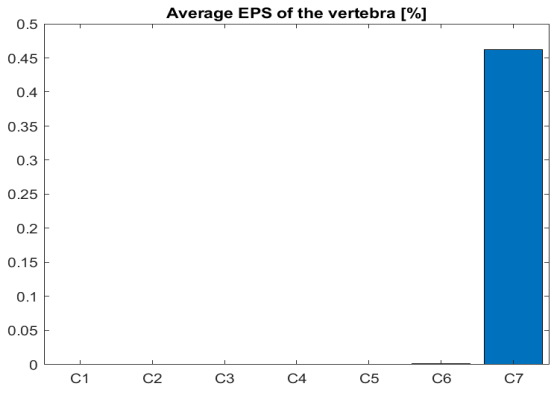

(e)

Figure A.27: Plastic strain of vertebrae; graphs; 90ms

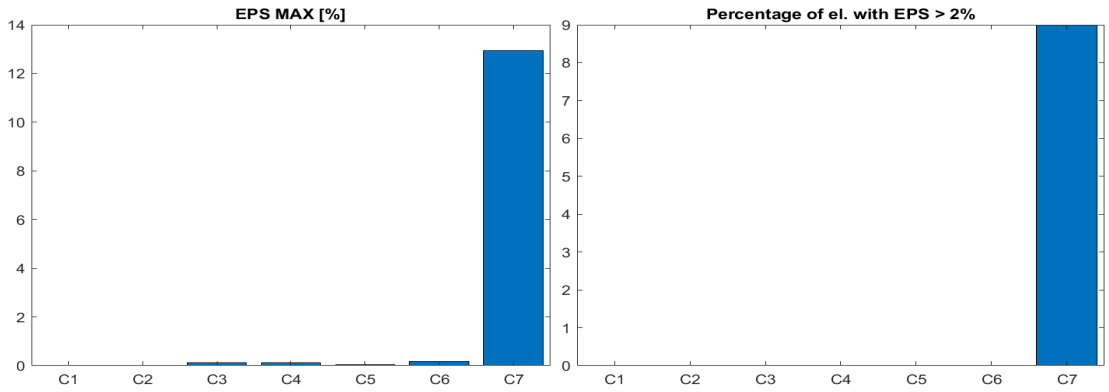

(a)

(b)

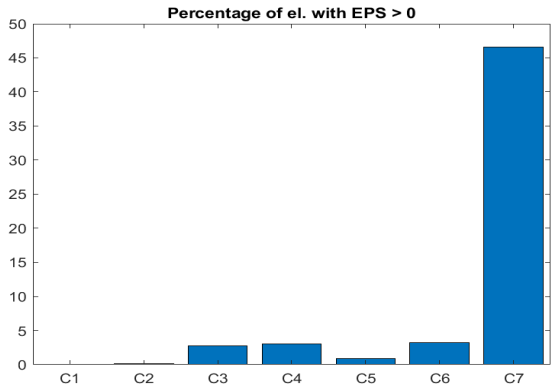

(c)

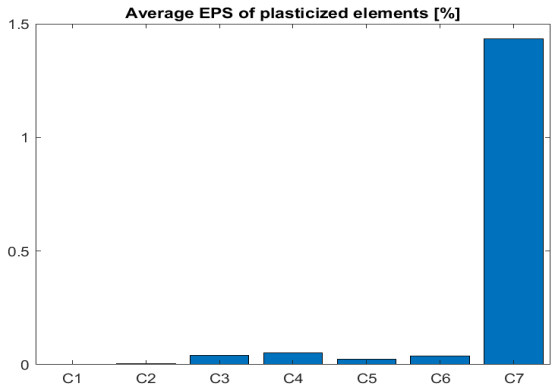

(d)

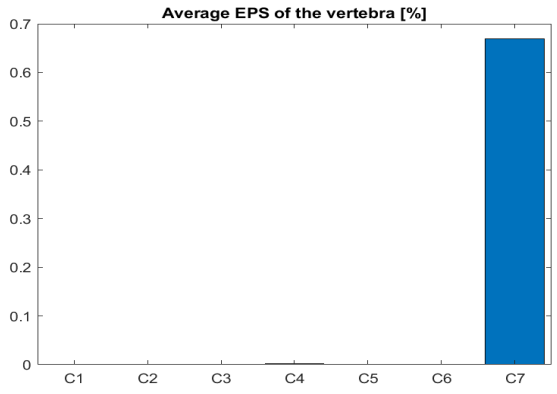

(e)

Figure A.28: Plastic strain of vertebrae; graphs; 100ms

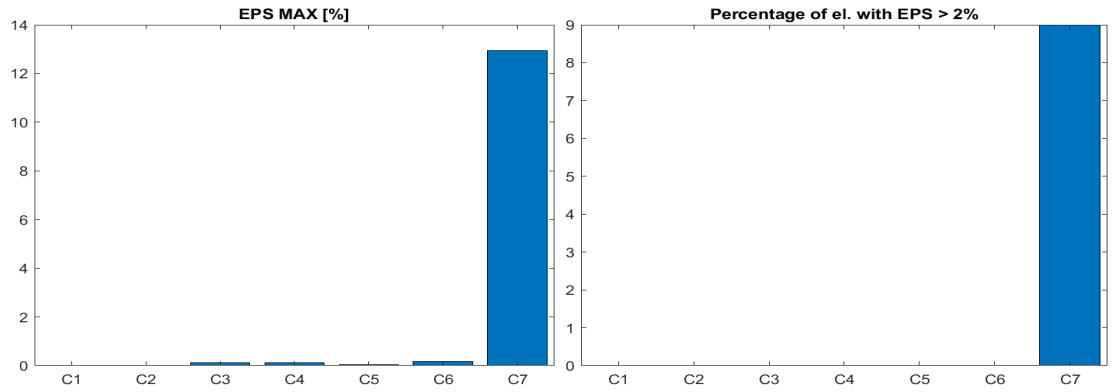

(a)

(b)

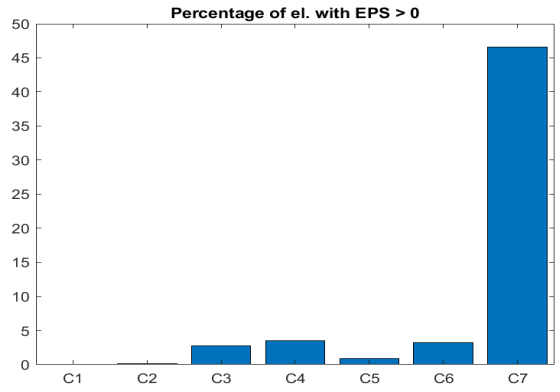

(c)

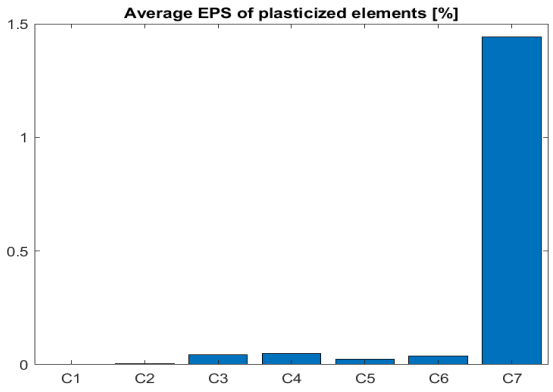

(d)

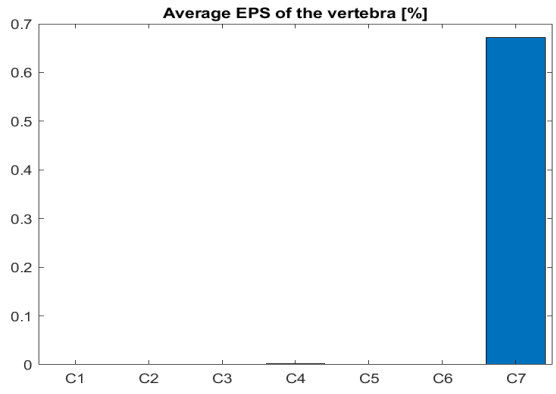

(e)

Figure A.29: Plastic strain of vertebrae; graphs; 110ms

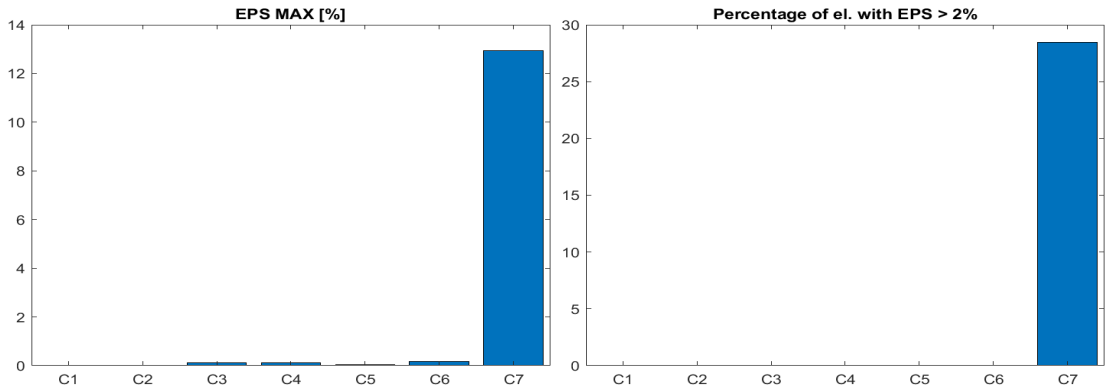

(a)

(b)

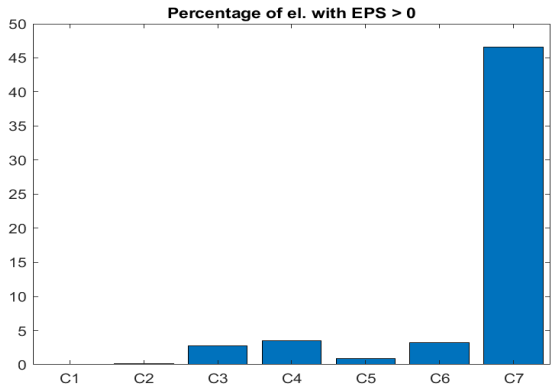

(c)

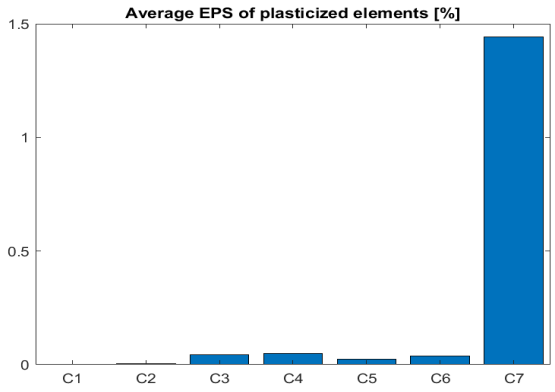

(d)

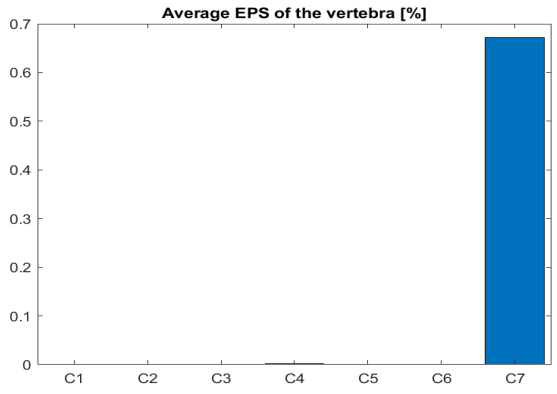

(e)

Figure A.30: Plastic strain of vertebrae; graphs; 120ms

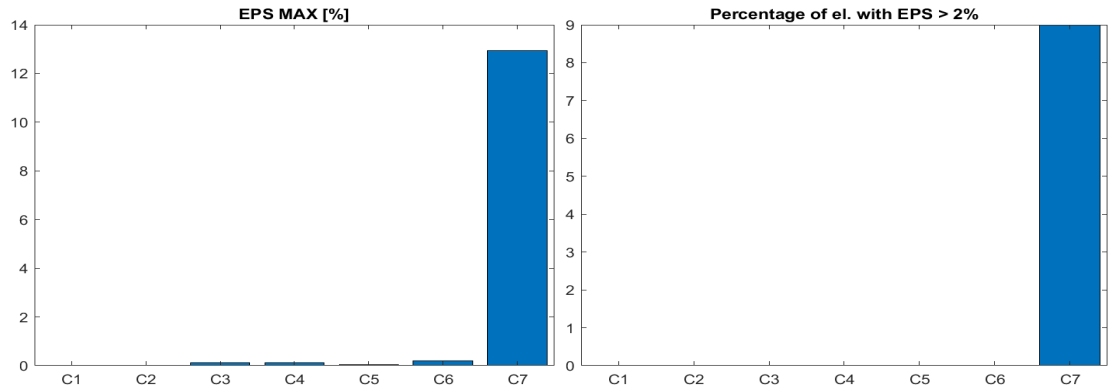

(a)

(b)

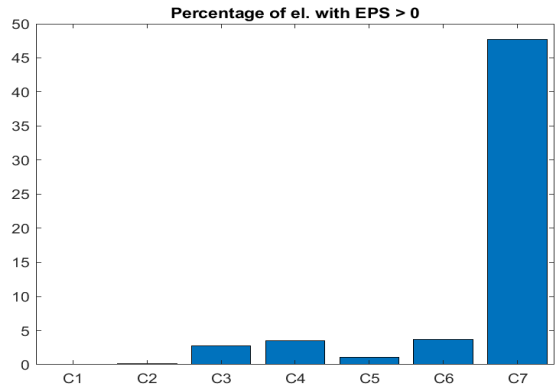

(c)

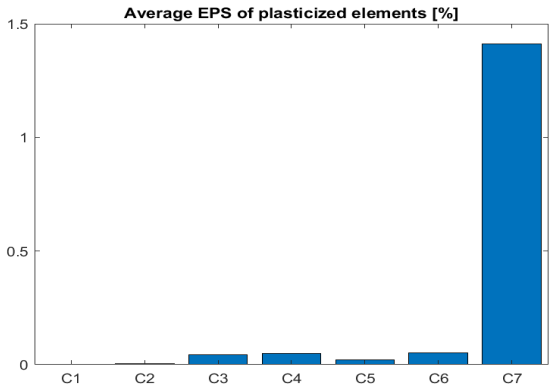

(d)

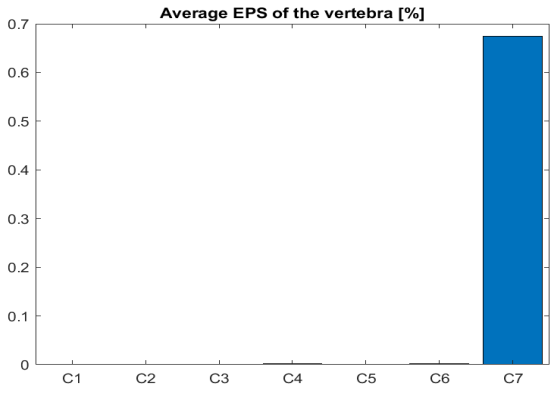

(e)

Figure A.31: Plastic strain of vertebrae; graphs; 130ms

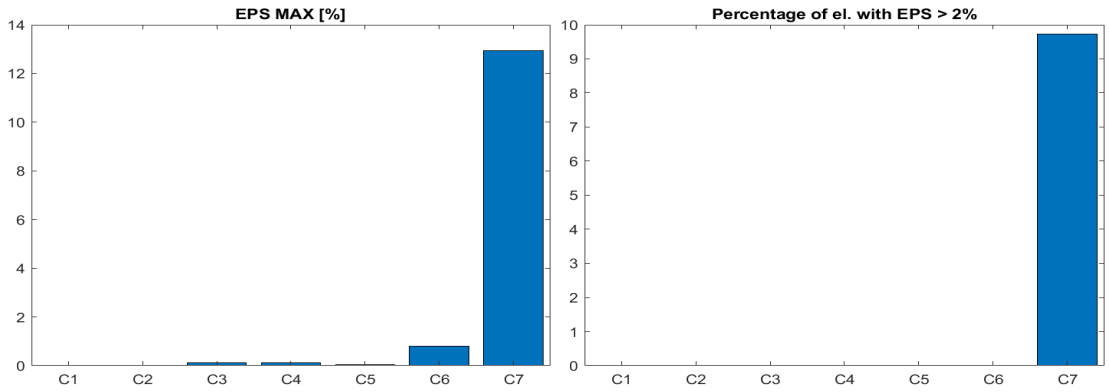

(a)

(b)

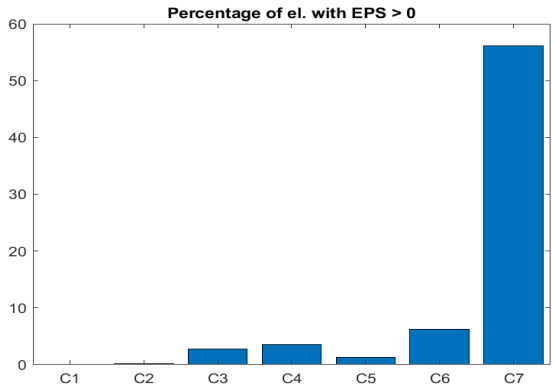

(c)

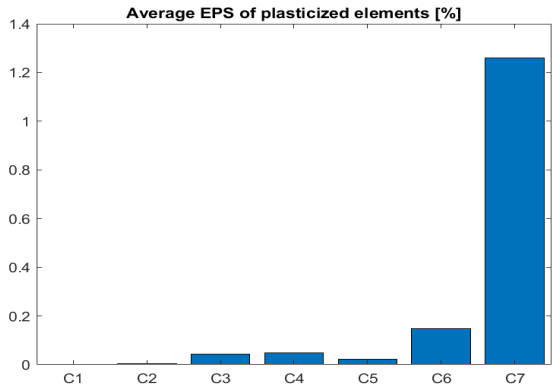

(d)

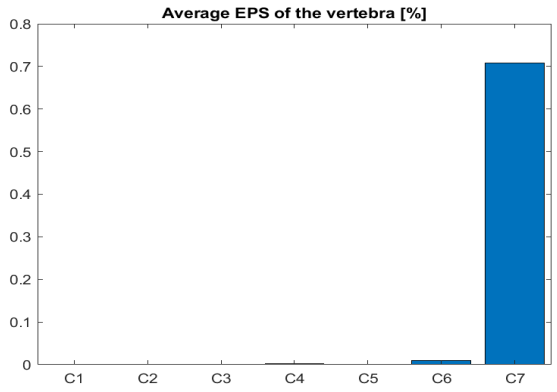

(e)

Figure A.32: Plastic strain of vertebrae; graphs; 140ms

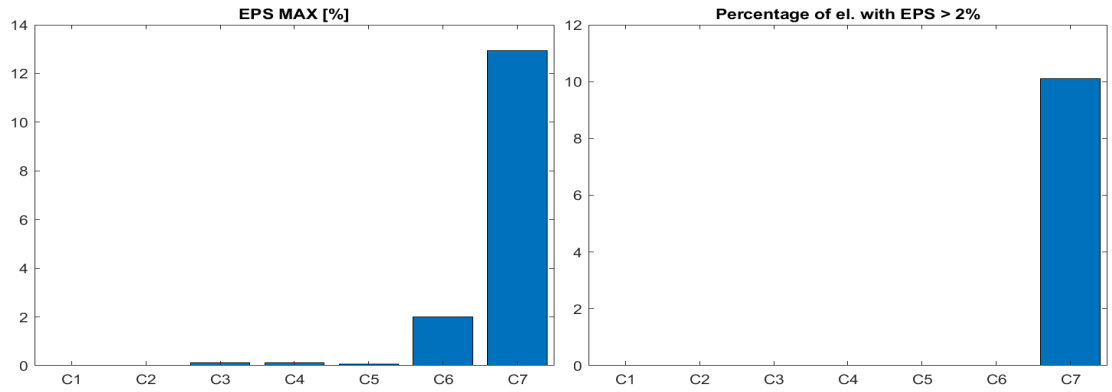

(a)

(b)

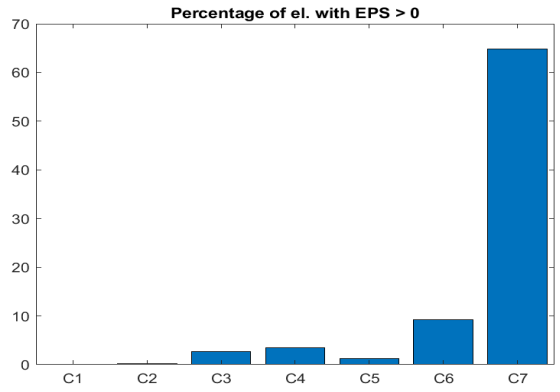

(c)

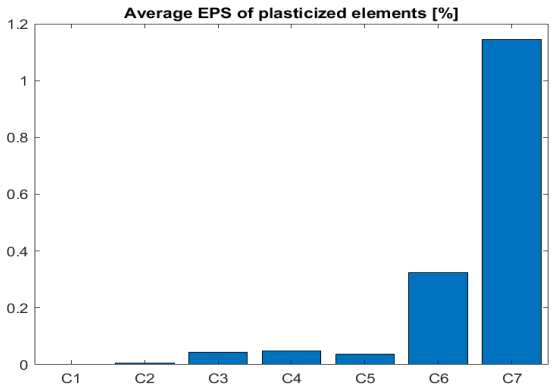

(d)

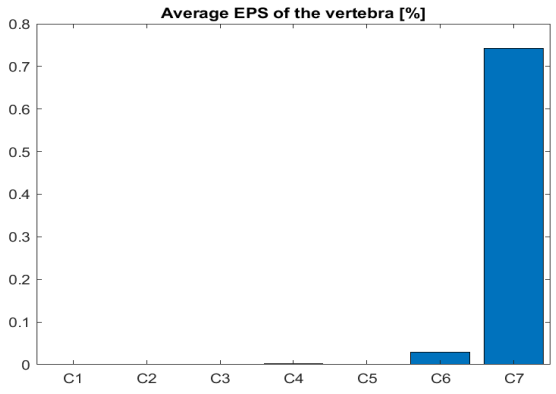

(e)

Figure A.33: Plastic strain of vertebrae; graphs; 150ms

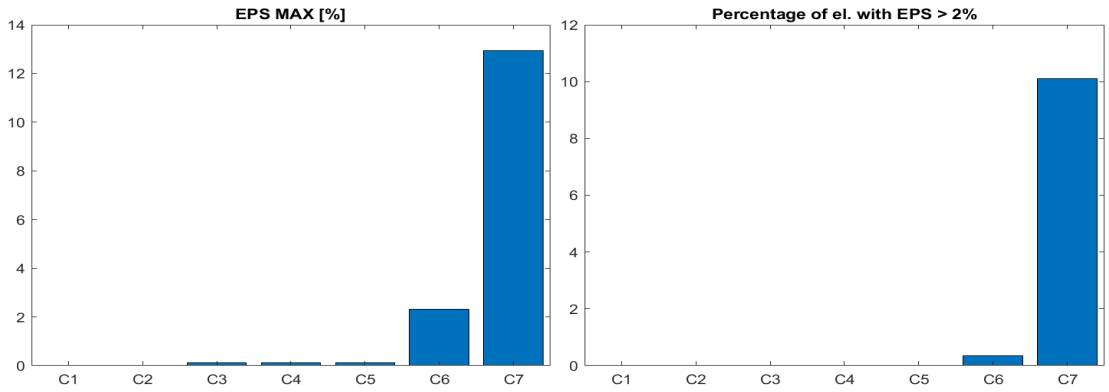

(a)

(b)

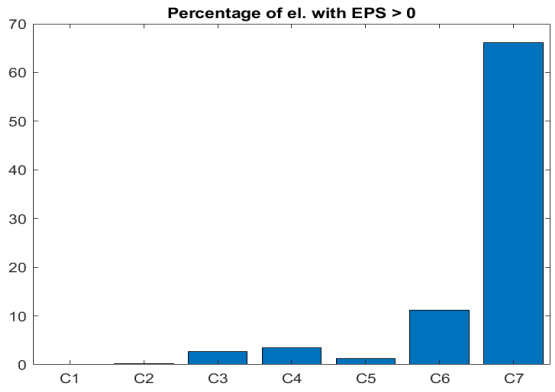

(c)

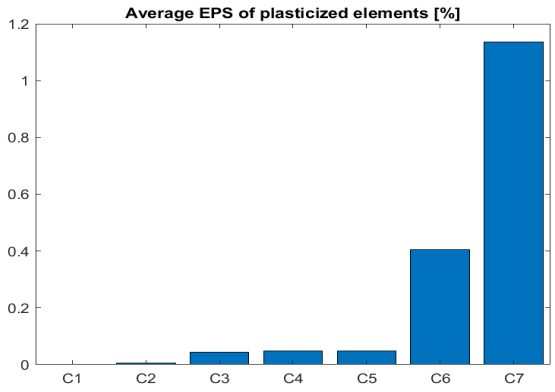

(d)

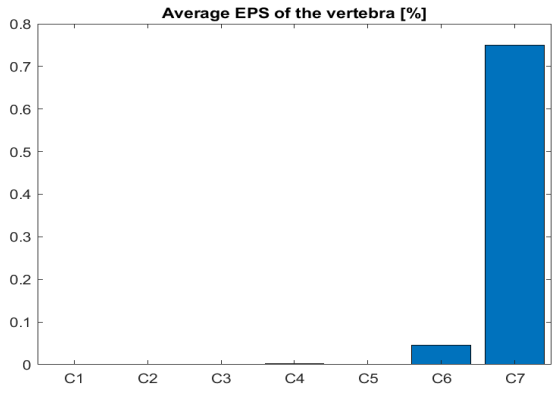

(e)

Figure A.34: Plastic strain of vertebrae; graphs; 160ms

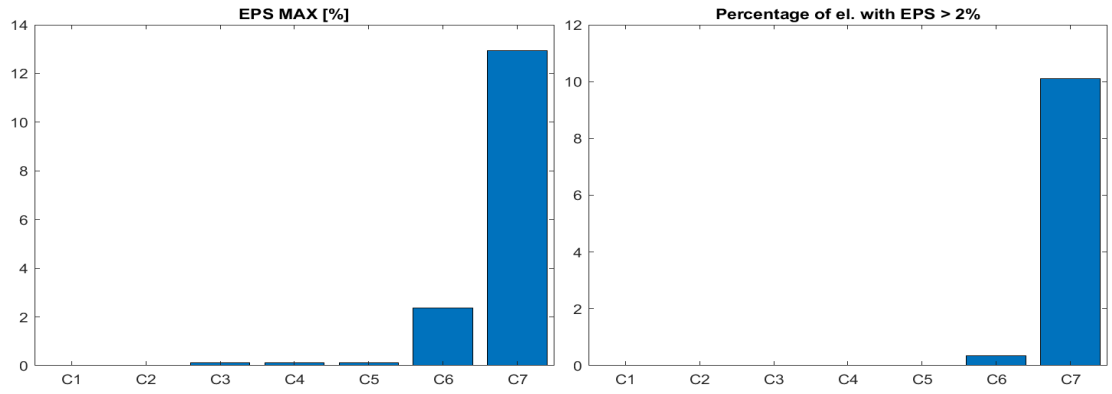

(a)

(b)

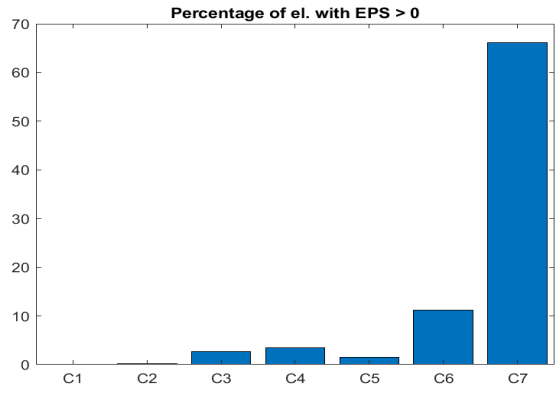

(c)

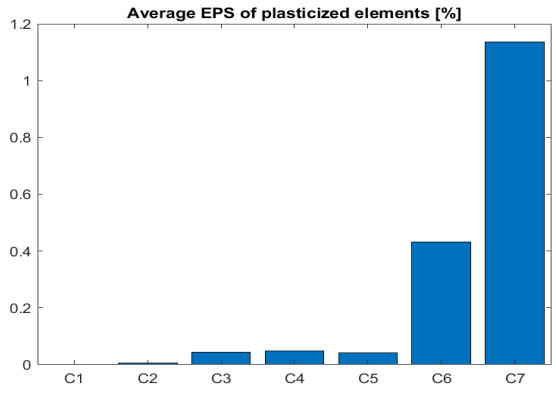

(d)

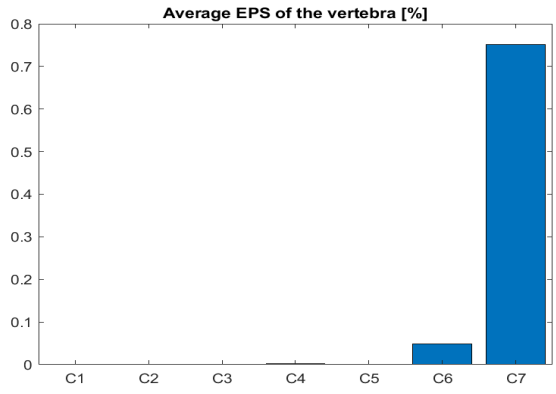

(e)

Figure A.35: Plastic strain of vertebrae; graphs; 170ms

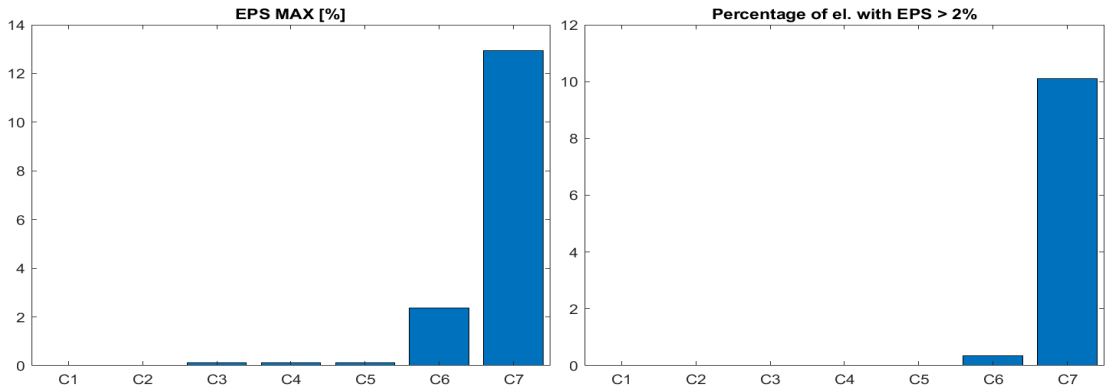

(a)

(b)

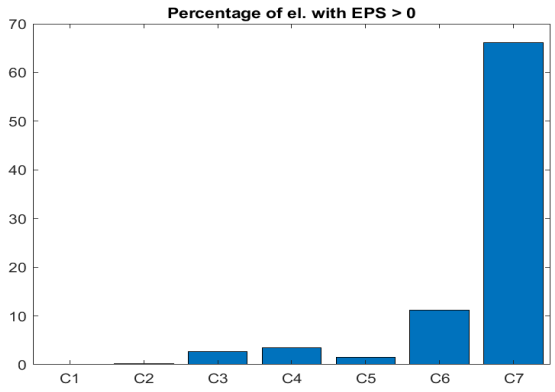

(c)

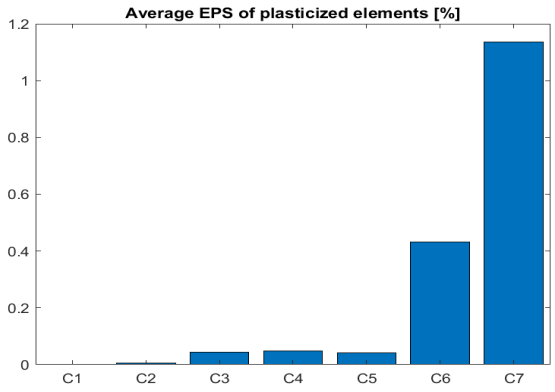

(d)

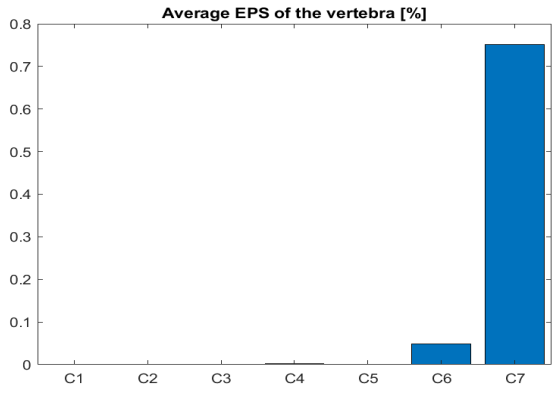

(e)

Figure A.36: Plastic strain of vertebrae; graphs; 180ms

Effective plastic strain figures

Effective plastic strain figures for THUMS simulation with $50ms$ of adjustment and termination time equal to $180ms$.

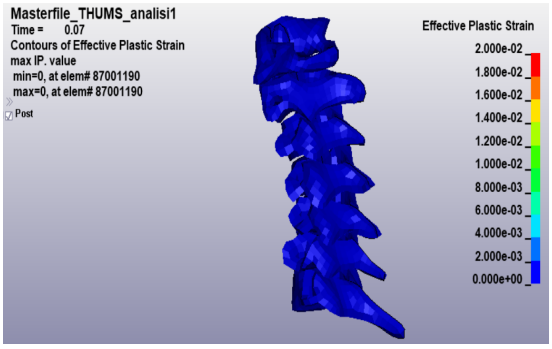

(a) 70ms

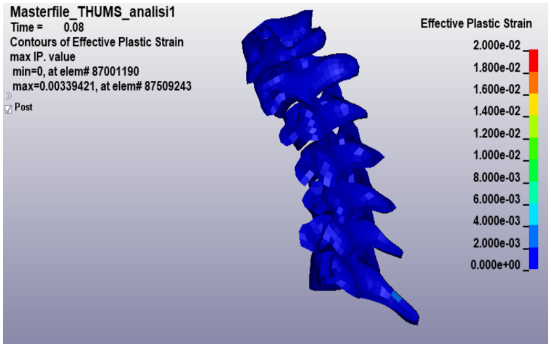

(b) 80ms

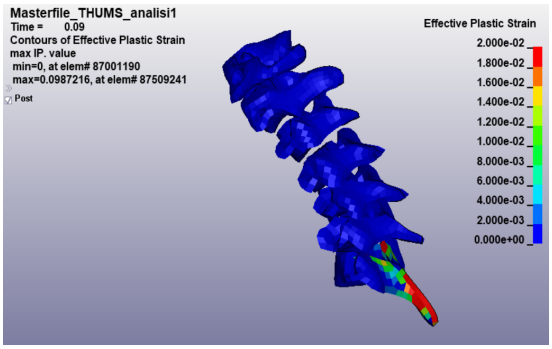

(c) 90ms

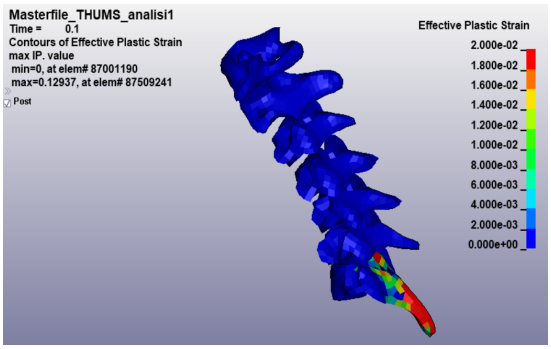

(d) 100ms

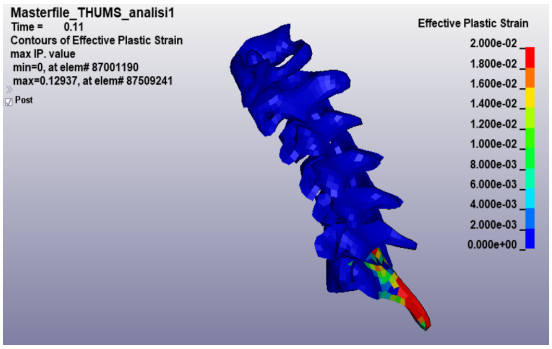

(e) 110ms

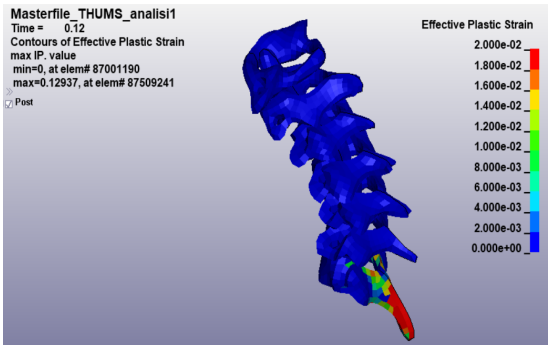

(f) 120ms

Figure A.37: Plastic strain of vertebrae; figures; 70-120ms

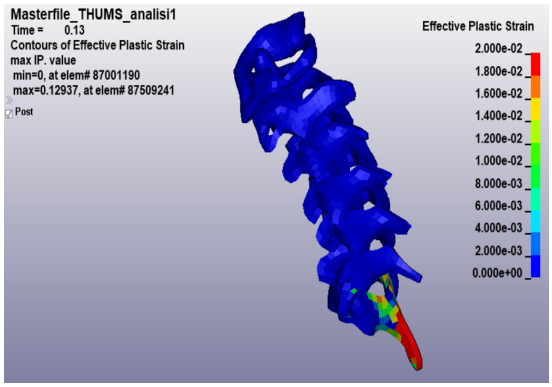

(a) 130ms

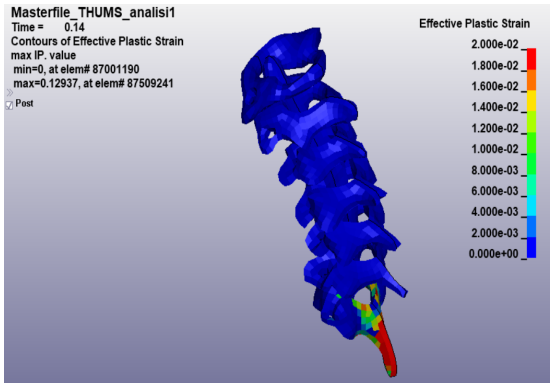

(b) 140ms

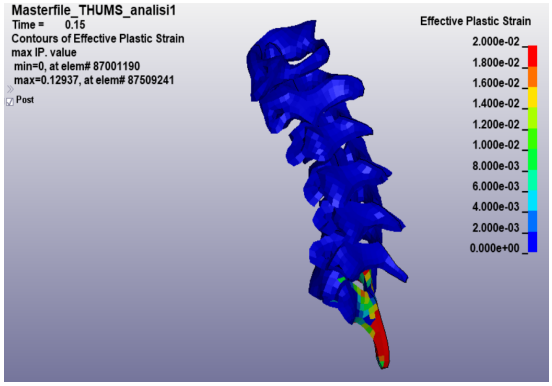

(c) 150ms

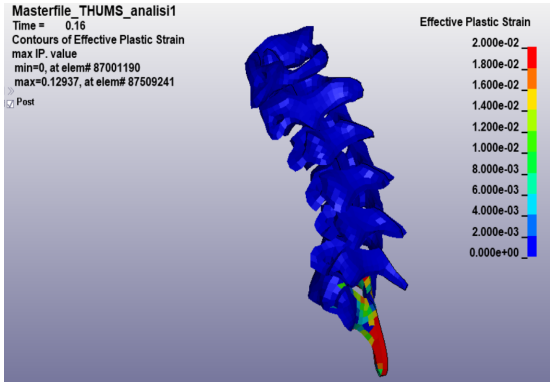

(d) 160ms

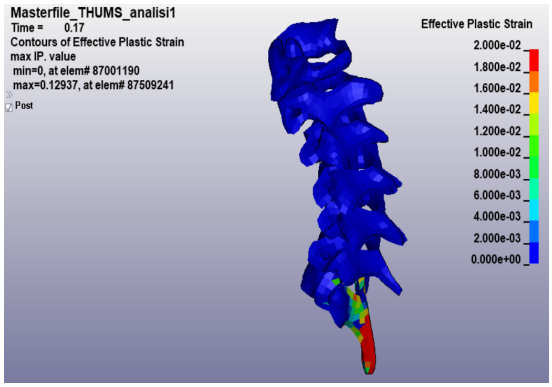

(e) 170ms

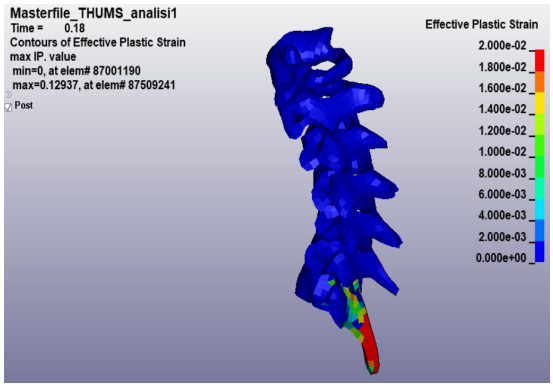

(f) 180ms

Figure A.38: Plastic strain of vertebrae; figures; 130-180ms

Appendix B

MatLab script

In order to organize the vertebral effective plastic strain output data of LS-DYNA, the following MatLab script have been used:

```
clear all

eps_max = [];
eps_gte2 = []; % number of element with eps > 2%
eps_gte2_p = []; % percentage of element with eps > 2% (on vertbra's number of ...
    element)
eps_gte0 = []; % number of element with eps > 0
eps_gte0_p = []; % percentage of element with eps > 0 (on vertbra's number of ...
    element)
mean_eps = [];
mean_eps_gte0 = [];

tab_el_id = readtable('tab_el_id.xlsx');
el_id = table2array(tab_el_id(:,2:end));

load('el_res');


for i = 1 : size(el_id,1)
    id_L_up = el_id(i,1);
    id_L_bot = el_id(i,2);
    id_R_up = el_id(i,3);
    id_R_bot = el_id(i,4);
    i_L_up = find(el_res(:,1)==id_L_up);
    i_L_bot = find(el_res(:,1)==id_L_bot);
    i_R_up = find(el_res(:,1)==id_R_up);
    i_R_bot = find(el_res(:,1)==id_R_bot);
    eps = [el_res(i_L_up:i_L_bot,2);el_res(i_R_up:i_R_bot,2)];

    eps_max(i) = max(eps);
    mean_eps(i) = mean(eps);

    % find number of elements with eps > 2%
    if eps_max(i) ≥ 0.02
        pos = find(eps ≥ 0.02);
        eps_gte2(i) = length(pos);
    else
        eps_gte2(i) = 0;
```

```
37      end
38      % normalization with number of elements of the vertebra
39      eps_gte2_p(i) = eps_gte2(i)/length(eps)*100;
40
41
42      % find number of elements with eps > 0
43      if eps_max(i) > 0
44          pos = find(eps > 0);
45          eps_gte0(i) = length(pos);
46          mean_eps_gte0(i) = mean(eps(pos));
47      else
48          eps_gte0(i) = 0;
49          mean_eps_gte0(i) = 0;
50      end
51      % normalization with number of elements of the vertebra
52      eps_gte0_p(i) = eps_gte0(i)/length(eps)*100;
53  end
54
55  xbar = categorical([1:size(el_id,1)],[1:size(el_id,1)],tab_el_id.Var1);
56
57  bar(xbar,eps_max*100)
58  title('EPS MAX [%]')
59
60  bar(xbar,eps_gte2_p)
61  title('Percentage of el. with EPS > 2%')
62
63  bar(xbar,eps_gte0_p)
64  title('Percentage of el. with EPS > 0')
65
66  bar(xbar,mean_eps_gte0*100)
67  title('Average EPS of plasticized elements [%]')
68
69  bar(xbar,mean_eps*100)
70  title('Average EPS of the vertebra [%]')
```

The script uses the table *table_ el_ id* and the table *el_ res*. The former defines the element id limits for each vertebra. The latter contains the effective plastic strain of each vertebra.

Appendix C

SAE J221 Butterworth filters

The SAE filtering operation performs two-pass, zero phase shift, second-order Butterworth filtering. A Butterworth four-poles digital filter is here described. A difference equation is used for filtering a sequence of data samples. The filtering results in an amplitude versus frequency response curve[27]. The difference equation in the time domain has this form:

$$Y[t] = a_0 X[t] + a_1 X[t-1] + a_2 X[t-2] + b_1 Y[t-1] + b_2 Y[t-2] \qquad \text{(C.1)}$$

where: $X[t]$ is the input data stream, $Y[t]$ is the filtered output data stream, $a0$, $a1$, $a2$, $b1$, $b2$ are constant depending on the cutoff frequency and sample period T.
Equation C.1 is for a two-pole filter. To make a four-pole filter, the data are passed through the filter twice. By passing the data through the filter forward and then backward, the filter will not phase shift the data. Peaks in filtered data set will occur at the same time as peak in the unfiltered data. However if the data set contains a step or a fast raise, filtered output will contain data prior to and after the actual event.
Startup of a digital filter yields the same response as switching a signal into the input of an analog filter. The digital filter sees nonzero initial data as a step function and responds with a typical underdamped second-order response.
In this work we used pass-low filters for specified cut-off frequencies. However, it possible to use class-specific operators filter for each of supported SAE filtering classes. This filters are named CFC[1]. Each class has its own characteristics defined by its identification number. This number is not the cutoff frequency but indicates the minimum sampling frequency for the input data. It is clear from the J211 filter specifications that they were derived from analog Butterworth filters whose corner frequency is equal to the CFC designation divided by 0.6. The characteristics of CFC60 are here reported as an example:
For CFC filters the Equation C.1 coefficients depend on the CFC class:

[1] channel frequency classes

$3dB$ limit frequency	$100Hz$
Stop damping	$-30dB$
Sampling frequency	$600Hz$

Table C.1: CFC60 characteristics

$$
\begin{aligned}
w_d &= 2\pi CFC \cdot 2.0755 \\
w_a &= \frac{\sin(w_d) \cdot 0.5T}{\cos(w_d) \cdot 0.5T} \\
b_0 &= \frac{w_a^2}{1 + \sqrt{2}w_a + w_a^2} \\
b_1 &= 2b_0 \\
b_2 &= b_0 \\
a_1 &= 2\frac{w_a^2 - 1}{1 + \sqrt{2}w_a + w_a^2} \\
a_2 &= -\frac{-1 + \sqrt{2}w_a - w_a^2}{1 + \sqrt{2}w_a + w_a^2}
\end{aligned}
$$

Bibliography

[1] University of Arizona. *Moment of Inertia and Properties of Plane Areas.* URL: https://wp.optics.arizona.edu/optomech/wp-content/uploads/sites/53/2016/10/OPTI_222_W61.pdf. (accessed: 05.05.21).

[2] B.Watier. *Etude expérimentale du rachis cervical: comportement mécanique in-vitro et cinématique in-vivo.* 1997.

[3] B.Watier. "Mechanical behaviour of cervical spine: literature update". In: *ITBM-RBM* 27 (2006), pp. 92–106.

[4] C.Niewiadomski et al. "Experimental assessment of cervical ranges of motion and compensatory strategies". In: *Chiropractic and Manual Therapies* (2019).

[5] Toyota Motor Corporation. *About THUMS.* URL: https://www.toyota.co.jp/thums/about/. (accessed: 05.05.21).

[6] *Crash test dummy.* URL: https://en.wikipedia.org/wiki/Crash_test_dummy. (accessed: 29.04.21).

[7] D.Johnson, B.Koya, and F.S. Gayzik. *Comparison of Neck Injury Criteria Values Across Human Body Models of Varying Complexity.* URL: https://www.frontiersin.org/articles/10.3389/fbioe.2020.00985/full. (accessed: 30.04.21).

[8] E.Munting et al. "Failure strains properties of the whole human vertebral body". In: 46th Annual Meeting of Orthopaedic Research Society, Orlando, Florida. March 12-15, 2000.

[9] E.N.Marieb et al. *Anatomie et physiologie humaines, 4th edition.* 2010.

[10] F.H.Netter. *Atlas of Human Anatomy, 6th edition.* 2014.

[11] H.J.Mertz et al. "An assessment of compressive neck loads under injury-producing conditions". In: *Phys. Sports Med* (1978).

[12] Humanetics. *Humanetics History.* URL: https://humanetics.humaneticsgroup.com/about-us/history. (accessed: 29.04.21).

[13] Humanetics. *Humanetics Online Documentation: Hybrid III 50th Male.* URL: https://humanetics.humaneticsgroup.com/products/anthropomorphic-test-devices/frontal-impact/hybrid-iii-50th-male/hybrid-iii-50th-male. (accessed: 05.05.21).

[14] J.G.Paver et al. "The development of IARVs for the hybrid III neck modified for dynamic rollover testing". In: 7th International Crashworthiness Conference. Washington D.C., 2010.

[15] J.H.Marcus. *Dummy and Injury Criteria for Aircraft Crashworthiness.* 1996.

[16] *LS-DYNA® KEYWORD USER'S MANUAL.* LIVERMORE SOFTWARE TECHNOLOGY (LST). 2020.

[17] *LS-DYNA® KEYWORD USER'S MANUAL*. LIVERMORE SOFTWARE TECHNOLOGY (LST). 2020.

[18] M.Kleinberg et al. "Development of improved injury criteria for the assessment of advanced automotive restraint systems". In: *NHTSA Docket* (1998).

[19] M.SHojaati. "Correlation between injury risk and impact severity index ASI". In: Proceedings of the 3rd Swiss Transport Research Conference. 2003, pp. 19–21.

[20] M.Y.Svensson et al. "Neck injuries in car collision-a review covering a possible injury mechanism and the developement of a new rear-impact dummy". In: *Accident Analysis and Prevention* 32.2 (2000), pp. 167–175.

[21] N.Schilke. "The HANS Device - a head and neck support system". In: *Motor Sport Magazine* (21 February, 2001).

[22] N.T.Spark. "The Fastest Man on Earth". In: *Improbable Research* (2003).

[23] P.Trott et al. "Three-dimensional analysis of active cervical motion: the effect of age and gender". In: *Clinical Biomechanics* 11.4 (1996), pp. 201–206.

[24] R.Eppinger et al. *Development of improved injury criteria for the assessment of advanced automotive restraint systems*. November, 1999.

[25] S.Guha. $LSTC_NCACHybridIII50thDummyPositioningPost-Processing$. LIVERMORE SOFTWARE TECHNOLOGY (LST). May 29, 2014.

[26] S.Motta. *Ottimizzazione di testa e collo di modelli FEM di Hybrid III e validazione attraverso il confronto con prove sperimentali*. a.a.2017/2018.

[27] *Sae J211-1: Instrumentation for impact test*. SAE International. March, 1995.

[28] Association for Safe International Road Travel. *Road Safety Facts*. URL: `https://www.asirt.org/safe-travel/road-safety-facts/#:~:text=More%20than%2038%2C000%20people%20die,for%20people%20aged%201%2D54.`. (accessed: 29.04.21).

[29] *The cervical spine*. URL: `https://teachmeanatomy.info/neck/bones/cervical-spine/`. (accessed: 05.05.21).

[30] *Total Human Model For Safety (THUMS): revolutionizing crash simulation to support safe mobility for all*. Toyota Motor Corporation. 2021.

[31] *Total Human Safety Model AM50 Occupant Model, Version 4.1*. Toyota Motor Corporation Toyota Central R&D Labs., Inc. 2021.

[32] V.J.Miele, M.M.Panjabi, and E.C.Benzel. "Anatomy and biomechanics of the spinal column and cord". In: *Handbook of clinical neurology* (2012), pp. 31–43.